UC Riverside

UC Riverside Electronic Theses and Dissertations

Title

A Photophysical Study of Rylene Family Members in the Search for Singlet Fission Candidates Using Optical Spectroscopy

Permalink

https://escholarship.org/uc/item/09f851px

Author

Nichols, Valerie Maureen

Publication Date

2015

Peer reviewed|Thesis/dissertation

UNIVERSITY OF CALIFORNIA
RIVERSIDE

A Photophysical Study of Rylene Family Members in the Search for Singlet
Fission Candidates Using Optical Spectroscopy

A Dissertation submitted in partial satisfaction
of the requirements for the degree of

Doctor of Philosophy

in

Chemistry

by

Valerie Maureen Nichols

August 2015

Dissertation Committee:
        Dr. Christopher J. Bardeen, Chairperson
        Dr. Eric Chronister
        Dr. Gregory Beran

The Dissertation of Valerie Maureen Nichols is approved:

_____

_____

_____
                                        Committee Chairperson

University of California, Riverside

ACKNOWLEDGEMENTS

"Call it a clan, call it a network, call it a tribe, call it a family. Whatever you call it, whoever you are, you need one." – Jane Howard

To My Second Family:

Although it seems logical to thank one's first family first, I cannot begin to express my gratitude and appreciation for anyone other than my advisor, Christopher J. Bardeen (let's call him Chris), first. None of this work, certainly, or the last five years of my life would have been as successful without him. I like to think that one of the first moments Chris knew he was in trouble was when I tried to integrate 'bras' and 'kets' on the whiteboard in his office hour my very first year of graduate school. It was his wisdom, guidance, persistence, and probably mostly his patience that got me through Quantum II before Quantum I, and through the rockiest and most rewarding journeys I have ever had the nerve to embark on. I want to say thank you for allowing me to feel like I belong, for teaching me how to be and think like a scientist, and above all else, thank you for being my advisor and mentor.

To Dr. Kerry Hanson, a colleague and mentor turned friend for life, I want to say thank you for all of your love and support. Many times you gave me the strength and smiles that made these last five years genuinely enjoyable. Thank you for having faith in me when I didn't know how to have my own. To the rest of the Bardeen group members I have had the pleasure of knowing, thank you for all of the laughs, memories, support, and encouragement. You have been my second family. In the future, if you ever get

discouraged, I want to leave you with a quote from Albert Einstein that has become quite near and dear to my heart:

"If we knew what it was we were doing, it would not be called research, would it?"

To My First Family:

To my husband, Aaron, thank you for being my rock. When you know what hit the fan, you have always been there for me behind the scenes holding me up and cheering me on. Never stop being unapologetically you and thank you for keeping me calm and away from the deep end.

To my parents, that planetarium and microscope went a lot further than you ever imagined they might. Thank you for raising me how you did and where you did, for encouraging my curiosity and interest in learning and my love for all things natural and scientific. Without your emotional, mental, and (let's be honest) financial support, I wouldn't be here today.

This work is dedicated to my Grandad:

Ralph Jerald Carter
May 5th, 1935 – December 13th, 2012

ABSTRACT OF THE DISSERTATION

A Photophysical Study of Rylene Family Members in the Search for Singlet
Fission Candidates Using Optical Spectroscopy

by

Valerie Maureen Nichols

Doctor of Philosophy, Graduate Program in Chemistry
University of California, Riverside, August 2015
Dr. Christopher J. Bardeen, Chairperson

As human's global energy consumption increases, reaching 17.5 TW annually in 2012, and continues to grow, the need for improved efficiencies of current renewable energy sources, such as solar energy, becomes vital. A majority of solar photons that are absorbed by photovoltaic cells are higher in energy than the bandgap material and lose that excess energy as heat. Singlet fission is a multi-electron process which fissions one excited singlet state into two separate triplet states. Incorporating singlet fission materials into a photovoltaic cell is one route to improving the efficiency of photovoltaic cells. An ideal singlet fission molecule for use in a photovoltaic cell requires three distinct improvements over current candidates: (1) increased photostability given the nature of photovoltaics and their constant exposure to sunlight, (2) increased triplet energy level so as to facilitate energy transfer at the silicon bandgap and (3) high singlet fission efficiencies. For these reasons, the rylene family with its reputation for photostability and multiple candidates with suitable energetics for singlet fission is explored in this work.

Ultrafast time resolved optical spectroscopy methods are used to study two rylene candidates: peropyrene and diindenoperylene. The crystal structure of solid peropyrene consists of a herringbone arrangement of π-stacked molecular

pairs and diindenoperylene's crystal structure consists of edge-to-face herringbone arrangement. We find no evidence for rapid singlet fission in the peropyrene crystals, due to the large shift of the singlet state to lower energy where it no longer fulfills the energy condition for singlet fission. Additionally, no evidence for singlet fission is found in diindenoperylene for which singlet fission would be 2,000 cm^{-1} uphill. These results demonstrate how both energetics and crystal packing influence the ability of a molecule to function as a singlet fission material and offer tools for surveying in the future.

A high pressure absorption cell is also built and tested in this work. The cell manipulates Beer's Law and increases the transition dipole moment between a molecule's S_0 state and its T_1 state, offering the unique ability to directly measure a molecules lowest triplet state energy.

TABLE OF CONTENTS

List of Figures

CHAPTER 1

Introduction

1.1 Photovoltaics as an Alternative Energy Source Need Higher Efficiencies

As of 2012, the worldwide total energy consumption reached 17.5 TW annually.[1] The sun alone provides 89,300 TW of solar energy **PER** year, more than 5,000 times the current energy usage, impressively providing the planet's human energy requirements in under two hours.[2] The average solar flux reaching the Earth's surface, after taking into account factors such as atmospheric absorption and widely ranging climates, is 175 W/m^2.[2] The thermodynamic maximum power production of other alternative energy sources such as biomass (2 W/m^2) and wind (16 W/m^2) pale in comparison to solar energy's potential power production.[3,4] Current organic photovoltaics (OPV) efficiencies of 10-15% produce 20 – 30 W/m^2 with considerable room for improvement.[5] Converting to square miles, in order to power the United States alone (3.5 TW)[1], solar farms covering an area roughly the size of Kansas would suffice. In addition, residential installation of solar panels costs a total of about $4.50 W while the panels themselves are produced for as little as $0.50/W and are projected to cost as little as $0.37/W by 2017.[6,7] Essentially, the costs of solar energy to the average customer lies heavily, upwards of 85 – 90%, in factors other than the actual panels themselves, such as balance of system, labor, and actual land area used. Ideally, the near future alternative energy will consist of maximizing the usage of

renewable solar energy and minimizing the usage of fossil fuels. In addition, it is also desirable to increase PV usage and availability by making PV's more affordable to the average residential customer, commercial customer, and investor. Clearly, increasing the current efficiencies of PV's is of utmost importance.

1.2 Photovoltaic Efficiency Limitations

The Shockley-Queisser limit states that the maximum efficiency of any normal p-n single junction cell is about 33%.[8] This relatively low maximum efficiency is the consequence of poor solar spectrum utilization. The vast majority of the available solar spectrum is not utilized to produce energy efficiently. Solar photons that have energies higher than the band gap of a PV, or with
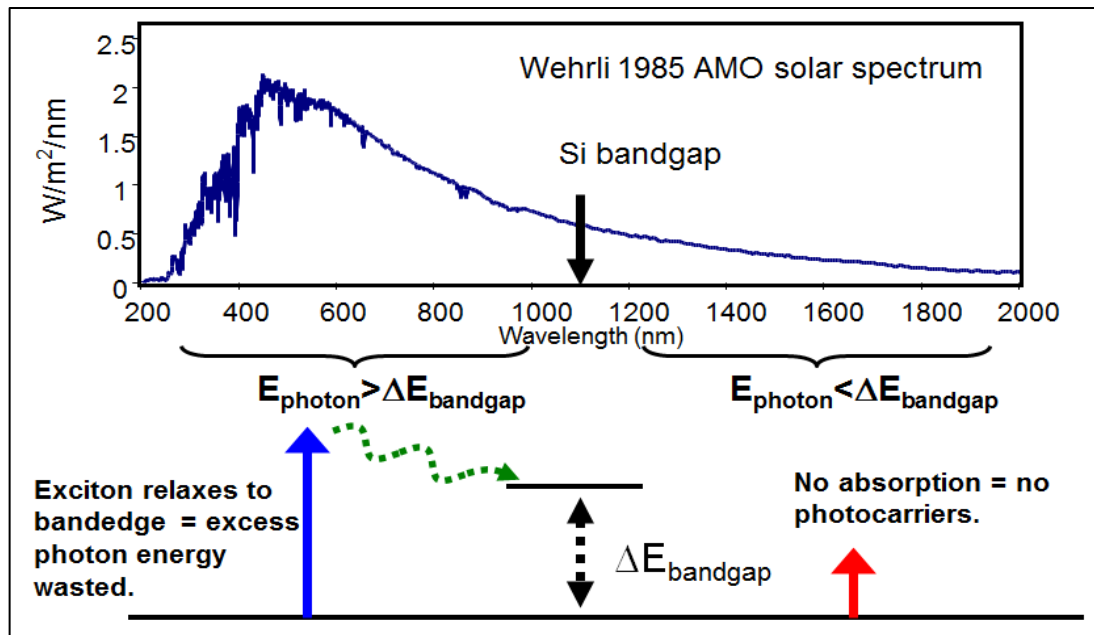
Figure 1.1 Top: Wehrli 1985 AMO solar spectrum showing intensity of solar photons that reach Earth. Bottom: diagram of photons with energy above and below the bandgap being absorbed. Photons with energy higher than the bandgap relax down to the bandedge and lose excess energy as heat.

2

wavelengths shorter than the band gap, will excite electrons that lose excess energy as heat as they relax down to the band edge (see Figure 1.1). Photons with energy below the band gap, or with wavelengths longer than the band gap, go un-absorbed and produce no excitations in the PV material at all. As a result of this single bandgap, Shockley and Queisser also calculated that the optimum PV bandgap for maximum efficiency should be between 1.0 and 1.5 eV. Silicon PV's dominate the present market and have a bandgap at 1.1 eV, or 1100 nm, which falls into the desired bandgap range. Strategies for surpassing the Shockley-Quisser limit utilize solar photons more efficiently, either by altering the way light is absorbed by creating tandem photovoltaic cells with multiple p-n junctions or by altering the efficiency of individually absorbed photons by taking advantage of multi-electron processes discussed in the following section.

1.3 Singlet Fission as a Downconversion Process to Increase Photovoltaic Efficiency

Multiple electron processes such as upconversion and downconversion serve as avenues to more efficiently utilize solar spectrum photons with energies that lie considerably above or below the silicon bandgap. For photons with longer wavelengths, upconversion would allow multiple low energy excited states to combine to produce one higher energy excited state that can access the silicon bandgap. Conversely, downconversion occurs when photons with energies much higher than the bandgap create a higher energy excited state that splits into multiple lower energy excited states, which would still be higher in energy than

3

1.1 eV. One possible method for improving the efficiency of a PV, and an example of downconversion already well established in small organic molecules, is singlet fission.[9] In singlet fission, a 4-electron process takes a high energy excited singlet state created by a high energy photon and fissions it into two lower energy triplet states (see Figure 1.2). These triplet states have longer lifetimes than a singlet state and can diffuse to the donor material in a PV, doubling the efficiency of high energy solar photons absorbed yielding electron hole pairs.
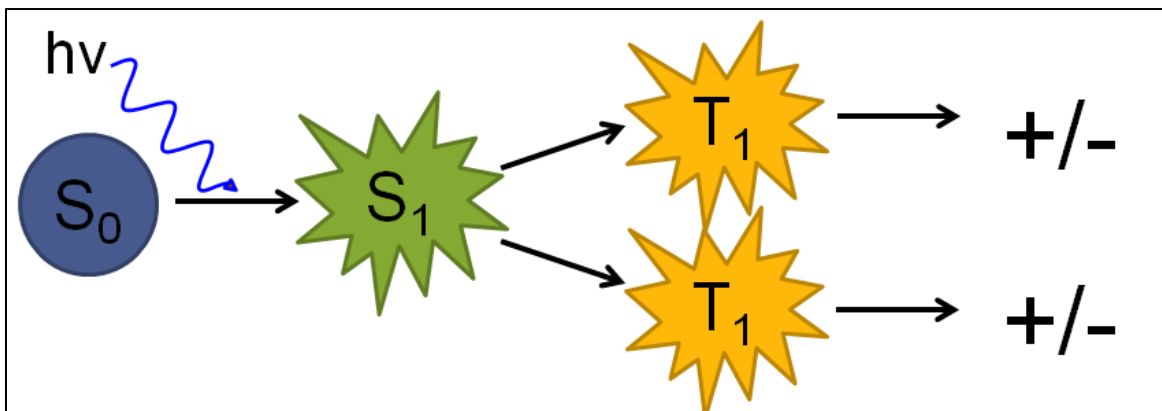
Figure 1.2 Singlet Fission illustration depicting excitation of a ground state (S0) upon absorption of a photon to an excited singlet state (S1) which then fissions into two separate triplet states (T1). Each of these triplet states could theoretically go on to form an electron hole pair in a photovoltaic cell.

1.4 Mechanism of and Requirements for Singlet Fission

Normal intersystem crossing involves a single singlet state going to a single triplet state, which requires a spin flip. However, when two triplets are created, superpositions of triplet pair spin states can have overall singlet character[10] making singlet fission a spin allowed and very fast process, on the

order of femtoseconds to picoseconds.[11] The mechanism for singlet fission involves a simultaneous forward and back electron transfer (see Figure 1.3), as suggested by experiments done in the Bardeen group here at UCR.[12,13] While the process is facilitated by the fact that spin is conserved, there are three requirements that an organic molecule must meet in order to undergo singlet fission. First, due to the singlet state fissioning into two triplets, the energy of the relaxed singlet must be approximately equal to twice the triplet energy, $E(S_1) \geq 2E(T_1)$ (see Figure 1.4). Secondly, in comparison with the radiative relaxation rate, other non-radiative processes must be slow in order to prevent competition for singlet fission. Last, in order to accommodate the resulting pair of triplets, there must be two excitation sites available.
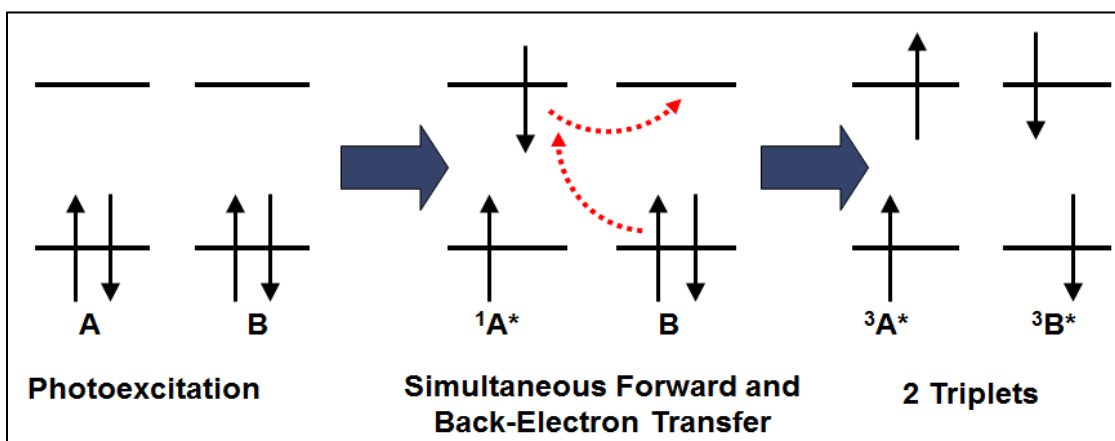
Figure 1.3 Schematic showing the mechanism of singlet fission and the movement of each of the 4 electrons involved in the process. A and B represent separate molecules, each originating in the ground state and resulting in a triplet state.
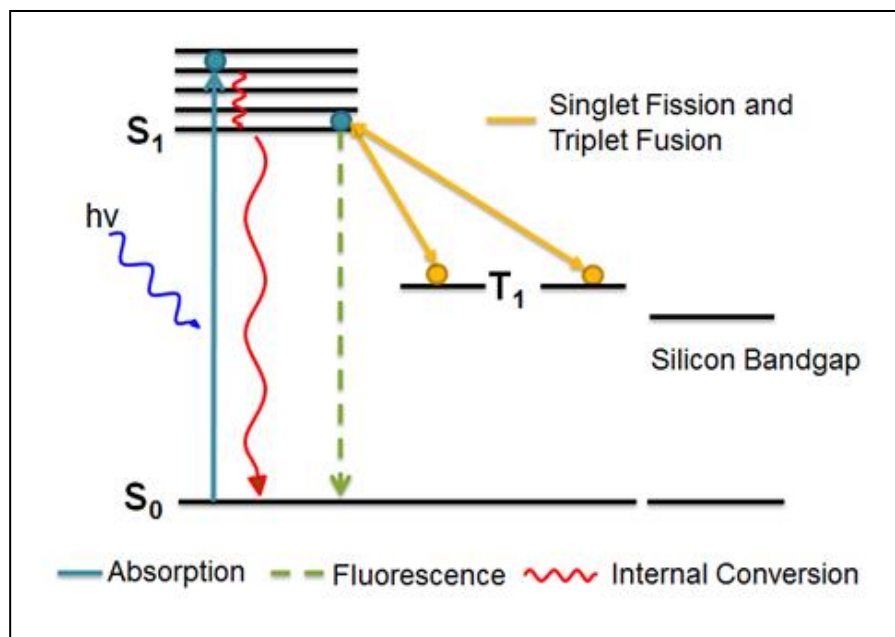
Figure 1.4 Jablonski diagram depicting excited state electronic transitions including singlet fission.

1.5 Controlling Singlet and Triplet Energy Levels

Clearly, to fulfill the first requirement for singlet fission, a molecule's triplet energy level must be lower than the singlet, which it is in virtually all molecules. This trend is indirectly due to the fact that electrons are fermions, which means that their overall wave function must be anti-symmetric. An electron's overall wave function is comprised of a spin portion and a spatial portion. A singlet state's spin wave function is anti-symmetric and so their spatial wave function must be symmetric. A symmetric spatial wave function means that the two electrons will have similar electron density maps and spend more time closer together, increasing the electron-electron repulsion interaction. On the other hand, a triplet state has a symmetric spin wave function and so the spatial wave function will be anti-symmetric, allowing each electron to spend more time away from the other,

6

resulting in a lowering of the energy level. Figure 1.5 shows the 1-D 2 electron charge density contour diagrams of symmetric and antisymmetric wave space wavefunctions.[13] Rather than being a 2-D map with x and y planes, this figure
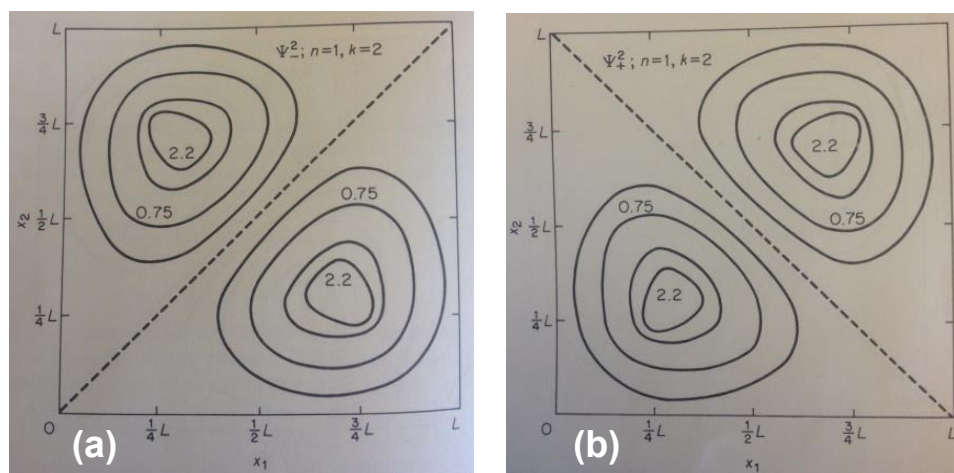
Figure 1.5 Contour diagram showing relative charge density of two electrons with (a) symmetric space wavefunction (triplet) and (b) antisymmetric space wavefunction (singlet) between the limits of the box, O and L. Images are taken from reference 14.

illustrates the most probable locations of each of the two electrons in the system based on one another's position. Each axis corresponds to a 1-D box length assigned to either electron, x_1 and x_2. The energy to exchange two electrons occupying the same state, whether it is the singlet or triplet, is responsible for triplet levels being lower in energy than the first excited singlet. Despite being lower in energy, the triplet level is usually not half the energy of the singlet level, as is necessary to undergo singlet fission. However, some classes of molecules do exist that have suitable energetics for singlet fission including the polyacenes, the carotenoids, designed molecules such as isobenzofuran, and even some members of the rylene family.[9] All of these are discussed in more detail in Section 1.6.

For classes of molecules that do not have $E(S_1) \geq 2E(T_1)$, the ability to control either the singlet or triplet energy merits some discussion as the energy levels of some states in molecules can be controlled to a certain extent. Different environments affect energy levels by changing the molecular environment. The general trend is a red-shift going from gas-phase to liquid and then from liquid to solid state. Solvent molecules can orient themselves around a chromophore and if a molecule has a permanent dipole, this reorientation usually stabilizes the molecules energy levels. If an electronic transition results in a change in dipole, the energy difference between the ground state and the excited state can change from solvent to solvent, depending on the solvent polarity. The larger the transition dipole moment, the larger the solvent effect. Allowed transitions have much larger transition dipole moments than transitions that are not allowed, for example, a spin-forbidden transition. Since the transition from a ground singlet to an excited singlet preserves spin, it is allowed, whereas the transition from a ground singlet to a triplet involves a spin flip and is spin-forbidden. Interaction of a solute with its environment results in a decrease of the excitation energy of a transition by the following equation: $h(v-v_0) = a^{-3}[n^2-1)/(n^2+2)][E/(E'+E)]$, where a is an effective solute cavity radius, n is the refractive index of the solvent, E and E' are mean excitation energies of the solvent and solute.[15] It can be seen that energy levels of states with a transition dipole moment are expected to change under changing refractive index, including phase change. However, those with negligible or zero transition dipole moment will not be affected. This is why the

energy of the excited singlet changes when a molecule goes from solution to a solid, but the triplet level remains relatively unchanged. Due to the unlikeliness of optimizing a molecule's energetics for singlet fission through controlling the singlet energy alone, it is more efficient instead to focus on the previously mentioned molecular classes whose energetics are already known to satisfy $E(S_1) \geq 2E(T_1)$.

1.6 Molecular Classes of Singlet Fission Molecules in the Literature

Singlet fission was first observed in the late 1960's in crystalline anthracene by Singh, et al.[16] Recently, the practical application of using singlet fission in photovoltaics was suggested causing a resurgence of interest in the phenomenon.[17] Since then it has become a very hot topic and a couple different classes of molecules have been discovered to exhibit singlet fission. The first class is the polyacenes and Figure1.6 below shows the general structure as well as the structures of known singlet fission polyacenes studied recently.[9] Singlet fission was first observed in tetracene in 1968 by Swenberg, et al.[18] and has since been studied by the Bardeen group at UCR,[12-13,19-20] the Zhu group from University of Texas,[21] Marc Baldo's group at MIT,[22] Damrauer at University of Colorado, Boulder,[23] Gao at Shandong University,[24] and others.[25-29]
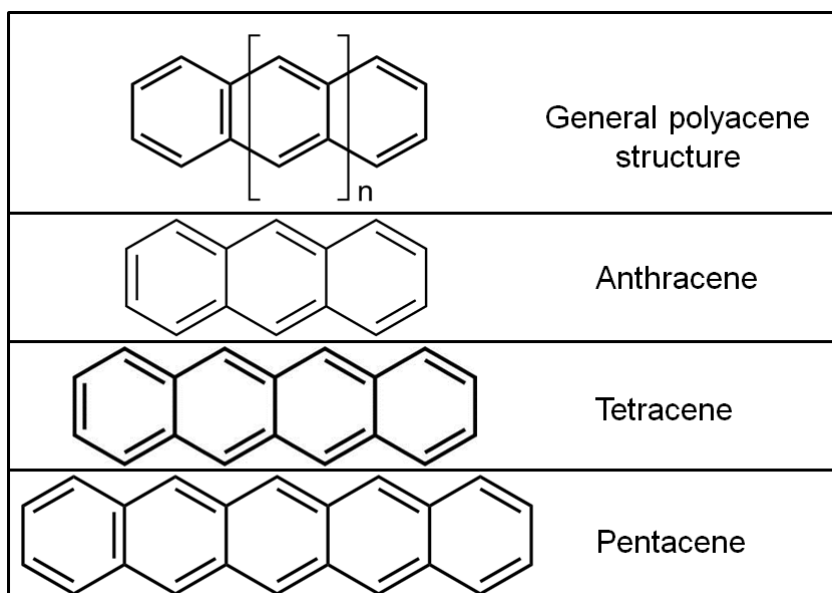
Figure 1.6 General structure of polyacenes and specific structures of anthracene, tetracene, and pentacene.

The Bardeen group's studies of tetracene have included elucidating the singlet fission mechanism, observation of quantum beats, and determining a triplet quantum yield of 200%.[12-13,17-18] Zhu's group studies pentacene/fullerene bilayers, using pentacene (**PEN**) to generate multiple excitons from the absorption of a single photon.[21] They report directly observing the multiple exciton state and suggest that it is in a coherent superposition with the singlet state. In addition, multiple electron transfer to the fullerene occurs on an order of magnitude faster (sub picosecond) timescale than transfer from a triplet state would occur. Baldo's work[22] focuses on using a longer wavelength absorber in conjunction with a singlet fission material by using copper phthalocyanine to absorb photons between the singlet and triplet energy gap of tetracene. The third polyacene, **PEN**, has been studied by many groups,[29-34] and probably most

notably by Richard Friend at University of Cambridge[35-36] and Michael Wasielewski from Northwestern University.[37] Friend's group studies polycrystalline thin films of **PEN** and pentacene/C_{60} bilayers, showing charge separation on a longer timescale of 2-10 ns, consistent with longer lived diffusing triplet excitons. Wasielewski and his group also study bilayers using 6,13-bis(triisopropylsilylethynyl)pentacene (TIPS-Pn, Figure 1.7) as their fissioning material and perylene derivatives as the acceptor material. They also discuss the importance of triplets formed from intersystem crossing from charge transfer states in addition to triplets formed from singlet fission, further increasing the triplet yield.

The second class of singlet fission molecules are isobenzofurans[9], studied by Josef Michl from University of Boulder.[38] They are the first to report a 200% yield from a molecule designed specifically for singlet fission, 1-3-diphenylisobenzofuran (Figure 1.8). A third class of singlet fission molecules are the carotenoids. Michael Tauber and his group at UCSD[39] study Zeaxanthin
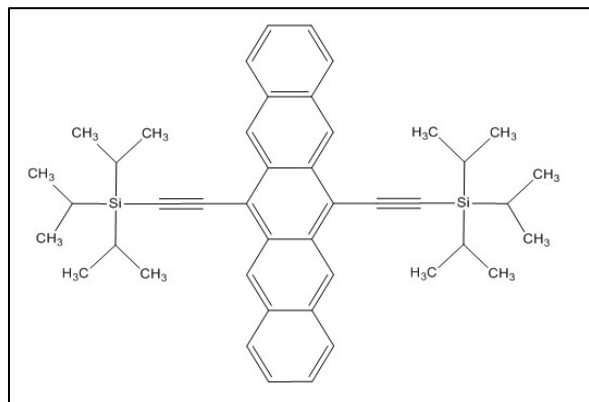
Figure 1.7 Structure of TIPS-Pn
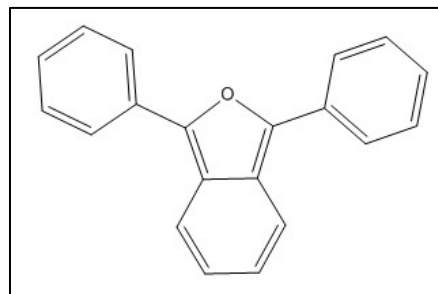
Figure 1.8 Molecular structure of 1-3-diphenylisobenzofuran.

aggregates (Figure 1.9) as their fissioning material. They report triplet quantum yields of 90%-200%, with the lower end of the yield being the consequence of triplet-triplet annihilation.
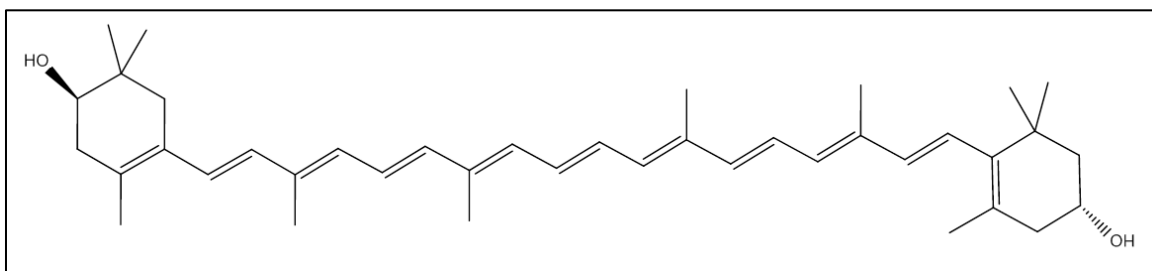
Figure 1. 9 Molecular structure of Zeaxanthin.

Lastly, a fourth possible category is the rylene family which comprises a class of polyaromatic hydrocarbon molecules that crystallize easily, have high stability, and support long exciton and charge carrier diffusion lengths. Current interest in this class of molecules has already been established by Michael Wasielewski from Northwestern University, who has studied tert-butyl-substituted
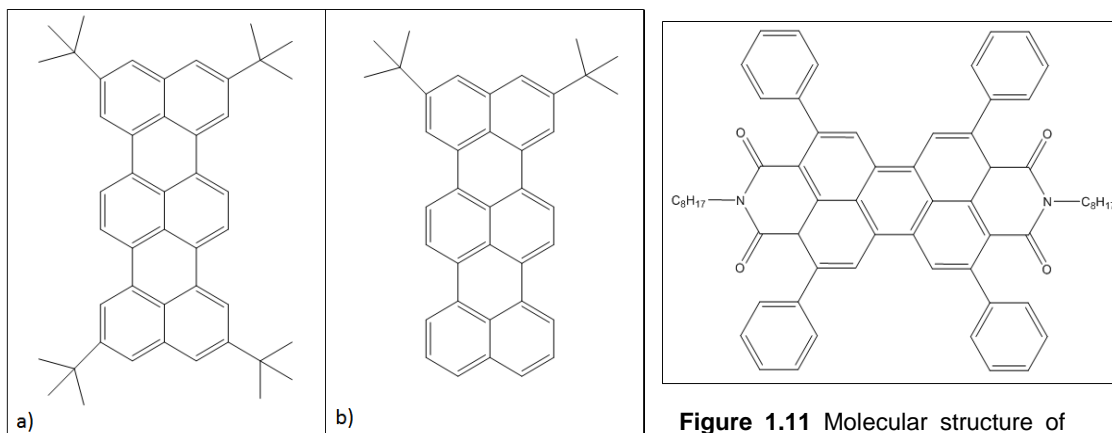
Figure 1.10 Molecular structure of 2,5,10,13-tetra-(tert-butyl)terrylene (a) and 2,5-di(tert-butyl)terrylene (b).

Figure 1.11 Molecular structure of perylenediimide.

12

terrylenes[40] (Figure 1.10) and perylenediimide[41] (Figure 1.11). Two other rylene family members, peropyrene (**PP**, Figure 1.Za) and diindenoperylene (**DIP**, Figure 1.12), are presented in this work (Chapter 3 and 4). **PP**, a derivative of perylene (**PER**), is of interest for multiple reasons (covered in detail in section 1.8 of this chapter), including a high triplet energy level and photostability.
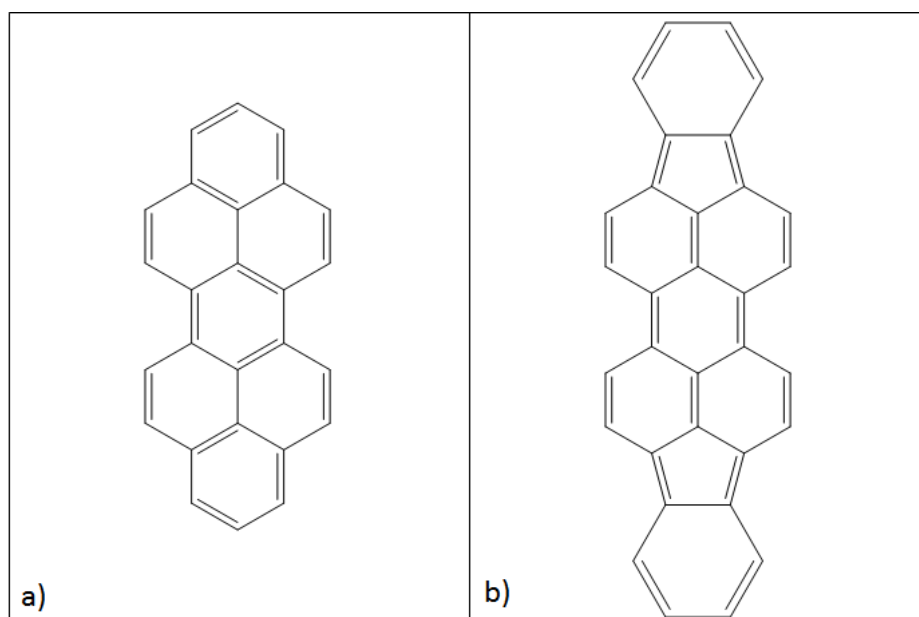
Figure 1.12 Molecular Structure of Peropyrene (a) and Diindenoperylene (b).

1.7 Experimental Methods for Singlet Fission Detection

When choosing to study a molecule, there are different methods available for detecting singlet fission. Currently, the prominent methods include transient absorption and time-resolved fluorescence while less common methods include Raman resonance spectroscopy and external quantum efficiency measurements. Tauber utilizes time resolved Raman resonance spectroscopy for the advantage of directly measuring triplet state signal rather than indirect triplet monitoring by

measuring other state's signal.[39] Baldo creates devices and measures the external quantum efficiency which is the ratio of charge carriers produced by the device to photons put into the device.[22] An advantage of transient absorption is the ability to watch populations change in real time and the ability to compare lifetimes of these population changes. A second very useful advantage of transient absorption is the ability to directly monitor triplet populations in samples with little to no fluorescence, but which might still exhibit singlet fission. However, the major disadvantage is the overlapping of spectra. It can be difficult to identify or extract the triplet absorption and different types of absorptions can have different excitation densities. On the other hand, using time-resolved fluorescence experiments as a tool to detect singlet fission can show specifically the singlet population change with high temporal resolution. Since the two resulting triplets created from singlet fission can diffuse away and eventually recombine with other triplets also formed from singlet fission in the crystal to reform the initial excited singlet state, late time fluorescence can also give information about triplet population dynamics. A Jablonski diagram (Figure 1.4) can be used to visualize the different rates of excited singlet and triplet population changes and shows how many of these kinetics can be monitored using fluorescence. The spectra of the emitting singlet state can also be elucidated. However, a major disadvantage of this method is that it is difficult to tell whether the depopulation and repopulation of the singlet state involves transfer to and from triplet states or some other dark state. However, imposing a

high (800+ Gauss) external magnetic field on a sample can give information indicating whether or not triplet states are interacting with the population and depopulation of a singlet state (described in detail in Chapter 3). A second disadvantage of time resolved fluorescence experiments is the inability to study molecules or samples with little to no fluorescence, such as **PEN** whose created excited singlet states fission into triplets before they can fluoresce.[35]

Pairing time resolved fluorescence with transient absorption can prove to be a very powerful tool when searching for singlet fission as the time resolved fluorescence gives both spectral and temporal components that are expected to be seen in the transient absorption experiments. This means that, by also taking into account absorption spectra, triplet state information can be easier to extract from complicated experimental data. This powerful pair of experimental methods provides the bulk of the data presented in this work.

1.8 Identifying a New Singlet Fission Candidate

The goal of this work has been to identify a new highly photostable source of high energy triplets from singlet fission for use in photovoltaic applications. A high energy triplet would facilitate more efficient energy transfer at a charge separation medium's band edge. The first step taken was to investigate and identify new molecule classes, specifically the rylene family, and studying promising candidate molecules within that family. While the acenes have been studied extensively, rylenes have only recently attracted attention as photovoltaic candidate singlet fission materials.[40-41] When considering a new candidate for

singlet fission with the future goal of use in a PV, there are three distinct improvements over current candidates to be considered: (1) increased photostability given the nature of PV's and their constant exposure to sunlight, (2) increased triplet energy level so as to facilitate energy transfer at the silicon bandgap and (3) high singlet fission efficiencies, preferably with a triplet yield near 200%. In addition to all three of these improvements, a candidate would also have to satisfy the three previously mentioned requirements for singlet fission to occur in the first place. **PP**, with **PER** as its parent molecule, is expected to retain the photostability of the rylene family and the reported energy levels for **PP** are 22,500 cm^{-1} for the relaxed singlet, and 11,000 cm^{-1} for the triplet.[42] Compared with a triplet level of 9,700 cm^{-1} for tetracene (see Figure 1.13)[19-29], **PP** has an advantage from a higher triplet energy because it can transfer energy to the donor band gap in a device more efficiently. Crystalline **PP** has one confirmed and one proposed crystal packing structure: **α-PP** (face-to-face paired herringbone motif, confirmed in this work) and **β-PP** (edge-to-face herringbone motif, proposed), similarly to **PER** which has both α and β crystal packing motifs confirmed.[43] Both of these crystal packing motifs would fulfill the need for two excitation sites for singlet fission. The literature has reported fluorescence quantum yields of 0.87 and 0.93 for **PP** in acetonitrile and toluene[42] and was confirmed in this work to have a nearly constant fluorescence quantum yield value of 0.90 in eight different solvents tested (see Chapter 3). Having quantum yields near unity are a good indication that the radiative rate of

relaxation is dominant and thus the rate of singlet fission would not have great competition from other non-radiative forms of relaxation. Based on this information, **PP** is a very promising candidate for singlet fission.

Tetracene Perylene Peropyrene

S_1 —— 19,350 cm^{-1} S_1 —— 22,500 cm^{-1} S_1 —— 22,500 cm^{-1}

T_1 —— 9,700 cm^{-1} T_1 —— 12,500 cm^{-1} T_1 —— 11,000 cm^{-1}

S_0 —— S_0 —— S_0 ——
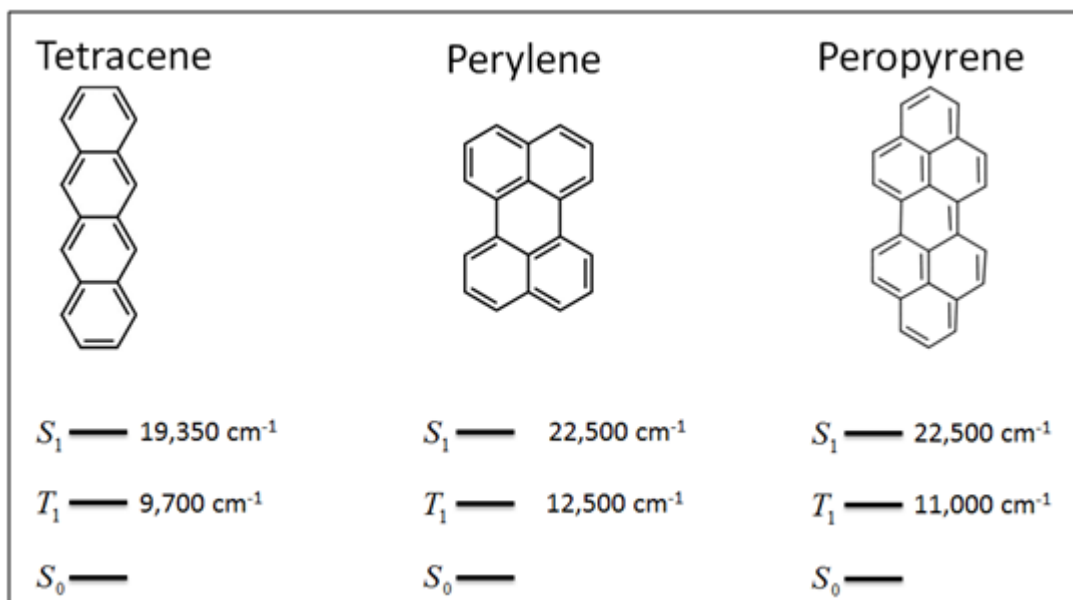
Figure 1.13 Structures and energy levels for tetracene, perylene, and peropyrene.

The crystal packing structure of **α-PP** ended up being the demise of **PP** for use as a singlet fission material, as the face-to-face pairwise packing lead to excimer formation and singlet energy stabilization (discussed in more detail in Chapter 3). However, an important lesson about just how the crystal packing structure of a molecule can affect its ability to function as a singlet fission material was shown, adding yet another "tool to the toolbox" used when surveying molecules for singlet fission candidates.
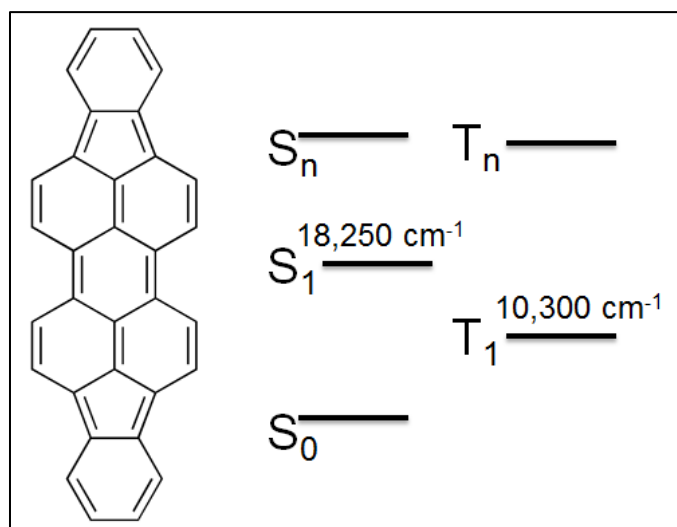
Figure 1.14 Molecular structure and energy levels of diindenoperylene.

The second rylene family member studied in this work, **DIP,** whose structure is shown in Figure 1.14, is an extended rylene that has become a prevalent component in OPV's due to its high degree of order and excellent charge transport properties.[44-47] Additionally, **DIP** has the unique ability to form crystalline mixtures with other conjugated molecules of similar size and crystal packing motif, such as pentacene (**PEN**), allowing for the production of well-defined and highly ordered composite materials.[48-52] However, even though it has been extensively studied in solid-state thin films, far less research has been done and relatively little is known on its basic photophysics. In fact, **DIP** itself is another decent candidate for singlet fission since it avoids the face-to-face pairwise crystal packing motif of **α-PP**. However, DIP has an energy difference of nearly 2,000 cm^{-1} between its $2E(T_1)$ and $E(S_1)$.[53] Tetracene is a model singlet fission molecule with despite having a singlet energy level 500 cm^{-1} lower than

$2E(T_1)$.[12] Possible explanations for singlet fission being able to overcome an energy barrier where the singlet energy is not technically sufficiently high enough to accommodate two triplet energies include available room temperature energy and even entropic gains from going from one excited state to two. The steady-state and solution photophysics of **DIP** are presented and discussed in Chapter 4 of this work. While **DIP** was not capable of functioning as a singlet fission material, it did provide an upper limit to the energetic uphill capability of singlet fission and also showcased the importance of a molecule's energetics in relation to its ability to function as a singlet fission material.

Finally, recalling the molecular energy requirement for singlet fission, it is clear that knowing the exact triplet energy of a molecule is necessary and valuable information. Separate from our work on SF in the rylenes, we also developed a new high pressure absorption cell to measure S_0-T_1 energies.[55] It is a set-up using a new cylindrical long pathlength cell (~10 cm) capable of withstanding up to 3,000 psi of oxygen to induce and increase the $S_0 - T_1$ absorption. This has provided the unique ability to directly measure the triplet state energy and is much more time-effective and efficient than the sensitization experiments currently used to determine triplet energy levels.[42] The major benefit of this development is the ability to scan singlet fission candidates more quickly to check for proper energetics. Another benefit of this system would be the ability to aid in studies on the effects of substitution on singlet and triplet energy levels, determining if and to what extent fine-tuning of a molecule's energy levels is

possible through substitution. This would be of great interest in the case of singlet fission candidate molecules which satisfy all but the energetic requirements of singlet fission. Chapter 6 discusses this apparatus and preliminary studies in more detail. Finally, Chapter 7 summarizes this work and offers directions for future work within the rylene family and with the high pressure absorption cell.

References

1. http://www.eia.gov/cfapps/ipdbproject/IEDIndex3.cfm?tid=44&pid=44&aid=2, *accessed 04/29/2015*

2. http://www.sandia.gov/~jytsao/Solar%20FAQs.pdf, *accessed 04/29/2015*

3. http://wind.nrel.gov/public/Robi/Wind%20101%20GovEnergy/GOVENERGY_2010_CD/GOVENERGY_2010_Presentations/12%20Wind%20101%20Rooftop%20Wind%20-%20Robichaud.pdf, *accessed 04/29/2015*

4. http://www.vaclavsmil.com/wp-content/uploads/docs/smil-article-power-density-primer.pdf, *accessed 04/29/2015*

5. Scharber, M.C.; Saricifti, N.S., Efficiency of Bulk-Heterojunction Organic Solar Cells, *Progress in Polymer Science*, **2013**, *38*, 1929.

6. http://www.nrel.gov/docs/fy12osti/53938.pdf, *accessed 03/10/2015*

7. http://www.greentechmedia.com/articles/read/solar-cost-reduction-drivers-in-2017, *accessed 03/10/2015*

8. Shockley, W.; Queisser, H., Detailed Balance Limit of Efficiency of p-n Junction Solar Cells, *J. Appl. Phys.* **1961**, *32,* 510.

9. Smith, M.B.; Michl, J., Singlet Fission *Chem. Rev.* **2010**, *110,* 6891.

10. Piland, G.B.; Burdett, J.J.; Kurunthu, D.; Bardeen, C.J., Magnetic Field Effects on Singlet Fission and Fluorescence Decay Dynamics in Amorphous Rubrene, *J. Phys. Chem. C.* **2013**, *117*, 1224.

11. Piland, G.B.; Burdett, J.J.; Dillon, R.J.; Bardeen, C.J., Singlet Fission: From Coherences to Kinetics, *J. Phys. Chem. Lett.* **2014**, *5,* 2312.

12. Burdett, J.J.; Bardeen, C.J., Quantum Beats in Crystalline Tetracene Delayed Fluorescence Due to Triplet Pair Coherences Produced by Direct Singlet Fission, *J. Am. Chem. Soc.* **2012**, *116*, 5145.

13. Burdett, J.J.; Bardeen, C.J., The dynamics of Singlet Fission in Crystalline Tetracene and Covalent Analogs, *Acc. Chem. Res.*, **2013**, *46*, 1312-1320.

14. McGlynn. *Molecular Spectroscopy of the Triplet State*.; Prentice Hall, Inc.: Englewood Cliffs, N.J., 1969; pp 69-70.

15. E.C. Lim. *Excited States*. Vol. 6.; Academic Press: New York, 1982; pp 67.

16. Singh, S.; Jones, W.J.; Siebrand, W.; Stoicheff, B.P.; Schneider, W.G., Laser Generation of Excitons and Fluorescence in Anthracene Crystals, *J. Chem. Phys.* **1965**, *42*, 330.

17. Hanna, M.C.; Nozik, A.J., Solar Conversion Efficiency of Photovoltaic and Photoelectrolysis Cells with Carrier Multiplication Absorbers. J. App. Phys. 2006, 100, 074510-1-7.

18. Swenberg, C.E.; Stacy, W.T., Biomolecular Radiationless Transitions in Crystalline Tetracene, *Chem. Phys. Lett* **1968**, *2*, 327.

19. Burdett, J.J.; Gosztola, D.; Bardeen, C.J., The Dependence of Singlet Exciton Relaxation on Excitation Density and Temperature in Polycrystalline TetraceneThin Films: Kinetic Evidence for a Dark Intermediate State and Implication for Singlet Fission, *J. Chem. Phys.* **2011**, *135*, 8597.

20. Burdett, J.J.; Muller, A.M.; Gosztola, D.; Bardeen, C.J., Excited State Dynamics in Solid and Monomeric Tetracene: The Roles of Superradiance and Exciton Fission, *J. Chem. Phys.* **2010**, *133*, 144506/1.

21. Chan, W.; Zhu, X.Y.; et al., Observing the Multi-Exciton State in Singlet Fission and Ensuing Ultrafast Multi-Electron Transfer, *Science*. **2011**, *334*, 1541.

22. Jadhav, P.J.; Mohanty, A.; Sussman, J.; Lee, J.; Baldo, M.A., Singlet Exciton Fission in Nanostructured Organic Solar Cells, *Nano Lett.* **2011**, *11*, 1495.

23. Alguire, E.C.; Subotnik, J. E.; Damrauer, N.H., Exploring Non-Condon Effects in a Covalent Tetracene Dimer: How Important Are Vibrations I Determining the Electronic Coupling for Singlet Fission? J. Phys. Chem. A. 2015, 119, 299-311.

24. Shen, L.; Chen, Y.; Gao, J., Effects of Substituents on Tetracene Derivatives on Their Stabilities and Singlet Fission. Journal of Molecular Graphics and Modelling. 2014, 51, 86-96.

25. Wilson, M.W.B.; Rao, A.; Johnson, K.; Gelinas, S.; Pietro, R.; Clark, J.; Friend, R.H., Temperature-Independent Singlet Exciton Fission in Tetracene. *J. Am. Chem. Soc.*, **2013**, *135*, 16680-16688.

26. Qiao, X.; Luan, L.; Yuchu, L.; Zhigang, Y.; Hu, B., Inter-Triplet Spin-Spin Interaction Effects on Inter-conversion Between Different Spin States in Intermediate Triplet-Triplet Pairs Towards Singlet Fission. *Organic Electronics,* **2014,** *15,* 2168-2172.

27. Arago, J.; Troisi, A., Dynamics of the Excitonic Coupling in Organic Crystals. *Phys. Rev. Lett.,* **2015,** *114,* 026402-1-5.

28. Birech, Z.; Schwoerer, M.; Schmeiler, T.; Pflaum, J.; Schwoerer, H., Ultrafast Dynamics of Excitons in Tetracene Single Crystals. J*. Chem. Phys.*, **2014**, *140*, 114501-1-9.

29. Zimmerman, P.M.; Bell, F.; Casanova, D.; Head-Gordon, M., Mechanism for Singlet Fission in Pentacene and Tetracene: From Single Exciton to Two Triplets. *J. Am. Chem. Soc.*, **2011**, *133*, 19944-19952.

30. Zeng, T.; Hoffmann, T.; Ananth, N., The Low-Lying Electronic States of Pentacene and Their Roles in Singlet Fission. *J. Am. Chem. Soc.,* **2014,** *136*, 5755-5764.

31. Wong, C.Y.; Penwell, S.B.; Cotts, B.L.; Rodrigo, N.; Wu, H.; Ginsberg, N.S., Revealing Exciton Dynamics in a Small-Molecule Organic Semiconducting Film with Subdomain Transient Absorption Microscopy., *J. Phys. Chem. C.,* **2013,** *117,* 22111-22122.

32. Minami, T.; Nakano, M., Diradical Character View of Singlet Fission., *J. Phys. Chem. Lett.,* **2012**, *3,* 145-150.

33. Chan, W.; Ligges, M.; Jailaubekov, A.; Kaake, L.; Miaja-Avila, L.; Zhu, X.-Y., Observing the Multiexciton state in Singlet Fission and Ensuring Multielectron Transfer. *Science,* **2011,** *344*, 1541-1545.

34. Zimmerman, P.M.; Zhang, Z.; Musgrave, C.B., Singlet Fission in Petacene Through Multi-Exciton Quantum States. *Nature Chemistry,* **2010,** *2,* 648-652.

35. Wilson, M.W.B.; Friend, R.H.; et al., Ultrafast Dynamics of Exciton Fission in Polycrystalline Pentacene, *J. Am. Chem. Soc.*, **2011,** *133*, 11830-11833.

36. Rao, A.; Wilson, M.W.B.; Hodgkiss, J.M.; Albert-Seifried, S.; Bassler, H.; Friend, R.H., Exciton Fission and Charge Generation via Triplet Excitons in Pentacene/C60 Bilayers *J. Am. Chem. Soc.* **2010**, *132*, 12698.

37. Ramanan. C.; Smeigh, A.L.; Anthony, J.E.; Marks, T.J.; Wasielewski, M.R., Competition between Singlet Fission and Charge Separation in Solution-Processed Blend Films of 6,13-Bis(triisopropylsilylethynyl)pentacene with Sterically-Encumbered Perylene-3,4:9,10-bis(dicarboximide)s, *J. Am. Chem. Soc.* **2012**, *134*, 386.

38. Johnson, J.C.; Nozik, A.J.; Michl, J., High Triplet Yield from Singlet Fission in a Thin Film of 1,3-Diphenylisobenzofuran, *J. Am. Chem. Soc.* **2010**, *132*, 16302.

39. Wang, C.; Tauber, M.J., High-Yield Singlet Fission in a Zeaxanthin Aggregate Observed by Picosecond Resonance Raman Spectroscopy, *J. Am. Chem. Soc.* **2010**, *132*, 13988.

40. Eaton, S.W.; Miller, S.A.; Margulies, E.A.; Shoer, L.E.; Schaller, R.D.; Wasielewski, M.R., Singlet exciton Fission in Thin Films of tert-Butyl-Substituted Terrylenes. *J. Phys. Chem. A.,* **2015**, *119*, 4151-4161.

41. Eaton, S.W.; Wasielewski, M.R.; et al., Singlet Exciton Fission in Polycrystalline Thin Films of a Slip-Staked Perylenediimide., *J. Am. Chem. Soc.*, **2013**, *135*, 14701-14712.

42. Wenzel. U.; Löhmannsröben, H.-G., Photophysical and Fluorescence Quenching Properties of Peropyrene in Solution, *J. Photochem. Photobio. A.* **1996**, *96*, 13-18.

43. Yago, T.; Tamaki, Y.; Furube, A.; Katoh, R., Growth of β-Perylene Crystal, *Chem. Lett.* **2006**, *36,* 370.

44. Wagner, J.; Schreiber, F.; Brutting, W.; et al., High Fill Factor and Open Circuit Voltage in Organic Photovoltaic Cells with Diindenoperylene as Donor Material, *Advanced Functional Materials* **2010,** *20*, 4295.

45. Gruber, M.; Brutting, W.; et al., Thermodynamic Efficiency Limit of Molecular Donor-Acceptor Solar Cells and its Application to Diindenoperylene/C60-Based Planar Heterojunction Devices, *Advanced Energy Materials,* **2012,** *2*, 1100.

46. Gruber, M.; Brutting, W.; et al., Correlating Structure and Morphology to Device Performance of Molecular Organic Donor–Acceptor Photovoltaic Cells Based on Diindenoperylene (DIP) and C60, *Advanced Energy Materials,* **2013,** *3*, 1075.

47. Yu, S.; Brutting, W.; Koch, N.; et al., Performance Enhancement of Diindenoperylene-based Organic Photovoltaic Cells by Nanocolumn-arrays, *Organic Electronics,* **2014,** *15*, 2210.

48. Oteyza, D.G.; Barrena, E.; Dosch, H.; Ortega, J.E.; Wakayama, Y., Tunable Symmetry and Periodicity in Binary Supramolecular Nanostructures, *Phys. Chem. Chem. Phys.* **2011,** *13*, 4220.

49. Aufderheide, A.; Broch, K.; Novak, J.; Hinderhofer, A.; Nervo, R.; Gerlach, A.; Banerjee, R.; Schreiber, F., Mixing-Induced Anisotropic Correlations in Molecular Crystalline Systems, *Phys. Rev. Lett.* **2012,** *109*, 156102.

50. Hinderhofer, A. and Schreiber, F., Organic-Organic Heterostructures: Concepts and Applications, *ChemPhysChem,* **2012,** *13*, 628-643.

51. Broch, K.; Schreiber, F.; et al., Optical Properties of Blends: Influence of Mixing-Induced Disorder in Pentacene:Diindenoperylene versus Perfluoropentacene:Diindenoperylene, *J. Phys. Chem. C* **2013,** *117*, 13952.

52. Broch, K.; Gerlach, A.; Lorch, C.; Dieterle, J.; Novak, J.; Hinderhofer, A.; Schreiber, F., Structure Formation in Perfluoropentacene:diindenoperylene Blends and its Impact on Transient Effects in the Optical Properties Studied in Real-Time During Growth. *J. Chem. Phys.* **2013,** *139*, 174709.

53. Schael, F.; Lohmannsroben, H.G., Photophysical Properties of the Nonalternant Polycyclic Aromatic-Hydrocarbons Periflanthene and 1,16-Benzoperiflanthene in Solution, *Photochem. Photobio. A* **1992,** *69*, 27.

54. Evans, D., Perturbation of Sinlget-Triplet Transitions of Aromatic Molecules by Oxygen Under Pressure, *J. Chem. Soc.,* **1957,** 1351.

CHAPTER 2

Methods

2.1 Introduction

In this chapter, experimental details pertaining to research done in this work are described. The first section will cover sample preparation. Synthesis and crystallization of peropyrene (**PP**) and preparation of pentacene (**PEN**) and pentacene:diindenoperylene (**PEN:DIP**) thin films, done by collaborating groups, are described. The second section will cover all steady state absorption experiments. Standard steady state and fluorescence experiments were done as a first step towards characterization of the photophysics for each system studied. In light of **PP**'s interesting radiative lifetime dependence on solvent refractive index, discussed in detail in Chapter 3, fluorescence quantum yield measurements were made and a nonlinear two photon absorption experiment was built in order to detect any optically dark states. The temperature dependent experimental setup described in the steady state section also applies to time resolved temperature dependence studies. The next section will cover the three laser systems used in this work, followed by a section detailing all time resolved experiments performed using these laser systems. If a molecule exhibits delayed fluorescence, the presence of a strong external magnetic field will alter the kinetics of the prompt and delayed fluorescence by altering the number of triplet

pair states available to fission into. A magnetic field stage that can be used with either solution or solid state samples is used to test for magnetic field effects the on time resolved fluorescence. Femtosecond transient absorption experiments give the time resolution (~500 fs) needed to identify ultrafast processes and allow singlet and triplet populations to be studied in the **DIP** and **PEN:DIP** thin films. Lastly, details of **PP** energy level calculations, x-ray diffraction and a description of software and methods used for working up data conclude this chapter.

2.2 Sample Preparation

2.2.1 Peropyrene Synthesis and Crystallization – Youngblood Lab

This section was performed and written by the Youngblood Lab at the University of North Texas. **PP** was synthesized following a reported procedure.[1] $TiCl_4$ (160 μL, 1.44 mmol) was injected dropwise to a stirring suspension of $LiAlH_4$ (58 mg, 1.4 mmol) in dry THF (10 mL) at 0°C under argon. The mixture was allowed to warm slowly to room temperature and then was heated to reflux for 90 min. Phenalenone (0.20 g, 1.1 mmol) in THF (5 mL) was added to the mixture. Stirring and heating continued for three days, and additional THF was added as necessary. The reaction was then allowed to cool, and the remaining $LiAlH_4$ was quenched with isopropanol/hexanes (1:1) at 0°C. The emulsion was concentrated *in vacuo* and the solid was extracted with toluene. The product was purified by adsorption chromatography (SiO_2, hexanes, toluene 3:1) followed by size exclusion chromatography (Bio-Beads® SX-3, toluene) to give the

product as a yellow solid (11 mg, 5%). Recrystallization from hot *o*-xylene under argon gave yellow plates. The NMR data were consistent with previous reports.[1-2] ^{1}H NMR (500 MHz, C_6D_6) δ 7.92 (t, *J* = 7.6 Hz, 2H), 8.15 (d, *J* = 7.6 Hz, 4H), 8.16 (d, *J* = 9.2 Hz, 4H), 8.99 (d, *J* = 9.2 Hz, 4H); λ_{Abs} = 392, 415, 442 nm.

2.2.2 DIP and PEN:DIP Thin Films – Dr. Katharina Broch

This section was performed and written by Dr. Katharina Broch[1]: Pentacene was bought from Sigma Aldrich (purity 99.9%) and used as received. Diindenoperylene (**DIP**) was purchased from PAH Greifenwald and purified using gradient sublimation. Liquid solution samples of **DIP** were made by dissolving the solid in acetonitrile, toluene, chlorobenzene, and benzene at 10^{-5} - 10^{-6} M concentrations. All solvents were purchased from Sigma Aldrich (HPLC grade, >99.9%) and were used as received. Solid-state films of **DIP** with thicknesses of 100 nm were prepared using organic molecular beam deposition at a rate of 2 angstroms/min in ultra-high vacuum at a base pressure of 2×10^{-10} mbar simultaneously on two quartz glass substrates and on a Si(100) substrate with a native oxide layer of 2 nm thickness at a constant substrate temperature of 300K. The thickness of the samples was determined using a quartz crystal microbalance calibrated using X-ray reflectivity and confirmed by ellipsometry based on the optical constants of DIP published in the literature.[3]

2.2.3 Solution Samples

Perylene (**PER**) was purchased from Sigma Aldrich and used as received. All monomer samples were made by dissolving the solids in solutions of cyclohexane, acetonitrile, toluene, tetrahydrofuran, dichloromethane, dimethyl formamide, chlorobenzene, ethanol, and/or chloroform at 10^{-5}- 10^{-6} M concentrations. All solvents were purchased from Sigma Aldrich (HPLC grade, >99.9%) and were used as received.

2.3 Steady State Spectroscopy

2.3.1 Absorption Experiments

Absorption spectra of liquid samples were taken in a 1 cm quartz cuvette in a Cary 50 spectrometer. Scan resolution varied from 0.2 to 1.0 nm and integrations times varied from 100 – 600 nm/min, with longer integrations providing better signal to noise for samples with low concentrations. Solid state absorption spectra were taken using a Cary 500 spectrometer. In general, samples were measured under vacuum in a Janis ST100 cryostat which fit into the Cary 500 sample cavity. The cryostat was attached to metal baseplates which fit into the sample cavity, no further securing of the cryostat to the spectrometer was used. The sample was mounted in the cryostat using either earthquake putty (for non-temperature dependent studies) or with four screws and a metal faceplate. Thin indium flecks were placed between the sample

29

substrate and the cryostat sample finger in order to facilitate temperature equilibrium.

2.3.2 Two Photon Absorption Experiments

Two-photon excitation spectra of **PP** in solution were taken using a Mai Tai wide-band, mode-locked Ti:sapphire laser scanning in 10 nm increments from 710 to 920 nm. Samples were held in a 1 cm quartz cuvette and the laser pulse was focused onto the sample using a 10 cm focus lens. Fluorescence was collected at 90° and focused into a photomultiplier tube (see Figure 2.1) using a 3 cm focus lens. The fluorescence intensity was recorded using a lock-in amplifier. Multiple powers were tested to confirm that the fluorescence intensity was proportional to the square of the laser power, characteristic of a two-photon absorption process. Absorption values were corrected for varying excitation power dependent upon wavelength.
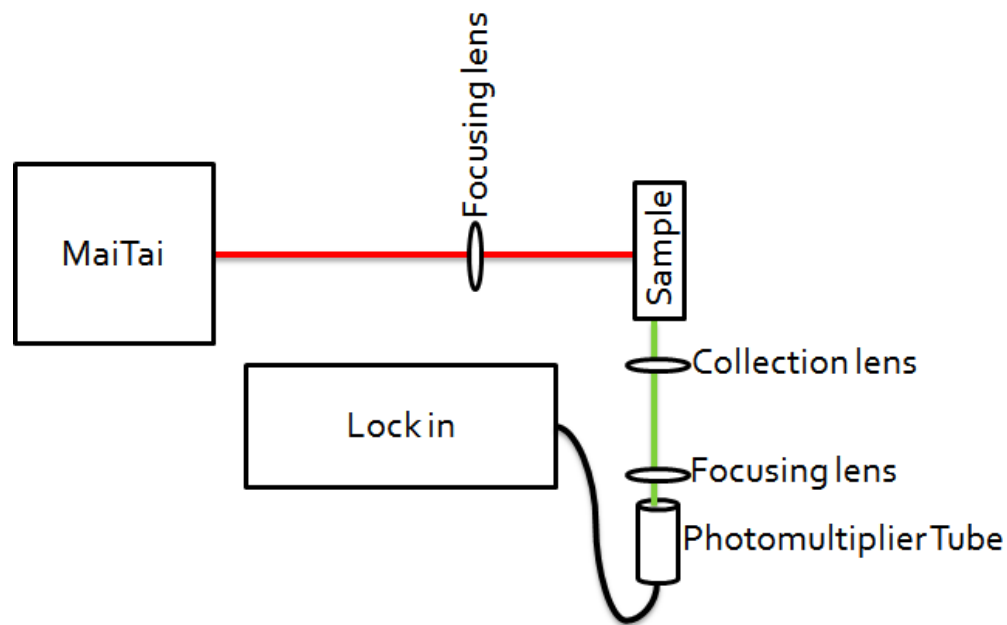
Figure 2.1 Two photon absorption experimental setup.

2.3.3 Fluorescence Experiments

Steady state fluorescence spectra were measured with a Fluorolog 3 spectrofluorimeter, typically using 400 nm excitation and front face detection (unless noted otherwise). Solution samples were held in a 1 cm quart cuvette and solid state samples were held under vacuum in a Janis ST100 cryostat. Sample mounting is described in Section 2.3.1, and cryostat was similarly attached to metal baseplates then placed into the Fluorolog sample cavity.

2.3.4 Fluorescence Quantum Yield Measurements

Fluorescence quantum yield measurements were performed using steady state absorption and fluorescence with the following equation[4]:

$$\phi_x = \phi_{ST}\left(\frac{grad_x}{grad_{ST}}\right)\left(\frac{n_x^2}{n_{ST}^2}\right)$$ Equation (2.1)

Where ϕ is the fluorescence quantum yield, $grad$ is the gradient, or the slope, from a plot of integrated fluorescence intensity versus absorbance, n is the refractive index of the solvent and subscripts x and ST signify the sample being tested and a standard sample with a previously determined fluorescence quantum yield. Liquid samples used had optical densities ranging from 0.02 to 0.1 to avoid self-absorption effects. The fluorescence data were taken using 385 nm excitation and **PER** in cyclohexane as the standard (quantum yield = 0.94[5]). To avoid quenching by O_2, samples were sealed in a 1 cm quartz cuvette with an overpressure of argon after being bubbled under argon for 15 minutes. This was achieved by using 10 mm screw cap UV-Quartz cuvettes with silicon/PTFE septa from Precision Cells (Item #: 41UV10). Two syringe needles were used to pierce the septa, one submerged in the liquid sample and connected to a very gentle flow of argon gas (gentle enough to barely produce a bubble stream, as solvent evaporation would change the overall concentration and affect the fluorescence quantum yield measurement), and the other needle tip above the solution, providing a gas escape from the cuvette (see Figure 2.2). After bubbling argon gas for 10-15 minutes, a balloon fixed to a plastic syringe barrel was filled with argon and attached to the gas escape needle head and the argon gas needle is removed. This ensures that there is a constant overpressure of argon in the

sample. The validity of this method was tested by using a solution of platinum octaethyl porphyrin whose fluorescence is quenched by oxygen. Upon removal of oxygen, the fluorescence is no long quenched and as oxygen diffuses through the septa and cap seal back into the cuvette, the fluorescence quenching returns. This method proved to be completely argon fast (zero fluorescence quenching return) for a minimum of 45 minutes, compared with only 10 – 15 minutes for a previously bubbled sample with no active overpressure.
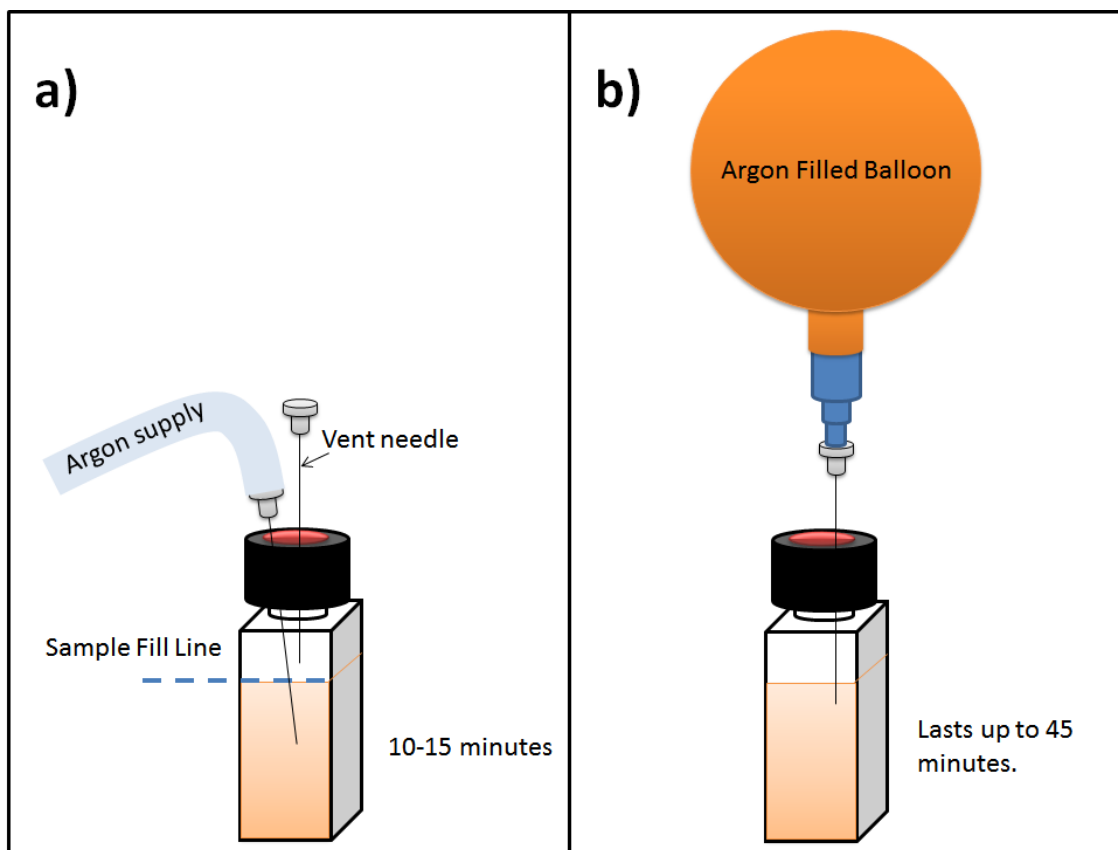
Figure 2.2 Solution degassing and experimental argon overpressure method. Panel a shows the needle placement during the actual degassing step and panel b shows the experimental setup with an argon filled balloon.

2.3.5 Temperature Dependence Experiments

Steady state temperature dependent fluorescence experiments were performed using the same setup described in **2.3.3**. A transfer line was used to transfer liquid nitrogen from a dewar to the cryostat holding the sample (see Figure 2.3) in the Fluorolog and a temperature sensor read off the internal cryostat temperature. Spectra were taken typically in 25 – 50 K increments from 77 K to 298 K. DIP thin film temperature dependent absorption experiments were performed using the same setup as described in section **2.3.1** with a temperature controller attached to the cryostat in order to heat the sample from 298 K to 500 K in increments of 50 K.
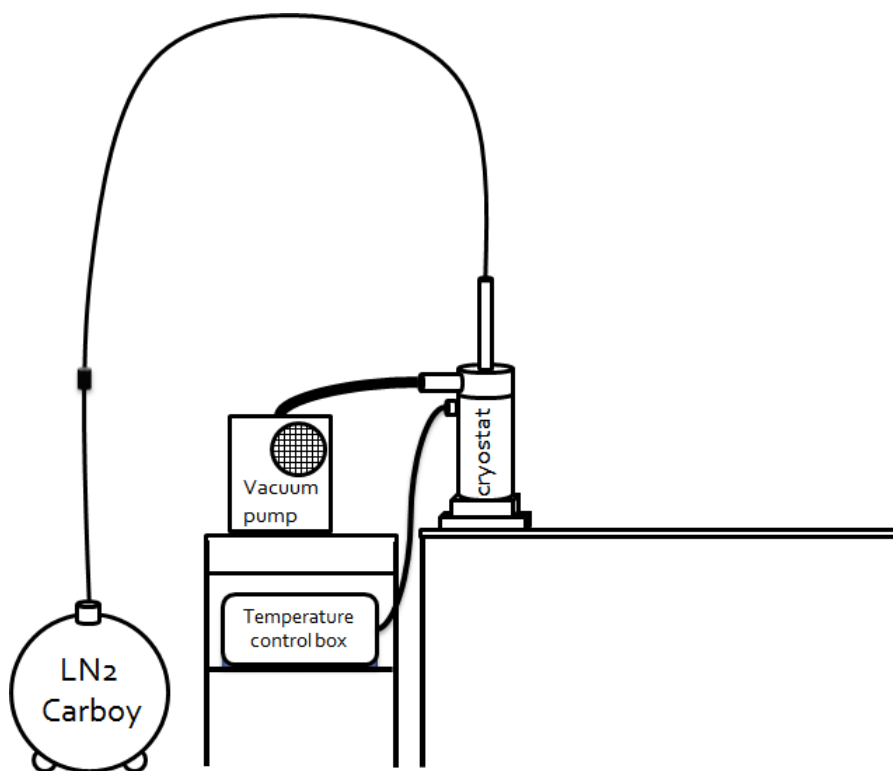
Figure 2.3 Temperature dependent experimental set. Cryostat would be integrated into relevant experimental setup (fluorolog, laser table top, Cary 500, etc.)

2.4 Laser Systems

2.4.1 40 KHz System

A Ti:sapphire regenerative amplifier (RGA) operating at 40 kHz provides the benefit of a high repetition rate, which allows for faster collection of data and lower fluences upon the sample. The RGA is seeded by a femtosecond Ti:sapphire oscillator (Kapteyn-Murnane Model TS laser kit, Figure 2.4), which is pumped by a diode-pumped Nd:VO4 laser (Millenia, Spectra Physics). With 3.30 W of pump power, the average output of the oscillator at 800 nm is ~245 mW at 91 MHz, which corresponds to ~2.5 nJ per pulse.

Figure 2.4 Optical layout for KML Ti:Sapphire oscillator, taken from operations manual.[6]

In order to generate powers high enough to induce nonlinear processes necessary for altering the excitation wavelength, the oscillator pulses are amplified with a Ti:sapphire amplifier system (Spitfire-50, Spectra Physics, Figure 2.5). The RGA is pumped by a frequency doubled Q-switched Nd:YLF laser (Merlin- 50, Spectra Physics), which outputs 532 nm with 5 W of power at 40 kHz

(~ 0.2 mJ per pulse). The output of the RGA is typically 200-250 mW, so that the pulses are approximately 5-6 µJ at 40 kHz. The output of the RGA is used in a non-linear process to frequency double in a beta barium borate (BBO) crystal to take the 800 nm output and turn it into 400 nm light. The 800 nm light is then filtered out with dielectric mirrors and color filters before the 400 nm light is used as an excitation source.
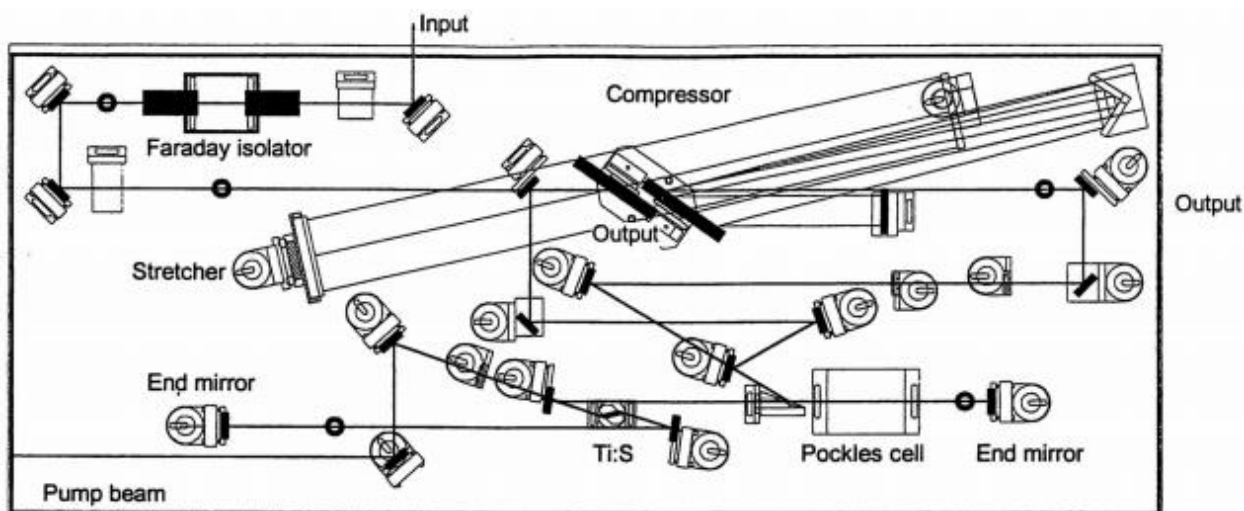
Figure 2.5 Optical layout for Spitfire-50, copied from operational manual.[7]

2.4.2 1 KHz System

A Ti:sapphire RGA operating at 1 kHz provides the pulses used for excitation in the transient absorption experiments and some time resolved fluorescence experiments. The benefits of this laser system are lower repetition rate, which allows for longer time windows in time resolved fluorescence and transient absorption experiments, and higher powers which allow for nonlinear processes that produce white light continuum. The Coherent RGA (Libra Femto HE 1K,

Coherent, Figure 2.6) has a closed box Ti:sapphire oscillator built in (Vitesse, Coherent). The oscillator is aligned by adjusting the peizo voltages, which is done automatically for maximum optimization, but can be done manually on the oscillator control box front panel in the event that a piezo goes bad. The modelocked output of the oscillator is 870-890 mW at an 80 MHz repetition rate, corresponding to 10-11 nJ per pulse. The Coherent RGA is pumped by a 1 kHz repetition rate diode-pumped, intracavity doubled, Q-switched Nd:YLF laser, which typically outputs 18 W of 527 nm light with a 1 kHz repetition rate and operating current of 21.0 A, corresponding to 18 mJ per pulse. The output of the RGA is 3.0-3.3 W at 1 kHz, corresponding to 3.0-3.3 mJ per pulse.

2.4.3 Mai Tai System

A Ti:sapphire oscillator (MaiTai – Spectra Physics) operating at 80 MHz provides the pulses used for excitation in the resolved fluorescence experiments. A benefit of this system is the controllable repetition rate, which is controlled by adjusting a ConOptics Model 305 Synchronous Countdown pulse picker coupled with a ConOptics Model 25 D, which controls the voltage bias for the pockel cell. Because of this unique laser modulation setup, the average power coming out of the pockel cell varies greatly with set repetition rate. For a repetition rate of 1 MHz, the 400 nm power (after the doubling crystal) is ~100 uW which corresponds to 0.1 nJ/pulse.
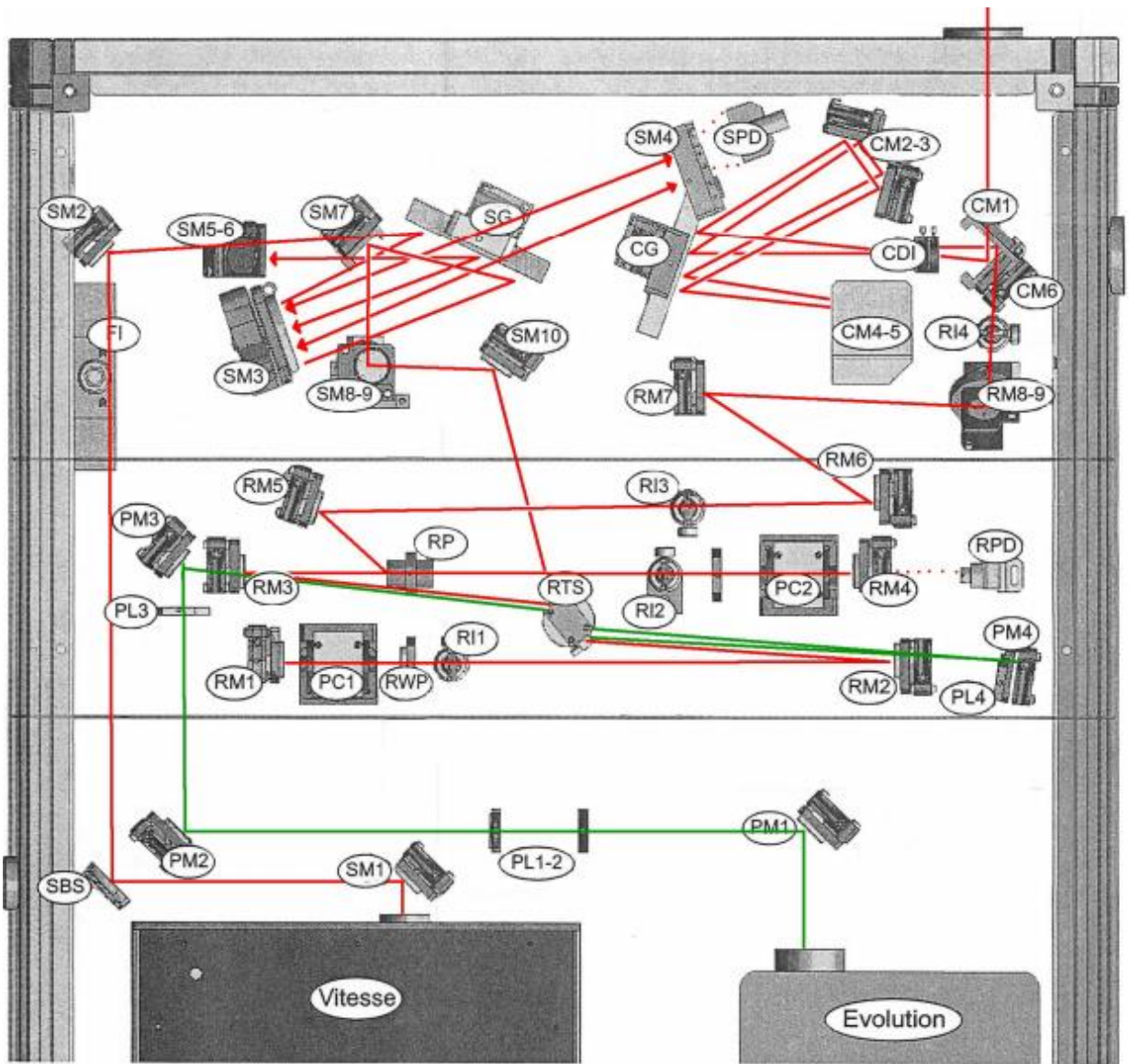
Figure 2.6 Optical layout of Coherent Libra RGA, copied from the operational manual with beam paths added by Dr. Jonathan Burdett, a previous member of the Bardeen Group at UCR.[8]

2.5. Time Resolved Spectroscopy

2.5.1 Time Resolved Fluorescence Using a Streak Camera

Fluorescence lifetime data were taken using front face detection with a Hamamatsu C4334 streakscope picosecond streak camera with a time resolution of 15 ps. The 400 nm excitation pulse was generated by frequency doubling the 800 nm pulse. A filter was used to remove remaining 800 nm in the beam before sample excitation. Scattered pump light was removed by placing a 450 nm long wave pass filter and 420 nm color filter on the input lens before the streak camera. For solution experiments, the fluorescence was detected at 54.7° (magic angle) relative to the pump polarization to eliminate rotational diffusion effects.[9] The pulse fluences were kept below 1.2 µJ/cm^2 for **PP** and 1.9 uJ/cm^2 for DIP and **PEN:DIP** samples. Measurements of the fluorescence decay at different laser intensities yielded similar decays, indicating that exciton-exciton annihilation did not influence the results. Figure 2.7 shows the optical layout for time resolved fluorescence experiments.
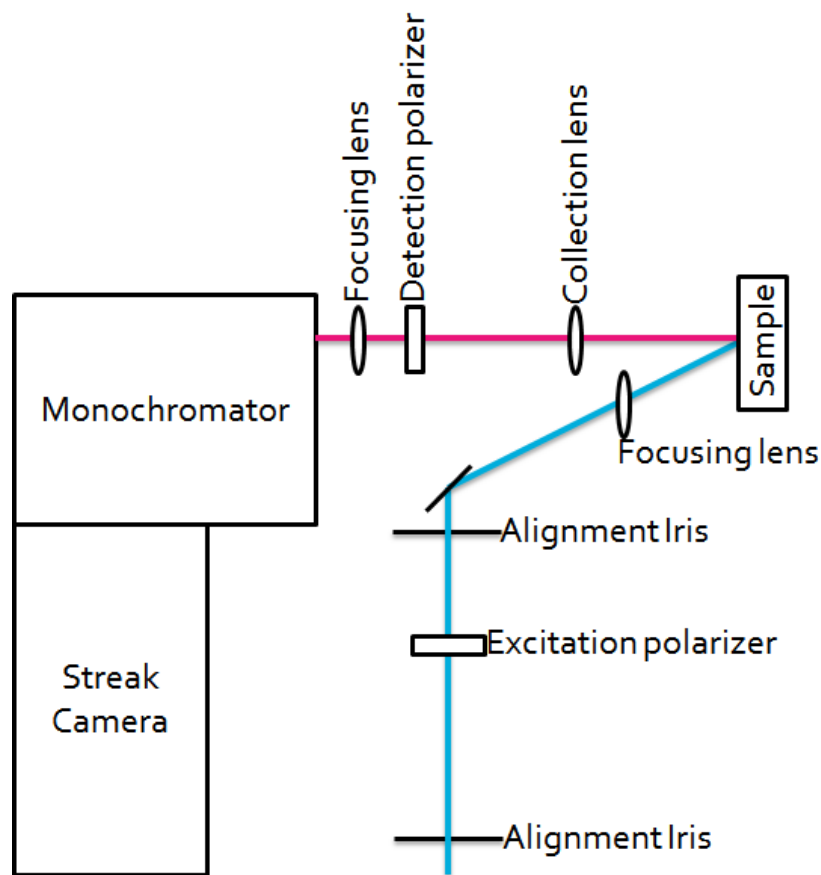
Figure 2.7 Optical layout for time resolved fluorescence experiments using a streak camera.

2.5.2 Time Resolved Temperature and Magnetic Field Dependence Experiments

Time resolved temperature dependence measurements were taken using the same cryostat and liquid nitrogen delivery system described in section **2.3.5**. For magnetic field experiments, the sample is held in a Janis ST-300 cryostat that is positioned at the center of a magnet stage (see Figure 2.8). The stage consists of two cylinder shaped Neodymium Permanent magnets (catalog #: DY0Y0-N50) with 2" diameter and 2" length that were purchased from K & J Magnetics. Each magnet is mounted in a non-magnetic mount which bolts onto

the stage in order to control the positions of the mounted magnets. The stage, constructed out of a combination of aluminum, Teflon, and brass parts, is able to keep the magnets at a specific distance despite their strong attractive forces. The position of the magnets are adjusted by rotating the brass handles at either end of the stage, which twists a threaded rod, forcing the magnet mounts either closer or farther away. Bringing the magnets up to within 1 mm of either side of the Janis ST-300 cryostat provides a field strength of about 6 kG. The magnetic field is measured with a Lakeshore Model 410 gaussmeter using the model HT 4658 transverse probe. The mounted magnets were only bolted on for magnetic field experiments and were removed and stored separately for zero field measurements and when not in use.
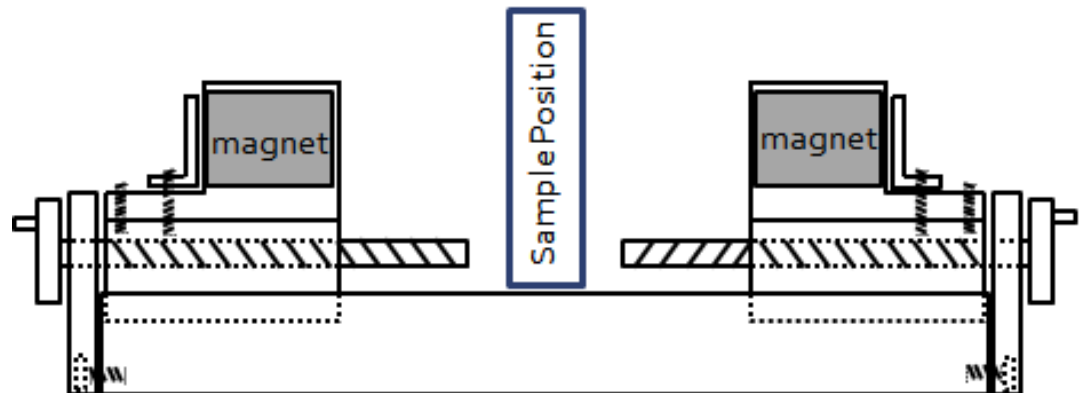
Figure 2.8 Magnetic field stage used for magnetic field effect experiments.

2.5.3 Transient Absorption Experiments

Transient absorption (TA) experiments were performed using the 1 KHz Coherent Libra Ti:sapphire regenerative amplifier described in section **2.4.3** with an Ultrafast Systems Helios transient absorption spectrometer. The 400 nm pump pulse was generated by frequency doubling the 800 nm Libra output and the white light continuum probe was generated by focusing a small portion (on the order of tens of mW) of the 800 nm fundamental onto a sapphire plate using a 3 cm focus lens. The power of the 800 nm beam being focused onto the sapphire plate was finely tuned using an iris just before the sapphire plate, and a white card can be used to identify an optimum continuum by eye. In addition to identifying a white continuum with a red halo (with no bright spot in the center of the beam which appears when the power on the sapphire plate is too high), the shape and stability of the continuum can also be monitored on the computer screen using the Helios software. The resulting continuum was collected and collimated using a 10 cm focus lens with a 15 cm focus lens used to focus the continuum onto the sample. The pump and probe were focused onto the same spot of the sample, and the transmitted probe beam was focused into an optical fiber coupled to an Ocean Optics S2000 spectrometer (see Figure 2.9). The best method for ensuring overlap of the two beams is to mount a known sample standard with a high fluorescence intensity (the Coumarins work well for solution samples and lumogen red works well for solid state samples) and overlap the beams by eye, adjusting the pump beam only since the probe beam is aligned

into an optical fiber. Then using the TA signal spectrum on the computer screen updating in live mode (every 1-2 seconds) maximize the signal by adjusting the position of the pump beam. The spectrometer and motorized delay stage were controlled with the Helios software. The motorized stage allows for a delay of up to 1.6 ns. The probe beam was intercepted and directed into an additional delay stage to obtain a probe delay of 7 ns. Pump fluences ranged from 0.80 to 8.3 mJ/cm^2. Excitation densities ranged from 7.8×10^{18} to 7.9×10^{19} per cubic centimeter for DIP and **PEN:DIP** studies.
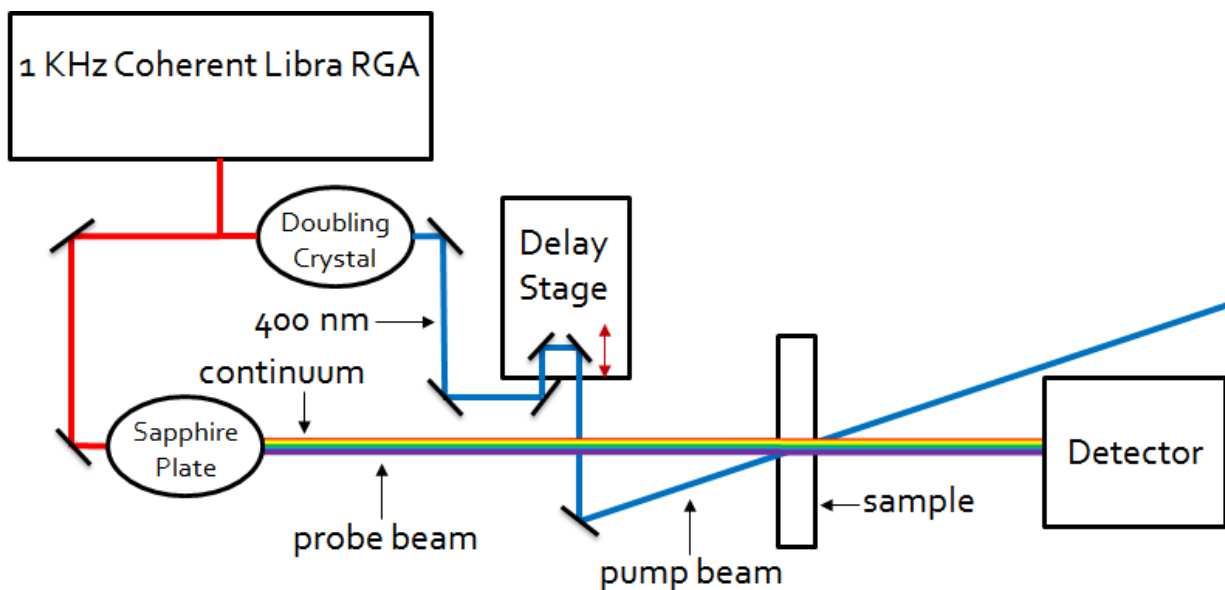
Figure 2.9 Optical layout for transient absorption experiments.

2.6 Other Experimental, Methods, and Data Workup

2.6.1 X-Ray Diffraction

Single-crystal X-ray diffraction was performed by Fook Tham at UCR. Data on **PP** crystals were collected on a Bruker APEX2 platform CCD X-ray diffractometer system (Mo-radiation, λ = 0.71073 Å, 50 kV/40 mA power) at 296. The frames were integrated using the Bruker SAINT software package and a narrow-frame integration algorithm. Absorption corrections were applied to the raw intensity data using the SADABS program. The Bruker SHELXTL software package was used for phase determination and structure refinement.

2.6.2 Calculations

All calculations for **PP** were performed by Geoffrey Piland in the Bardeen group and were done with the Gaussian 09 quantum chemistry package.[10] The computational method used for this work was TD-B3LYP using the 6-31 G* double zeta basis set.[11-12] Geometries converged with a force threshold of 0.00045 a.u. and a displacement threshold of 0.001800 a.u. Ground state geometries were obtained using B3LYP/6-31 G* with no symmetry restrictions and these geometries were subsequently used for calculating the vertical excitations of **PP**. Energy minima were confirmed by ensuring the Hessian contained no imaginary values.

REFERENCES

1. Pogodin, S.; Agranat, I., Large PAHs by Reductive Peri-Peri "Dimerization" of Phenalenones. *Org. Lett.* **1999,** *1*, 1387-1390.

2. Ueda, T.; Iwashima, S.; Aoki, J.; Takekawa, M., Complete Assignment and Additivity Rule for ^{1}H and ^{13}C Chemical Shifts of Non-Planar, Nonacyclic Aromatic Hydrocarbons. *Magn. Reson. Chem.* **1995,** *33*, 95-103.

3. Heinemeyer, U.; Scholz, R. et al., Exciton-phonon Coupling in Diindenoperylene Thin Films. *Phys. Rev. B.* **2008,** *8*, 085210

4. http://www.horiba.com/fileadmin/uploads/Scientific/Documents/Fluorescence/quantumyieldstrad.pdf

5. Dawson, W. Windsor, M. Fluorescence Yields of Aromatic Compounds. J. Phys. Chem. 1968. 9, 3251-3260.

6. Model TS laser kit oscillator manual; Labs, K.-M., Ed.

7. Spitfire-50 Preliminary User's Manual; Spectra-Physics, Ed., 1995.

8. Operator's Manual Libra Ultrafast Amplifier Laser System; Coherent, Ed., 2009.

9. Lakowicz, J.R., Principles of Fluorescence Spectroscopy. 2006: Springer.

10. Frisch, M. J.; Trucks, G. W.; Schlegel, H. B.; Scuseria, G. E.; Robb, M. A.; Cheeseman, J. R.; Scalmani, G.; Barone, V.; Mennucci, B.; Petersson, G. A.; et al, *Gaussian 09, B.01*, Gaussian Inc.: Wallingford, CT, 2009.

11. Becke, A. D., Density-Functional Thermochemistry. 3. The Role of Exact Exchange. *J. Chem. Phys.* **1993,** *98*, 5648-5652.

12. Schaefer, A.; Horn, H.; Ahlrichs, R., Fully Optimized Contracted Gaussian basis Sets For Atoms Li to Kr. *J. Chem. Phys.* **1992,** *97*, 2571-2577.

CHAPTER 3

Assessing the Potential of Peropyrene as a Singlet Fission Material:

Photophysical Properties in Solution and the Solid-State

3.1 Introduction

In this chapter, the photophysics of peropyrene (**PP**) both in dilute solution and in the solid-state are studied, with the goal of evaluating **PP** as a potential singlet fission (SF) material. The analysis of the spectroscopic properties of molecules in dilute solution provide evidence that the low-lying triplet states of this molecule affect the properties of the singlet state through mixing of an optically dark state with the bright ^1B_u state. This mixing, previously observed only in polyenes, leads to a dramatic dependence of the radiative rate on solvent polarizability. The crystal structure of solid peropyrene is reported for the first time, and it is found that its packing is very similar to that of the α -polymorph of perylene (**PER**). The face-to-face packing leads to large changes in the singlet fluorescence. No evidence is found for rapid SF in the **PP** crystals, most likely due to the large shift of the singlet state to lower energy in the crystal so that $E(S_1)<2E(T_1)$. These results demonstrate how both energetics and crystal packing influence the ability of a molecule to function as a SF material, and ways to improve the ability of **PP** to function as a SF material are suggested.

3.2. Steady State Solution Absorption and Fluorescence

PP is a highly absorbing molecule (ε = 1.1x10^5 M^{-1}cm^{-1} at its peak absorption[1]) that is very photostable. Solutions of the molecule left out in air at room temperature under room light showed no decrease in absorption after 1 week. **PP** is also highly fluorescent, with a quantum yield greater than 90% in most solvents. The molecule is very similar to **PER** in terms of its spectral properties and photostability, and despite its larger π-electron conjugation extent, its absorption and emission are only shifted by ~5 nm to the red as compared to **PER**. Figure 3.1 shows the absorption and fluorescence spectra of **PP** in
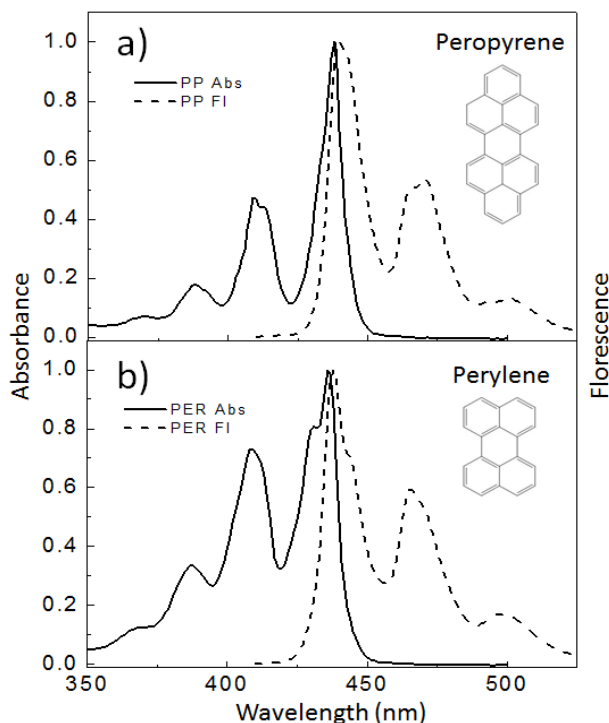
Figure 3.1 Normalized steady state absorption (solid) and the steady state fluorescence (dashed) of a) monomeric peropyrene (PP) and b) monomeric perylene (PER) in cyclohexane.

cyclohexane, which can be compared to those of **PER** in Figure 3.1b. A plot of the Stokes shift versus the solvent orientation polarizability, Figure 3.2, has a negligible slope, reflecting the fact that the absorption and fluorescence shift by similar amounts in different solvents. The lack of a Stokes shift dependence on solvent polarity indicates that there is little or no change in its polarity in going from the ground to excited state, as expected for this highly symmetric, nonpolar molecule.
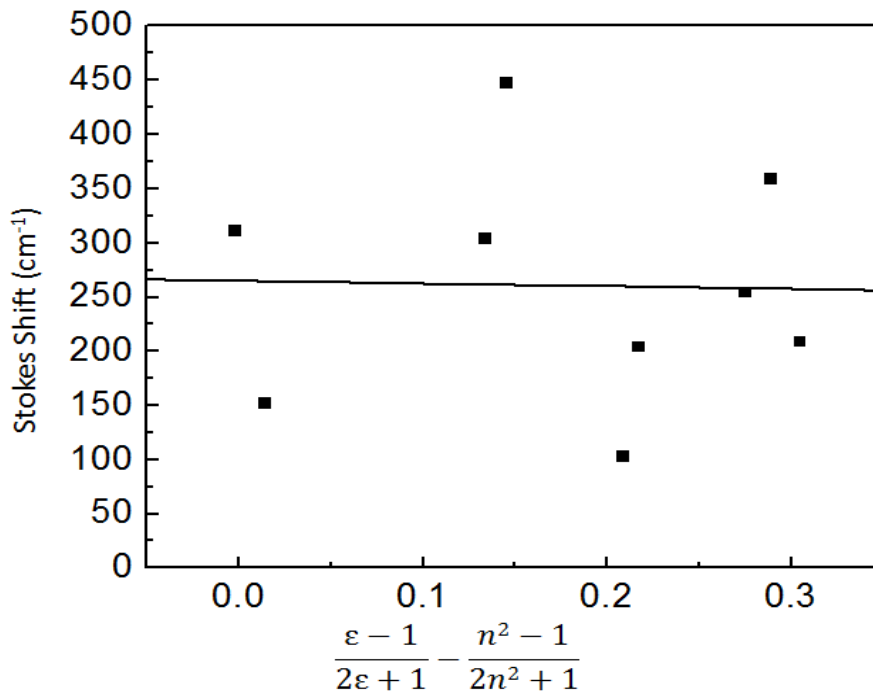
Figure 3.2 Lippert-Mataga plot of peropyrene: stokes shift in wavenumbers of peropyrene in different solvents as a function of solvent orientation polarizability. Solvents include cyclohexane, acetonitrile, ethanol, tetrahydrofuran, toluene, dichloromethane, dimethyl formamide, chloroform, and chlorobenzene.

3.3 Monomer Fluorescence Lifetime and Dependence on Solvent Refractive Index

In terms of its steady state spectroscopy, **PP** behaves in a straightforward manner. When the fluorescence lifetime was measured as a function of solvent, however, it was find that the lifetime increased by more than a factor of 2 in lower refractive index solvents. The measured fluorescence decay rates and quantum yields for peropyrene and perylene are given in Table 3.1, along with the relevant solvent parameters. The fluorescence lifetime showed no correlation with standard measures of solvent polarity, which ruled out the role of a charge transfer state. The quantum yield is essentially independent of solvent, suggesting that the radiative decay rate controls the solvent-dependent fluorescence lifetime. It is well known that the solvent index of refraction n controls the local density of electromagnetic modes around a molecule, which in turn affects the molecule's ability to radiate away its excited state energy. Most experimental and theoretical studies suggest that this local field effect leads to a factor of n^2 enhancement in the observed radiative rate of a planar molecule[2-5], *i.e.*

$$k_{rad}^{obs} = k_{fl}\phi_{fl} = n^2 k_{rad}^0 \tag{3.1}$$

where k_{rad}^0 is the intrinsic radiative rate of the molecule in a vacuum ($n = 1$). Thus a plot of k_{rad}^{obs} versus n^2 should yield a straight line where the value k_{rad}^0 can be obtained by the line's y-intercept at $n = 1$. This plot is shown in Figure 3.3 for

both **PER** and **PP**. Both data sets appear linear as a function of n^2, and the

slope for perylene yields a reasonable value of $k_{rad}^0 = 1.1 \times 10^8$ s^{-1}. The slope

obtained from the **PP** data, on the other hand, is much steeper and yields a

negative value for k_{rad}^0. Clearly, some other factor, beyond the usual local field

effect, is contributing to the solvent dependence of k_{rad}^{obs} for **PP**.

Table 3.1 Fluorescence decay rates and quantum yields for peropyrene and perylene

Solvent	Solvent Parameters[a]			$k_{fl}/10^8$ s^{-1} [c]		φ_{fl} [d]	
	ε_0	n	α	PP	PER	PP	PER
ACN	35.94	1.344	0.212	1.75	1.77	0.95	-
ETOH	24.55	1.361	0.221	1.82	-	0.99	-
THF	7.58	1.407	0.246	2.53	-	0.85	-
DCM	8.93	1.424	0.255	3.16	-	0.90	-
CH	2.02	1.426	0.256	2.38	2.03	0.90	0.94
DMF	36.71	1.431	0.259	2.88	-	0.90	-
CHCL$_3$	4.89	1.446	0.289	3.62	2.02	0.85	-
TOL	2.38	1.497	0.292	3.33	2.17	0.86	-
CB	5.62	1.525	0.304	3.92	2.15	0.90[b]	-

a) Values obtained from reference [64]
b) Estimated value; average of all other measured **PP** quantum yield values
c) Estimated error ±0.10
d) Estimated error ±0.03

3.3.1 Polyene Literature and Comparison with Peropyrene

The literature on the spectroscopy of polyenes provides an important clue as to the origin of the anomalous dependence of **PP**'s k_{rad}^{obs} on solvent. In the polyenes, the emission originates from a weakly allowed ^1A_g state while the bright ^1B_u state dominates the absorption. The ^1A_g state to ground state transition is formally forbidden, but gains oscillator strength by mixing with the nearby optically allowed ^1B_u state.[6-8] The relative energies of these states, and
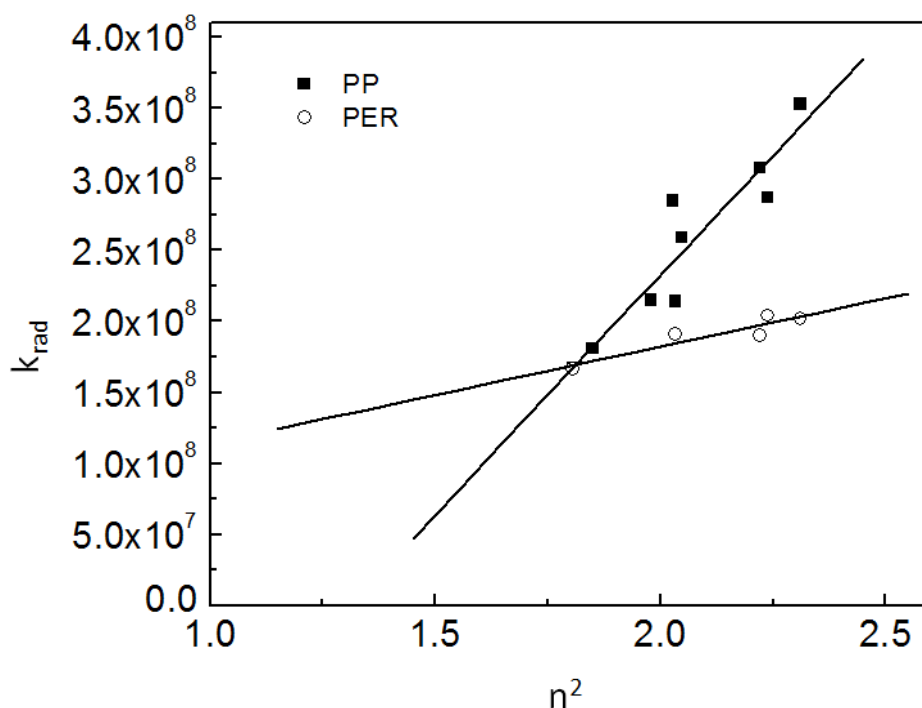
Figure 3.3 Rate of the radiative relaxation of monomeric peropyrene (black squares) and perylene (open circles) in different solvents plotted as a function of the solvent refractive index squared. The linear fits show that peropyrene has a negative y-intercept at y-intercept at n2 = 1 while perylene has a positive y-intercept at n^2=1.

thus their degree of mixing, change in different solvents. This solvent-dependence of the oscillator strength has been observed in at least one other

type of molecule[9], and Hudson and coworkers have developed a detailed theory for this phenomenon in the polyenes.[10] Following their approach, below perturbation theory is used to illustrate the main aspects of this phenomenon as applied to the case of **PP**. A 3-level system is considered where ϕ_0 is the ground
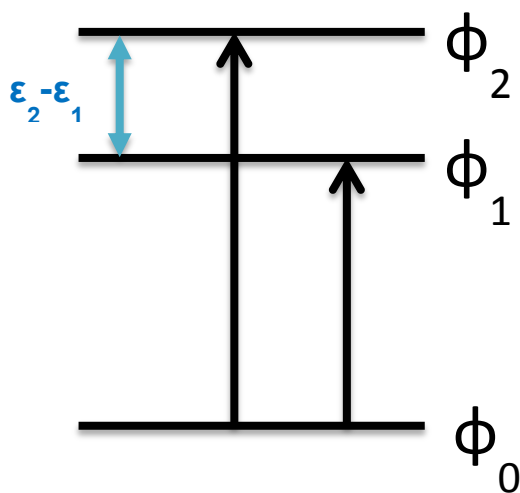
Figure 3.4 Energy diagram illustrating a 3-level system where φ_0 is the ground electronic state and φ_1 and φ_2 are two electronic excited states with energies ε_1 and ε_2 and an energy difference of ε_2-ε_1.

electronic state and there are two electronic excited states: ϕ_1 with energy ϕ_1 and ϕ_2 with energy ϕ_2 (see Figure 3.4). Furthermore, it is assumed that all three states are normalized and orthogonal, and that ϕ_1 is the bright state and ϕ_2 is the dark state, *i.e.*

$$\langle \phi_0 | \hat{\mu} | \phi_1 \rangle \neq 0$$
$$\langle \phi_0 | \hat{\mu} | \phi_2 \rangle = 0$$

(3.2a,b)

where $\hat{\mu}$ is the dipole moment operator. In this model, ϕ_1 corresponds to the ^1B_u state that is one-photon allowed due to its different symmetry from the ground

state ϕ_0. ϕ_2 corresponds to the ^1A_g state, which shares the same symmetry as the ground state and thus is one-photon forbidden, but two-photon allowed. If ϕ_1 and ϕ_2 are coupled through a generic operator $\hat{V}$, then first order perturbation theory gives the following expression for the perturbed bright state:

$$\left| \Psi_1^{(mixed)} \right\rangle = \left| \phi_1 \right\rangle + \frac{\left| \left\langle \phi_1 \left| \hat{V} \right| \phi_2 \right\rangle \right|^2}{\varepsilon_2 - \varepsilon_1} \left| \phi_2 \right\rangle \tag{3.3}$$

The normalized version of $\left| \Psi_1^{(mixed)} \right\rangle$ is defined to be $\left| \Psi_1 \right\rangle$, and the radiative decay rate from this state will be proportional to its transition dipole moment squared as well as the local field factor n^2,

$$k_{rad}^{obs} \propto n^2 \left| \left\langle \phi_0 \left| \hat{\mu} \right| \Psi_1 \right\rangle \right|^2 \tag{3.4}$$

Note that here the local field factor is taken to be n^2, rather than the factor of $\frac{9n^2}{(n^2 + 2)^2}$ assumed in reference [10]. If it is assumed that the perturbation term is small, Equation (3.4) can be written as,

$$k_{rad}^{obs} \propto n^2 \left| \left\langle \phi_0 \left| \hat{\mu} \right| \phi_1 \right\rangle \right|^2 \left[1 - \frac{\left| \left\langle \phi_1 \left| \hat{V} \right| \phi_2 \right\rangle \right|^2}{\left| \varepsilon_2 - \varepsilon_1 \right|^2} \right] \tag{3.5}$$

It can now be seen that k_{rad}^{obs} now depends on both the local field factor n^2 and the energy separation between states ϕ_1 and ϕ_2. The energies of these states depends on their interaction with the solvent dielectric, and to first order these energies are given by

$$\varepsilon_1 = \varepsilon_1^0 + P_1 \alpha$$
$$\varepsilon_2 = \varepsilon_2^0 + P_2 \alpha$$

(3.6a,b)

where ε_1^0 is the energy of state 1 in vacuum, P_1 is the polarizability of state 1, and α is the polarizability of the solvent. From this analysis, Equation (3.5) can be written in the form

$$\frac{k_{rad}^{obs}}{n^2} \propto k_{rad}^0 \left[1 - \frac{\Gamma^2}{(\Delta\varepsilon + \Delta P \alpha)^2} \right]$$

(3.7)

where

$$\Delta\varepsilon = \varepsilon_2 - \varepsilon_1$$
$$\Delta P = P_2 - P_1$$

(3.8a,b)

The polarizability of the solvent is estimated from its refractive index n,

$$\alpha = \frac{n^2 - 1}{n^2 + 2}$$

(3.9)

A plot of $\dfrac{k_{rad}^{obs}}{n^2}$ versus the solvent polarizability α should lead to a Lorentzian type dependence on α. In Figure 3.5 $\dfrac{k_{rad}^{obs}}{n^2}$ is plotted versus α for both **PER** and **PP**. As expected, the **PER** data is flat to within the experimental error, indicating that no significant state mixing exists. For **PP**, on the other hand, there is an obvious dependence on α, indicating that the second term in Equation (3.7) cannot be neglected and there is a solvent-dependent mixing of two excited electronic states. In the polyenes, the k_{rad}^{obs} of the low energy ^1A_g state increases due to mixing with the strongly allowed ^1B_u state.[43] In **PP**, it appears to have the

opposite situation, where the strongly allowed ^1B_u state is the low energy state whose k_{rad}^{obs} is decreased by the proximity of the dark state. A fit to the PP data using Equation (3.7) yielded values k_{rad}^0=4.2x10^{8}s^{-1}, $\dfrac{\Gamma^2}{\Delta\varepsilon^2}$ = 1.27, and $\dfrac{\Delta P}{\Delta\varepsilon}$ = 1.31. These values are reasonable when compared to values obtained for polyenes[45], although the value for k_{rad}^0 is almost a factor of 4 higher than **PER** and may overestimate the intrinsic radiative rate.
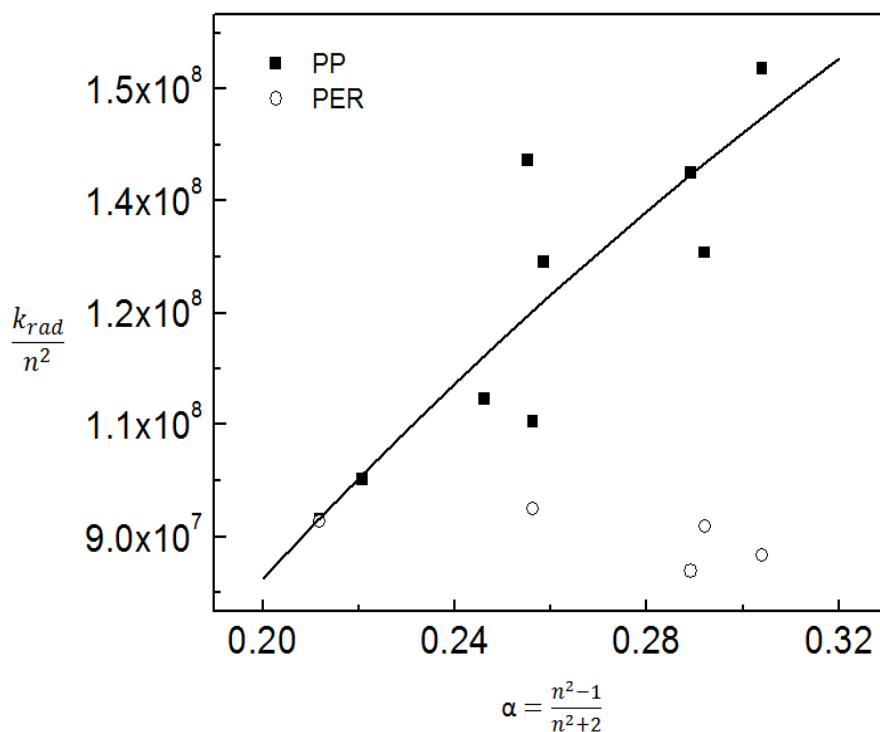
Figure 3.5 Rate of the radiative relaxation scaled by the solvent refractive index squared of PP (black squares) and PER (open circles) plotted as a function of the solvent property α, a function of the refractive index. Also shown is the fit of the PP data points (black curve) using see Equation (3.7) and the parameters given in the text. The PP rates change with α but those of PER do not.

3.3.2. Perturbation Theory and Two Photon Absorption: Evidence of Light and

Dark States Nearby in Energy

      To confirm that there is a dark state close in energy to the bright ^1B_u state,

the two-photon fluorescence excitation spectrum is measured, which should

reflect the shape of the $\phi_0 \rightarrow \phi_2$ transition. In Figure 3.6 two-photon fluorescence

excitation spectra is plotted in two different solvents: acetonitrile (α = 0.219) and

chlorobenzene (α = 0.304). Also shown are the one-photon absorption spectra

for comparison. The one- and two-photon lineshapes are completely different,

indicating that the two different excitation modes access different states. A

similar two-photon absorption lineshape has been measured for PER[11-12], and

other workers have shown that **PER** derivatives have different one- and two-

photon absorption spectra [13-14], as expected for this class of highly symmetric

molecules. In **PP**, the one- and two-photon spectra both exhibit similar vibronic

progressions with spacings of ~20 nm (corresponding to a 1000-1200 cm^{-1}

vibrational mode characteristic of PAH's). Looking at the 420 nm peak in the

two-photon spectra, it can be seen that it does not shift with solvent, while the

one-photon peak shifts from 437 nm to 450 nm. This shift moves the one-photon

peak farther from the two-photon peak located at ~420 nm. As the one-photon

peak shifts farther away from the two-photon peak in higher α solvents, the

degree of mixing should decrease and the k_{rad}^{obs} should increase, as observed

experimentally. It is suspected that the two-photon peak around 440 nm reflects

two-photon absorption to the bright $\left| \Psi_1 \right\rangle$ state that is now two-photon allowed by

virtue of the mixing between ϕ_1 and ϕ_2. The decrease in the amplitude of this peak as ϕ_1 shifts to lower energy in more polarizable solvents is consistent with a loss of its two-photon absorption strength which should accompany a decrease in mixing between ϕ_1 and ϕ_2. It is not thought that the two-photon spectrum due to ϕ_2 is sensitive to the polarizability because the higher energy peaks at 400 nm and 420 nm do not shift with solvent.
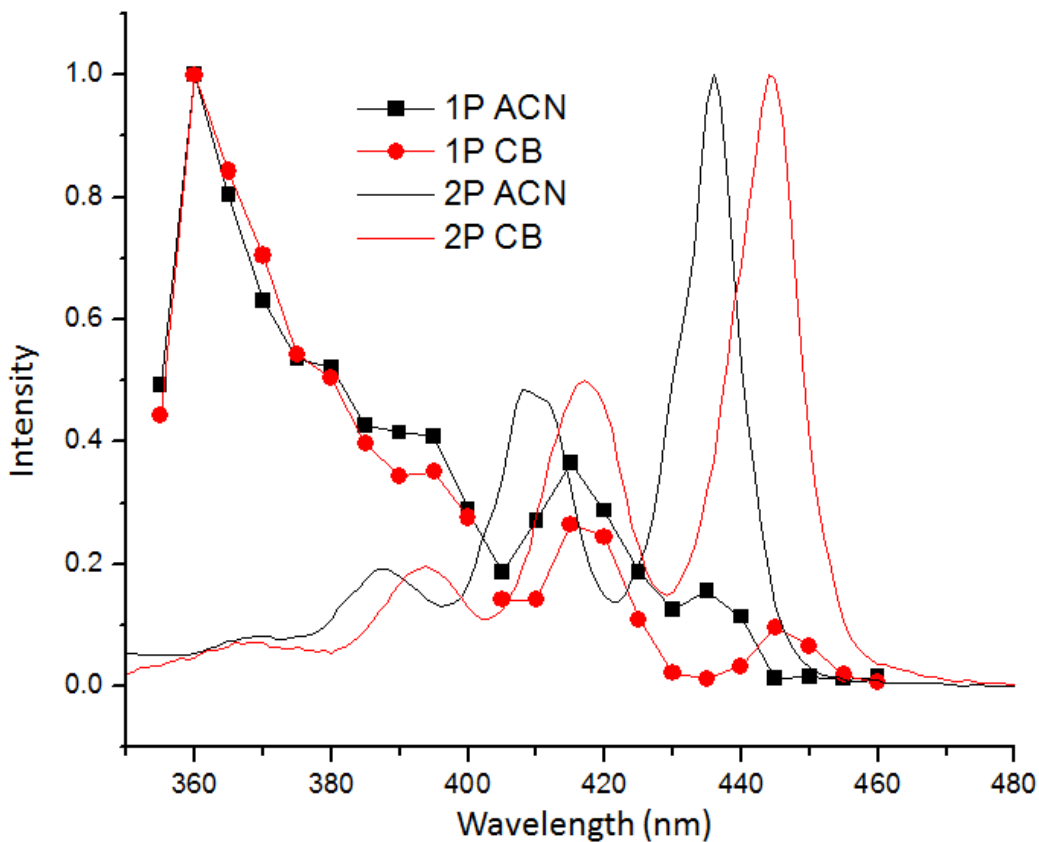
Figure 3.6 Normalized one-photon absorption (solid) and two-photon fluorescence excitation (symbols) spectra of PP in acetonitrile (ACN, black, n=1.34) and chlorobenzene (CB, red, n=1.52). The solvent-independent two-photon features at 400 nm and 420 nm are ascribed to the dark state, while the feature at ~440 nm that shifts with solvent is ascribed to residual two-photon absorption to the one-photon allowed state due to mixing with the dark state.

3.3.3. Identity of Dark and Bright States

The last question concerns the exact nature of the bright and dark states. It was originally suspected that the dark state ϕ_2 might have ^1A_g symmetry, in analogy with the situation in the polyenes. As Schulten and Karplus originally showed[15], this state can be thought of as a double excitation of two triplet states with overall singlet character. The existence of the T_1 state at almost exactly half the energy of the singlet $S_1{}^1$ would put this doubly excited state at the same energy as the singlet and approximately where the dark state is observed. Using time-dependent density functional theory (TDDFT) electronic structure calculations, we were able to assign ^1B_u symmetry to the bright state. The ground $^1A_g \rightarrow {}^1B_u$ transition is strongly dipole-allowed due to the change in state symmetry. Semi-empirical ZINDO and TDDFT calculations using B3LYP and wB97xd functionals all located a second singlet ^2B_u state at energies of 0.3-0.4 eV above the ^1B_u state, with an oscillator strength <1% of that of the bright ^1B_u state. The nearest ^1A_g state was at least 1 eV above the ^1B_u state, apparently ruling out any analogy with the polyenes. However, there are still some questions left remaining. If the dark state ϕ_2 that is observed experimentally corresponds to the ^2B_u state, it is strange that its two-photon cross-section is so much larger than that of the ^1B_u state. In molecules of high symmetry, like **PER** and **PP**, two-photon absorption should couple states of like symmetry, e.g. from a gerade ground state to a gerade excited state. Furthermore, standard *ab initio* methods

often fail to correctly account for doubly excited electronic configurations,[16] and it is possible that a gerade singlet state is missed by our relatively simple calculations. The identity of the dark state merits further study.

3.4. Crystal Growth and Packing Structure

To study **PP** in the solid-state, the crystals were grown from *o*-xylene and x-ray diffraction was used to determine the crystal structure. The crystal parameters are summarized in Table 2, and two views of the crystal packing are shown in Figure 3.7. **PP** crystallizes in a herringbone pair motif, with an almost 90° angle between the π-stacked molecular pairs. The slight offset between the two molecules within the pair is commonly seen in the packing of similar PAH molecules.[17] The overall structure is very similar to that of *α*-perylene[18], and this type of π -stacking is known to lead to strong electronic interactions and excimer formation.[19] The presence of such low energy states with charge-transfer character may provide a competing channel for relaxation of the initially excited singlet state and suppress SF.

Table 3.2. Crystal data and structure refinement for peropyrene

Empirical formula	C26 H14
Formula weight	326.37
Temperature	100(2) K
Wavelength	0.71073 Å
Crystal system	Monoclinic
Space group	P2(1)/c
Unit cell dimensions	a = 12.377(3) Å $\quad\square$= 90°.
	b = 8.994(2) Å $\quad\square$= 92.036(4)°.
	c = 13.897(3) Å $\quad\square$ = 90°.
Volume	1546.0(6) Å3
Z	4
Density (calculated)	1.402 Mg/m3
Absorption coefficient	0.080 mm-1
F(000)	680
Crystal size	0.49 x 0.33 x 0.01 mm3
Theta range for data collection	1.65 to 25.68°.
Index ranges	-15<=h<=15, -10<=k<=10, -16<=l<=16
Reflections collected	20835
Independent reflections	2926 [R(int) = 0.0852]
Completeness to theta = 25.68°	100.00%
Absorption correction	Semi-empirical from equivalents
Max. and min. transmission	0.9989 and 0.9620
Refinement method	Full-matrix least-squares on F2
Data / restraints / parameters	2926 / 0 / 235
Goodness-of-fit on F2	1.005
Final R indices [I>2sigma(I)]	R1 = 0.0500, wR2 = 0.1246
R indices (all data)	R1 = 0.0948, wR2 = 0.1565
Largest diff. peak and hole	0.240 and -0.211 e.Å-3
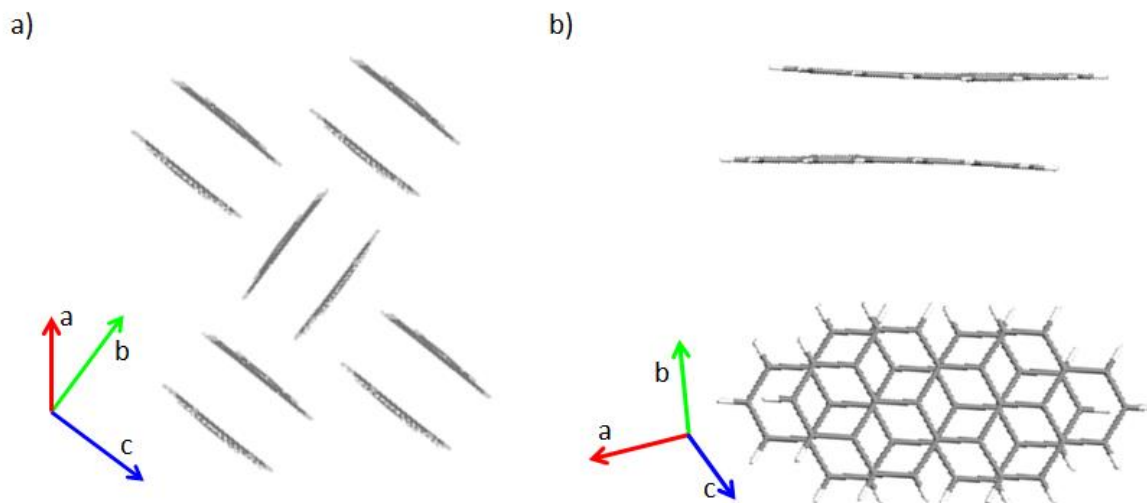
Figure 3.7 Two different views of crystalline PP: a) side-view showing pair-wise herringbone packing structure; b) side and top view of each pair showing offset alignment of the PP molecular pair. The crystal unit cell axes are shown in both figures.

3.5. Steady State and Time Resolved Spectroscopy of Peropyrene Crystals

To examine the effect of the crystal packing on the electronic dynamics, steady state and time-resolved spectroscopy of microcrystals of **PP** were measured. Figure 3.8 shows the fluorescence emission spectra for a collection of **PP** microcrystals at different temperatures. The spectra are redshifted by ~100 nm in the crystal relative to the solution spectrum in Figure 3.1a. Furthermore, the spectral shapes are quite different from those of the isolated molecule in solution; they are strongly broadened and the relative heights of the distinguishable peaks have changed. Some insight into the origin of these changes can be gained by examining the temperature dependence of the emission spectra. At lower temperatures, the peak at 550 nm becomes enhanced, while the shape of the emission at 650 nm and beyond remains constant. These separate changes suggest that at least two emitting species

contribute to the total spectrum. The same situation is encountered for *α*-perylene, where the high and low energy emission components have been assigned to the Y and E-type excimers, respectively.[18, 20]
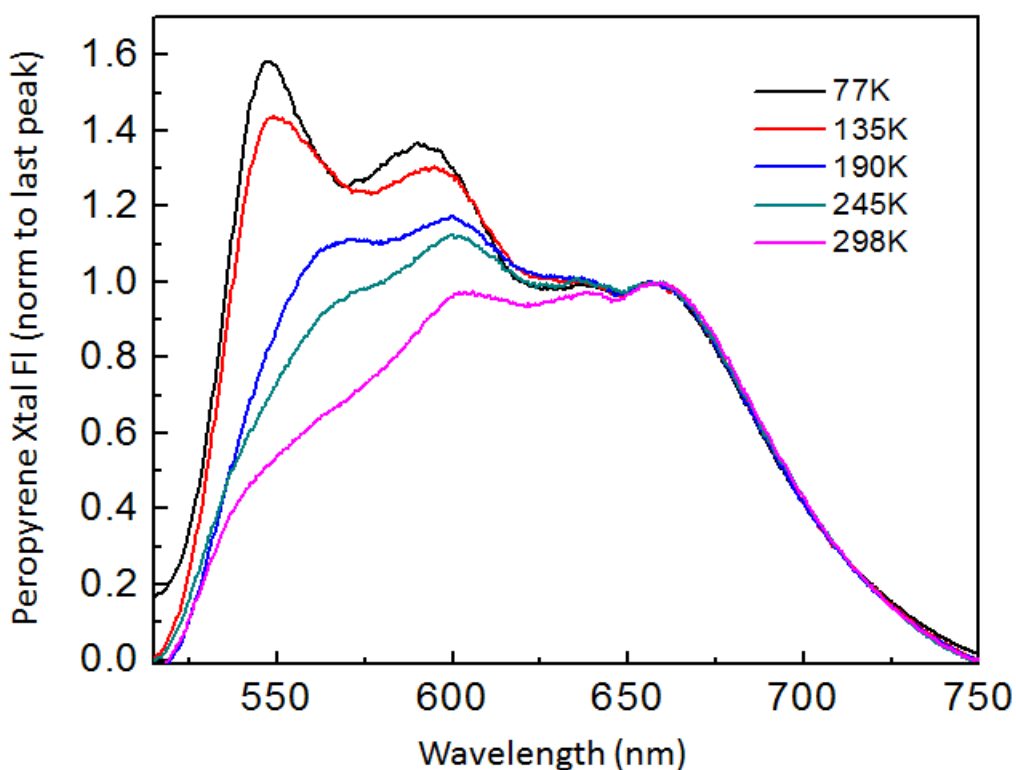
Figure 3.8 Normalized fluorescence emission spectra of crystalline PP at different temperatures. The higher energy peak at ~550 nm becomes more pronounced as the temperature is lowered.

Time-resolved measurements confirm the presence of two distinct emitting species that appear to be created in parallel. Figure 3.9 shows early (integrated from 0-1 ns) and late (integrated from 15-20 ns) luminescence spectra taken at room temperature. The early time emission is dominated by the 550-600 nm

emission, but this peak decays relatively quickly, leaving the longer time emission dominated by the double peaked spectrum (610 nm and 660 nm). The same qualitative shape change is also observed at 77 K, although at this temperature there is still appreciable 550-600 nm emission even in the long time window. The decay of the 550-600 nm peak depends on temperature, but that of the 610/660 nm feature is only weakly temperature dependent. This can be seen from the data in Figures 3.10a and 3.10b, which show the fluorescence decays centered at 550 and 650 nm, respectively. At both wavelengths, the decays are biexponential and can be fit using the parameters given in Table 3. It can be seen that the 550 nm peak decay time, τ_1, increases by a factor of 3.5 when the temperature is lowered to 77 K, while τ_2 doubles. The decay time of the 650 nm emission also lengthens at 77 K, but both components slow by less than a factor of 2. The nonexponential nature of the fluorescence decays could reflect disorder or a heterogeneous population of defects within the **PP** crystals. It was found that the decay of the excimer in crystalline **PER** is sensitive to crystal quality. While solution-grown crystals had decay times on the order of 5 ns or less, vacuum sublimed crystals had lifetimes on the order of 20 ns, decay times as long as 60-70 ns were observed in single crystals grown by sublimation of zone-refined material. There was not sufficient sample to attempt this level of purification for **PP**. For this reason, it is suspected that the decay times in Table 3 represent a lower bound on the true fluorescence lifetime of crystalline **PP**.
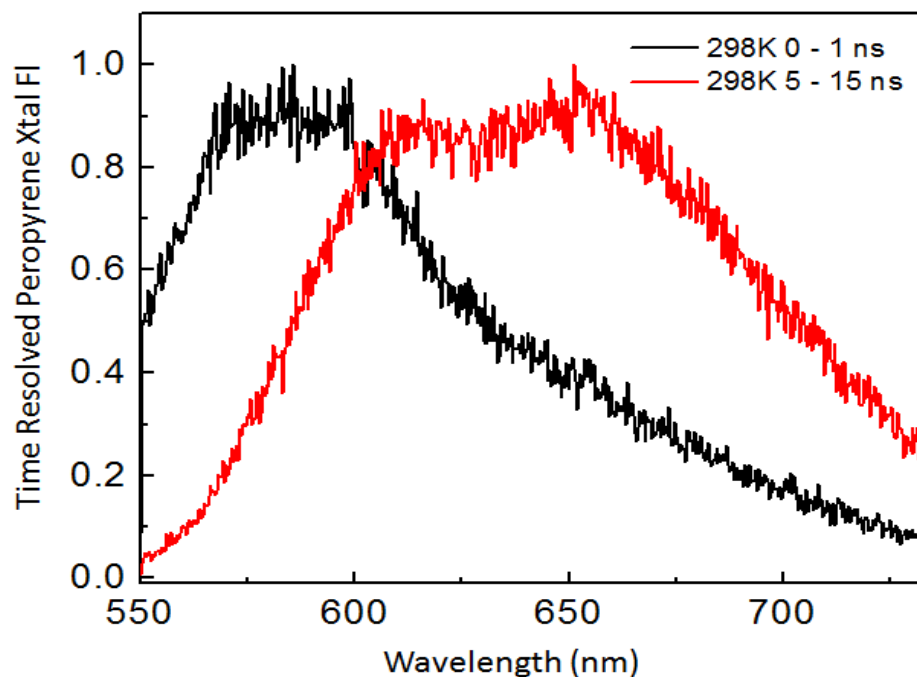
Figure 3.9 Normalized transient fluorescence spectra from crystalline PP at 298K showing the early (integrated from 0-1 ns, black) emission spectral shape and the late emission (integrated from 5-20 ns, red). The time-dependent shift of the spectrum reflects the presence of two different species with different decay rates.
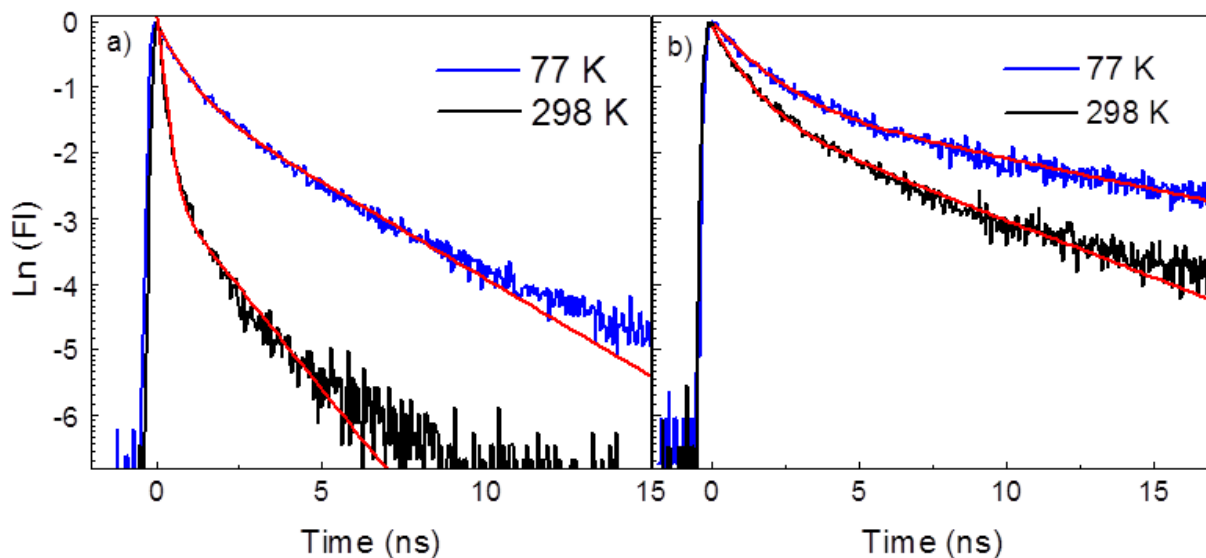
Figure 3.10 a) The normalized fluorescence decays of crystalline PP at 298K (black) and 77K (blue) integrated over a 10 nm window centered at 550 nm. The corresponding bi-exponential fits (red, see Table 3 for formula and parameters) are also shown. b) The same data as in panel a), but integrated over a 10 nm window centered at 650nm.

Table 3.3. Biexponential Decay Parameters used to fit the fluorescence decay data in Figure 3.10.

$$f(t) = A_1 e^{\frac{-t}{\tau_1}} + A_2 e^{\frac{-t}{\tau_2}}$$

Parameter	550 nm peak		650 nm peak	
	77K	298K	77K	298K
A1	0.61	0.92	0.69	0.70
τ1 (ns)	0.701	0.198	1.477	0.978
A2	0.39	0.08	0.31	0.30
τ2 (ns)	3.889	1.617	10.755	5.732

There is no sign that the population in the high energy states is transferring into the 610/660 nm state, since if this were the case, it would be expected to see the 610/660 nm component grow in on the τ_1 timescale. Neither signal exhibits a risetime, with both peaking within the 15 ps instrument response of the streak camera. Our data are consistent with an ultrafast relaxation of the initially excited state into two distinct emitting states that proceed to decay independently of each other (see Figure 3.11). Again, this is very similar to the situation for α-perylene, where the excimer emission appears within 15 ps or less.[21-23] Earlier work suggested the E and Y states were formed independently from an initially excited "free exciton" population that rapidly partitions between high energy Y-state and a low energy E state in α-perylene.[20, 24] Later temperature dependent measurements have suggested that there is population exchange between these states[25], but the molecular origin of these two emitting

species remains obscure.   Nevertheless, it can concluded that the structural similarity between the **PP** crystals and α -perylene leads to a similarity of their spectroscopic properties as well.
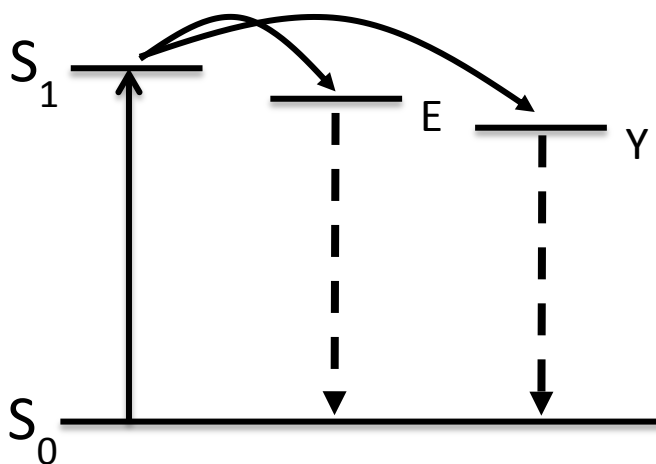
Figure 3.11 Energy level diagram illustration of crystalline peropyrene showing an absorption from the ground state to a high energy excited state that relaxes to states E and Y both of which then decay independently of each other.

3.6 Effects of Crystallization on Peropyrene's Suitability as a Singlet Fission Material

The large changes in the electronic states of **PP** when it is in crystalline form have strong implications for its suitability as a SF material. It is doubtful that the triplet state experiences as large a shift as the singlet state in the crystal, and thus the condition $E(S_1) \approx 2E(T_1)$ is likely no longer fulfilled. If the 550 nm peak is taken to reflect the energy of the relaxed singlet, then $E(S_1)$=18,100 cm^{-1}, and if $E(T_1)$ =11,000 cm^{-1}, the SF reaction will be quite endothermic and not competitive with other relaxation processes. It is possible that there exists a short-lived higher energy state, analogous to the "free exciton" postulated for α-

perylene, where SF is more favorable. However, the short lifetime (<15 ps) of such a state requires a rapid SF rate if it is going to generate a significant number of triplets. Our excitation wavelength of 400 nm (25,000 cm^{-1}) should provide sufficient excess energy to generate a pair of triplets, yet there was no sign of delayed fluorescence that would indicate the creation of a large triplet population. Preliminary experiments also failed to observe a magnetic field effect on the fluorescence decay, which would also provide evidence for SF.[26-27] It is possible that triplets could be formed more efficiently from a higher-lying singlet state that is not accessed by our 400 nm excitation. Direct detection of triplets after variable wavelength excitation, for example using transient absorption with femtosecond time resolution, might provide some evidence for the existence of SF at very early times. But if SF can only occur from high-lying electronic states, its efficiency will be limited due to competition from internal conversion to the lowest-lying singlet state. While the lack of delayed fluorescence and a magnetic field effect does not conclusively prove that SF is completely absent, crystalline **PP** certainly does not behave like crystalline tetracene, a polyaromatic hydrocarbon with similar energetics where SF from the lowest singlet state plays a dominant role in the photophysics.

3.7 Conclusion

In dilute solutions, **PP**'s radiative rate shows an anomalous dependence on solvent polarizability that can be explained by mixing of the bright ^1B_u state

with a higher energy dark state. It was hoped that this dark state might be a precursor to a separated triplet pair state in the solid. However, the herringbone pair packing motif of the **PP** crystal appears to result in lower energy singlet excimer states that no longer satisfy the condition $2E(T_1) \leq E(S_1)$. This result suggests that control of the crystal packing could improve **PP**'s potential as a SF material. For example, the *β*-form of perylene has a herringbone packing motif[18, 28], similar to that of tetracene, and apparently undergoes more facile SF[29]. If conditions can be found under which a similar crystal polymorph of **PP** is formed, excimer state formation may be avoided which would provide more time for SF to occur. Chemical substitution has also been shown to change the crystal packing of peropyrene derivatives[30], providing a second way to crystal engineer a more promising SF material.

REFERENCES

1. Wenzel, U.; Lohmannsroben, H. G., Photophysical and Fluorescence Quenching Properties of Peropyrene in Solution. *J. Photochem. Photobio. A* **1996,** *96*, 13-18.

2. Shibuya, T., The Refractive-Index Correction to the Radiative Rate Constant. *Chem. Phys. Lett.* **1983,** *103*, 46-48.

3. Lampert, R. A.; Meech, S. R.; Metcalfe, J.; Phillips, D.; Schaap, A. P., The Refractive Index Correction to the Radiative Rate Constant in Fluorescence Lifetime Measurements. *Chem. Phys. Lett.* **1983,** *94*, 137-140.

4. Hirayama, S.; Iuchi, Y.; Tanaka, F.; Shobatake, K., Natural Radiative Lifetimes of Anthracene Derivatives and Their Dependence on Refractive Index. *Chem. Phys.* **1990,** *144*, 401-406.

5. Toptygin, D., Effects of the Solvent Refractive Index and its Dispersion on the Radiative Decay Rate and Extinction Coefficient of a Fluorescent Solute. *J. Fluoresc.* **2003,** *13*, 201-219.

6. Hudson, B. S.; Kohler, B. E., A low-lying weak transition in the polyene a,w-diphenyloctatetraene. *Chem. Phys. Lett.* **1972,** *14*, 299-304.

7. Birks, J. B.; Tripathi, G. N. R.; Lumb, M. D., The Fluorescence of All-Trans Diphenyl Polyenes. *Chem. Phys.* **1978,** *33*, 185-194.

8. Hudson, B. S.; Kohler, B. E.; Schulten, K., Linear Polyene Electronic Structure and Potential Surfaces. *Excited States* **1982,** *6*, 1-95.

9. Mohanty, J.; Nau, W. M., Refractive Index Effects on the Oscillator Strength and Radiative Decay Rate of 2,3-diazabicyclo[2.2.2]oct-2-ene. *Photochem. Photobio. Sci.* **2004,** *3*, 1026-1031.

10. Andrews, J. R.; Hudson, B. S., Environmental Effects on Radiative Rate Constants with Applications to Linear Polyenes. *J. Chem. Phys.* **1978,** *68*, 4587-4593.

11. Yu, J. A.; Nocera, D. G.; Leroi, G. E., Two-Photon Excitation Spectrum of Perylene in Solution. *Chem. Phys. Lett.* **1990,** *167*, 85-89.

12. Vivas, M. G.; Diaz, C.; Echevarria, L.; Mendonca, C. R.; Hernandez, F. E.; Boni, L. D., Two-Photon Circular-Linear Dichroism of Perylene in Solution. *J. Phys. Chem. B* **2013,** *117*, 2742-2747.

13. Belfield, K. D.; Bondar, M. V.; Hernandez, F. E.; Przhonska, O. V., Photophysical Characterization, Two-Photon Absorption and Optical Power Limiting of Two Fluorenylperylene Diimides. *J. Phys. Chem. C* **2008,** *112*, 5618-5622.

14. Piovesan, E.; Silva, D. L.; Boni, L. D.; Guimaraes, F. E. G.; Misoguti, L.; Zalesny, R.; Bartkowiak, W.; Mendonca, C. R., Two-Photon Absorption of Perylene Derivatives: Interpreting the Spectral Structure. *Chem. Phys. Lett.* **2009,** *479*, 52-55.

15. Schulten, K.; Karplus, M., On the Origin of a Low-Lying Forbidden Transition in Polyenes and Related Molecules. *Chem. Phys. Lett.* **1972,** *14*, 305-309.

16. Dreuw, A.; Head-Gordon, M., Single-Reference *Ab Initio* Methods for the Calculation of Excited States of Large Molecules. *Chem. Rev.* **2005,** *105*, 4009-4037.

17. Hunter, C. A.; Sanders, J. K. M., The Nature of P-P Interactions. *J. Am. Chem. Soc.* **1990,** *112*, 5525-5534.

18. Tanaka, J., The Electronic Spectra of Aromatic Molecular Crystals. II. The Crystal Structure and Spectra of Perylene. *Bull. Chem. Soc. Jap.* **1963,** *36*, 1237-1249.

19. Birks, J. B., Excimers. *Rep. Prog. Phys.* **1975,** *38*, 903-974.

20. Freydorf, E. V.; Kinder, J.; Michel-Beyerle, M. E., On Low Temperature Fluorescence of Perylene Crystals. *Chem. Phys.* **1978,** *27*, 199-209.

21. Inoue, A.; Yoshihara, K.; Kasuya, T.; Nagakura, S., Excimer and Monomer Defect Emissions of Perylene and Pyrene Crystals as Studied by the Nanosecond Time-Resolved Spectroscopy Technique. *Bull. Chem. Soc. Jap.* **1972,** *45*, 720-725.

22. Kobayashi, T., The Observation of the Excimer Formation Process in Pyrene and Perylene Crystals Using a Picosecond Ruby Laser and Streak Camera. *J. Chem. Phys.* **1978,** *69*, 3570-3574.

23. Nelson, K. A.; Dlott, D. D.; Fayer, M. D., Excited State Dynamics in Pure Molecular Crystals: Perylene and the Excimer Problem. *Chem. Phys. Lett.* **1979,** *64*, 88-93.

24. Hochstrasser, R. M.; Nyi, C. A., Dynamical Effects from Resonance Raman and Fluorescence Studies of the Molecular Exciton System Perylene. *J. Chem. Phys.* **1980,** *72*, 2591-2600.

25. Walker, B.; Port, H.; Wolf, H. C., The Two-Step Excimer Formation in Perylene Crystals. *Chem. Phys.* **1985,** *92*, 177-185.

26. Geacintov, N.; Pope, M.; Vogel, F., Effect of Magnetic Field on the Fluorescence of Tetracene Crystals: Exciton Fission. *Phys. Rev. Lett.* **1969,** *22*, 593-596.

27. Piland, G. B.; Burdett, J. J.; Kurunthu, D.; Bardeen, C. J., Magnetic Field Effects on Singlet Fission and Fluorescence Decay Dynamics in Amorphous Rubrene. *J. Phys. Chem. C* **2013,** *117*, 1224-1236.

28. Albrecht, W.G.; Coufal, H.; Baberkorn, R.; Michel-Beyerle, M.E., Excitation Spectra of Exciton Fission in Organic Crystals. *Phys. Stat. Solid. B* **1987,** *89,* 261-265.

29. Albrecht, W.G.; Michel-Beyerle, M.E.; Yakhot, V., Exciton Fission in Excimer Forming Crystal. Dynamics of an Excimer Build-Up in a-Perylene. *Chem. Phys.* **1978,** *35,* 193-200.

30. Beer, L.; Mandal, S. K.; Reed, R. W.; Oakley, R. T.; Tham, F. S.; Donnadieu, B.; Haddon, R. C., The First Electronically Stabilized Phenalenyl Radical: Effect of Substituents on Solution Chemistry and Solid-State Structure. *Cryst. Growth & Design* **2007,** *7*, 802-809.

CHAPTER 4

Excited State Dynamics of Diindenoperylene in Liquid Solution and in Solid Films

4.1 Introduction

In this chapter, the excited state dynamics of diindenoperylene (**DIP**) in both dilute solution and in a polycrystalline solid film at room temperature is presented. Also a member of the rylene family, DIP's molecular structure is very similar to that of peropyrene (**PP**), introduced and discussed in Chapter 3. In light of **α-PP's** inability to undergo sinlget fission (SF) most likely due to its excimer forming crystal packing structure (pair-wise herringbone), **DIP** offers a more desirable edge-to-face herringbone crystal packing motif (see Figure 4.1 for molecular structure and crystal packing comparison of **PP** and **DIP**). In solution, **DIP** undergoes internal conversion back to the ground state on a subnanosecond timescale. This rapid internal conversion, seen in other acene molecules that incorporate a five-membered ring, has been attributed to a lack of resonance stabilization.[1-2] In solid form, **DIP** exhibits a complex decay that involves multiple emitting species. The time-resolved photoluminescence (PL) signal is dominated by the intrinsic exciton decay on a timescale of 170 ps. Emission from lower energy excimer-like species then persists for >10 ns. These results suggest that despite its herringbone crystal motif, **DIP** does not support phenomena like long-lived singlet exciton states (anthracene[3-4]) or singlet fission (as in crystalline perylenes[5-6], tetracene[7-8] and pentacene[9-11]) seen in crystals with similar packing

72

motifs Instead, rapid internal conversion leads to transient heating, with a small fraction (<10%) of the excitons surviving in longer-lived trap or defect states. It is hypothesized here that **DIP**'s success in organic photovoltaic applications stems largely from its ordered packing in thin films and high charge carrier mobilites, as opposed to excitonic contributions.
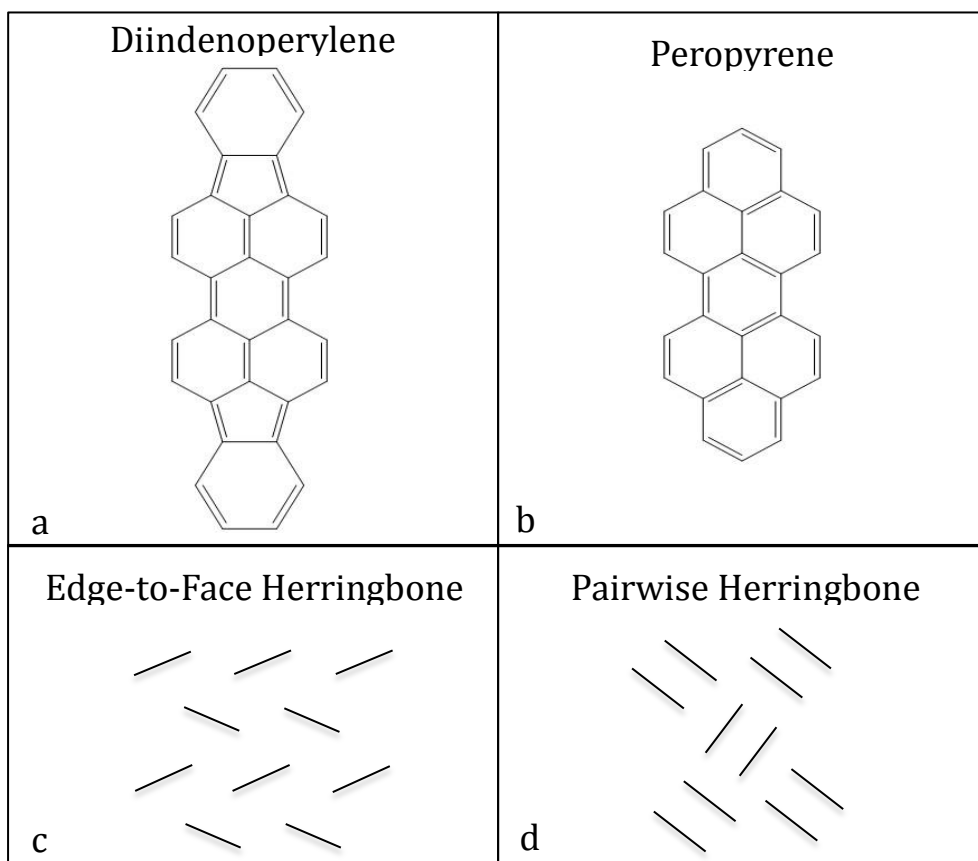
Figure 4.1 Molecular structures of Diindenoperylene (a) and Peropyrene (b) above the corresponding crystal packing structure of each: DIP's Edge-to-Face Herringbone motif (c) and Peropyrene's Pairwise Herringbone motif (d).
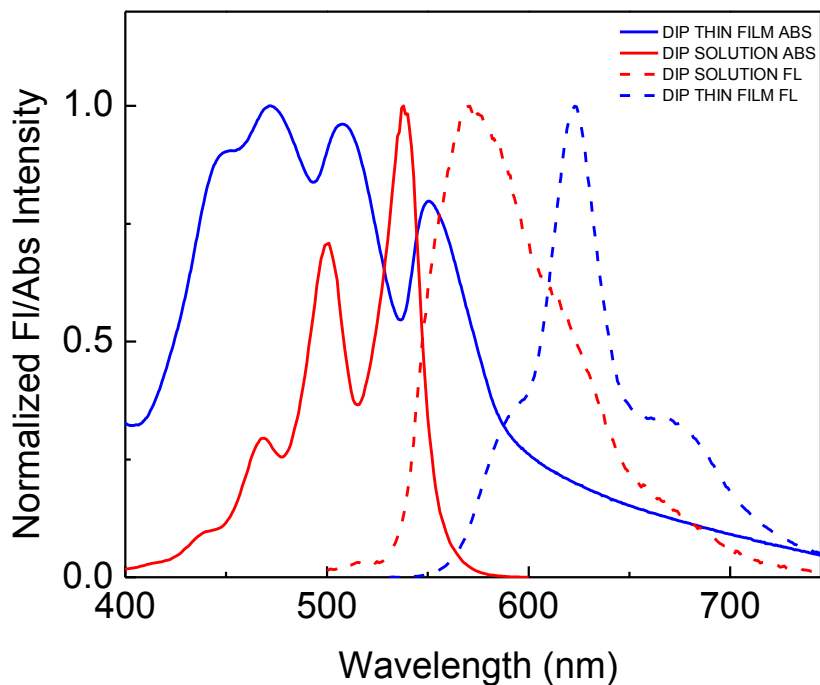
Figure 4.2 Absorption (solid) and fluorescence (dotted) spectra of DIP monomer in benzene (red) and 100 nm thick thin films (blue).

4.2. Monomeric Steady State and Time Resolved Absorption and Fluorescence

The absorption lineshape of **DIP** in solution has a vibronic progression that resembles those of smaller members of the rylene family, like perylene and peropyrene.[12] But the increased conjugation leads to a redshift of about 100 nm relative to those molecules, with the lowest energy peak at 540 nm. A more profound difference is that **DIP**'s fluorescence spectrum does not mirror its absorption but is broadened with a different vibronic intensity pattern (Figure 4.2). Lohmansroben and coworkers deduced that the emitting state was different from the absorbing state, with a lower oscillator strength that leads to a radiative lifetime of 58 ns.[13] This state also has a low fluorescence quantum yield, on the

order of 1-2%. This low yield results from a rapid fluorescence decay. Figure 4.3 shows the fluorescence decay in two solvents with different polarities: cyclohexane and chlorobenzene. The fluorescence decay was single exponential on all timescales with a lifetime of 0.890 ns in all solvents tested, in good agreement with the value measured by Lohmansroben and coworkers.[13]

Figure 4.3 Normalized fluorescence intensity of DIP in chlorobenzene (blue) and cyclohexane (red) exhibits a single exponential fluorescence lifetime of 890 ps in both solvents.

4.3. Monomeric Femtosecond Transient Absorption

Lohmansroben and coworkers attributed the short fluorescence lifetime to rapid internal conversion.[13] To confirm this, femtosecond transient absorption spectroscopy is used to see 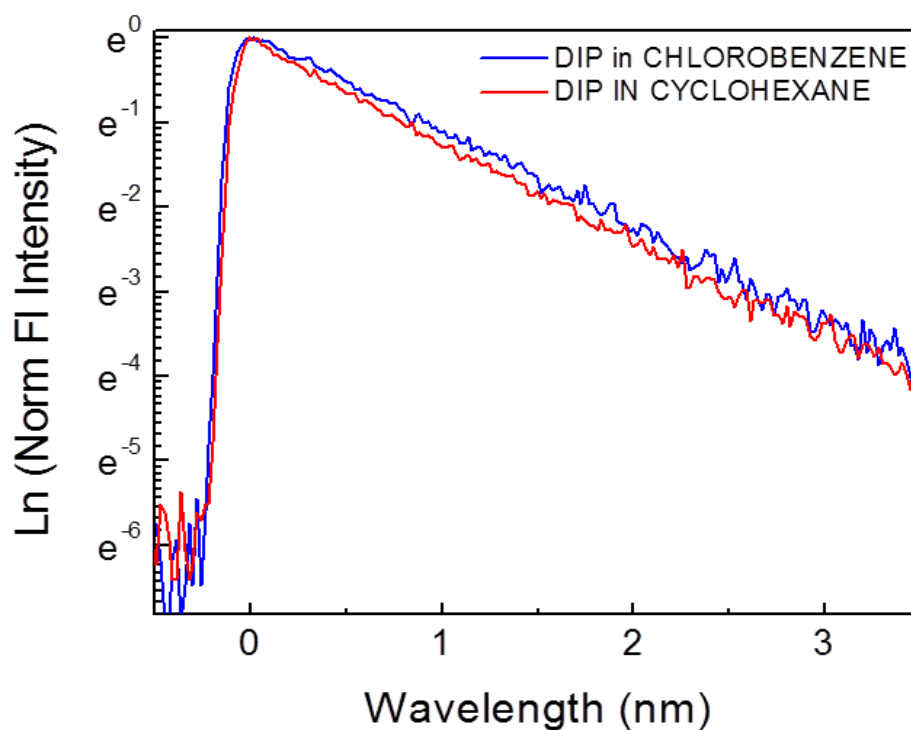if there was any evidence for the formation of any other species (triplet, charge-transfer state) during the decay of the singlet state. These experiments were challenging due to the low solubility of **DIP** in common solvents, and benzene was eventually chosen to provide the highest concentration of 10^{-5} M. Figure 4.4a shows the transient spectra at delays of 1 ps, 500 ps, 1 ns and 7 ns. At 1 ps, the negative bleach signal at 540 nm overlaps a large induced absorption stretching from 600 nm well into the near-infrared. The time resolution of these experiments was limited to ~500 fs, and there is no further evolution of the TA spectrum after the pump pulse has finished interacting with the sample. Thus the relaxation from the initially excited bright state into the less emissive state that dominates the PL behavior must be complete within 1 ps. Note that this relaxation could not be resolved in the PL measurements due to the 15 ps time resolution of the streak camera system. After 1 ps, both the negative and positive TA signals decay with the same rate, and there is no sign of any new spectral features growing in. By 7 ns, there is no detectable TA signal, indicating that all the **DIP** molecules return to their ground state without forming long-lived intermediates. Given the triplet absorption coefficient is on the order of 40000 $M^{-1}cm^{-1}$, even a few percent of this species should be able to be detected, if it were formed.[13] The TA delay line limited the

time range over which the TA decays could be directly measured, but over this limited time range, at all probe wavelengths, it was found that the TA signal could be fit using a single exponential with a time constant fixed to 890 ps, the value extracted from the PL decays (Figure 4.5).

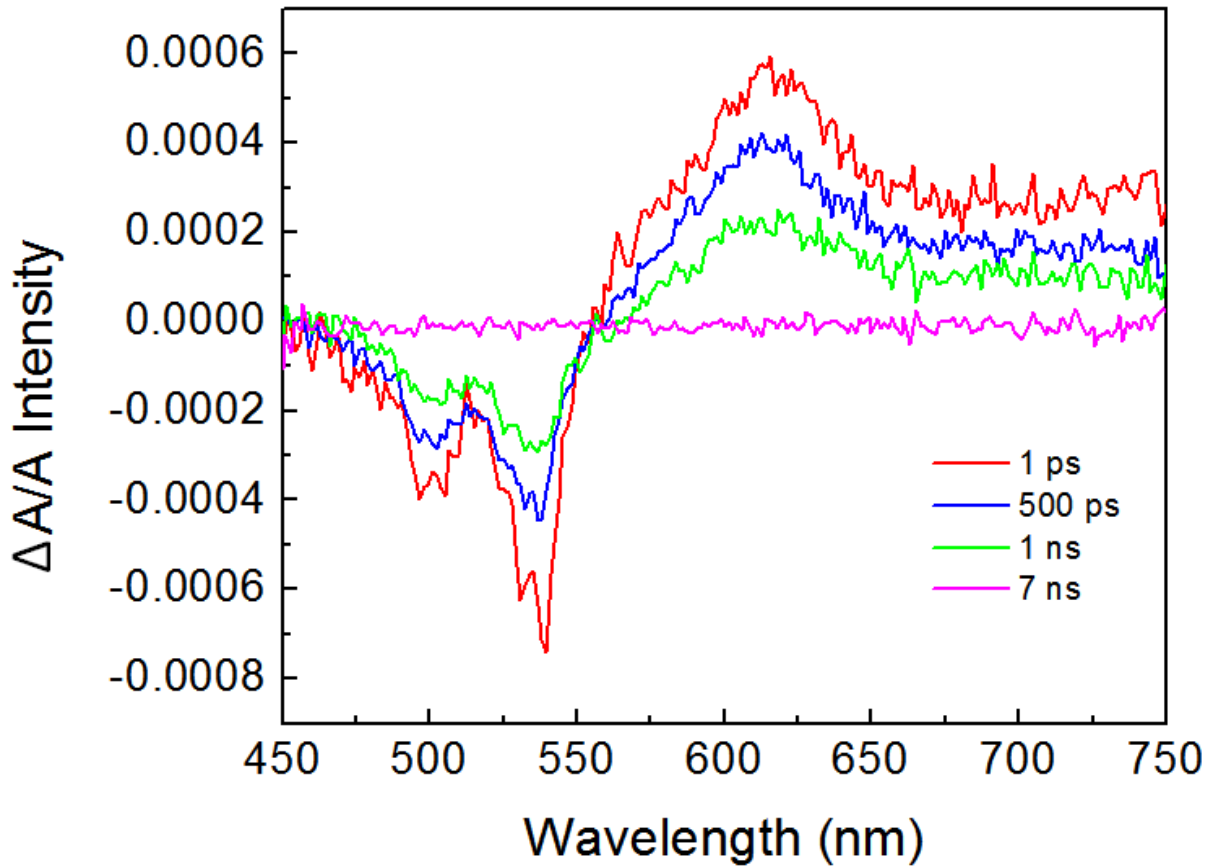**Figure 4.4** Transient absorption spectra $\Delta A/A$ of 100 nm thick DIP crystalline thin film at 1 ps (red), 500 ps (blue), 1 ns (green), and 7 ns (pink).
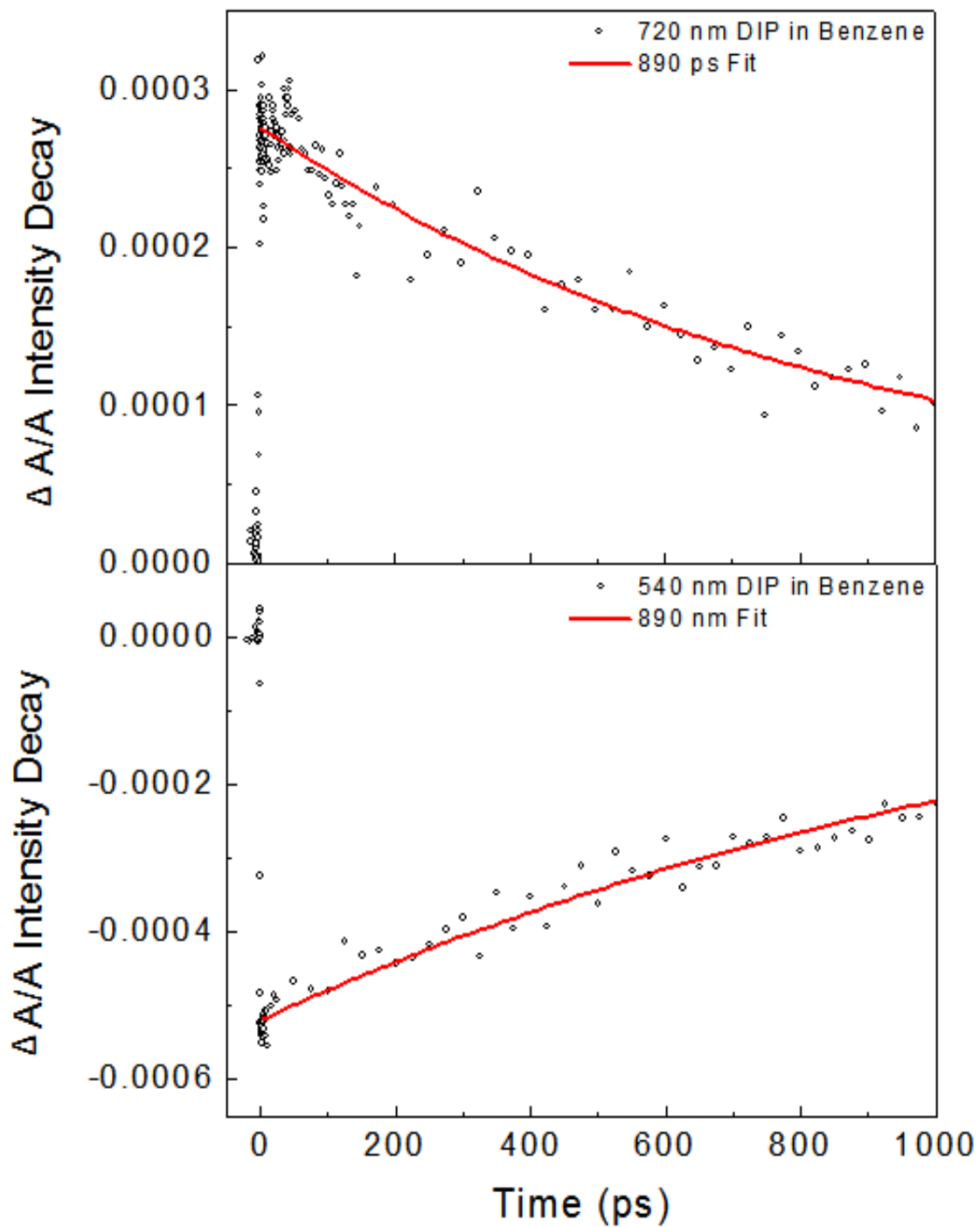
Figure 4.5 Decays of transient absorption signal (open circles) at 720 nm (top) and 520 nm (bottom) of DIP in benzene. Each is fit to a single exponential decay (red lines) of 890 ps – agreeing well with fluorescence lifetime data.

78

4.4. Thin Film Femtosecond Time Resolved Fluorescence

In solution, **DIP**'s photophysical behavior is determined by two sequential internal conversion processes. First, the initially excited singlet state quickly (<1 ps) relaxes to the lower lying singlet state. This state then relaxes back to the ground state within a nanosecond via a second internal conversion process. Some hint of a rapid, pulsewidth-limited decay can be seen in the TA trace in Figure 4.5b, which probably reflects the subpicosecond relaxation to the lower singlet state. This state then relaxes back to the ground state via a second internal conversion process with the characteristic 890 ps decay time as determined by fitting the data in Figure 4.5. The behavior of this molecule is similar to that of well-studied polyene systems in which the emission also takes place from a low-lying state, close in energy to the strongly allowed ^{1}Bu state but possessing a much smaller transition dipole moment.[14-15] Once **DIP** crystallizes into solid form, however, its excited state behavior changes significantly. The absorption and fluorescence spectra of solid **DIP** are clearly different from those of **DIP** in dilute solution, as can be seen from Figure 4.2. The absorption and PL spectra of **DIP** are both redshifted from those in solution. The absorption retains three distinct vibronic peaks, located at 560 nm, 520 nm, and 480 nm, but they are broadened by at least a factor of 2. The relative intensities of these peaks are similar, in contrast to the well-defined Franck-Condon progression seen in the monomer. The PL spectrum also retains features that can be associated with vibronic structure, but whose relative intensities are completely different from

those of the monomer.[16] The change in vibronic lineshape can be taken as evidence for the formation of intermolecular exciton states.[17] The side-by-side herringbone packing motif, coupled with orientation of the transition dipole along the long axis of the molecule, would be expected to result in H-type aggregate states similar to what is observed in the oligothiophenes.[18-19] In H-type aggregates, it is expected to see a 0-0 peak that is reduced in intensity from the monomer, as observed experimentally.[20] However, as shown below, the steady-state PL actually consists of contributions from multiple emitting states. Because of these varied contributions, a detailed lineshape analysis to determine the exact nature of the exciton state was not performed.

Heilig et al. studied the PL behavior of **DIP** thin films and deduced the presence of multiple emitting species with lifetimes ranging from less than 30 ps to 6.4 ns.[21] They found that the PL decay at 300 K consisted of two components: an excitonic state with a lifetime of ~100 ps and a redshifted, unstructured emission with an undetermined lifetime. In this work, the room temperature behavior is focused on using a streak camera to measure the PL dynamics. As shown in Figure 4.6, the picosecond time-resolved PL experiments gave rise to multiexponential decays at all wavelengths, indicating the presence of several different emitting populations In the 1 ns window, we found that ~70% of the singlet decayed with a 166 ps time constant, with an additional ~30% component with a time constant of 1.1 ns. Using a longer 20 ns time window (inset to Figure 4.6), we also identified a 6.4 ns decay component that has an amplitude of a few

percent of the total.   The bulk of the PL signal (~80%) decays within 1 ns (Figure 4.6, inset).   There was not any growth in the PL signal at longer wavelengths seen that would indicate that the initial excited state population is relaxing to lower energy emissive states, e.g. trapping to excimer sites. Instead, the different emitting states appear to decay independently.

The bright initial exciton state must relax either back to the ground state or to a dark excited state. One candidate for such a dark state is the triplet exciton, which could be formed by either rapid intersystem crossing or by singlet fission (SF). Since 166 ps is very rapid for intersystem crossing in the absence of heavy atoms, SF would be the most likely mechanism for rapid triplet formation.[22-23] The
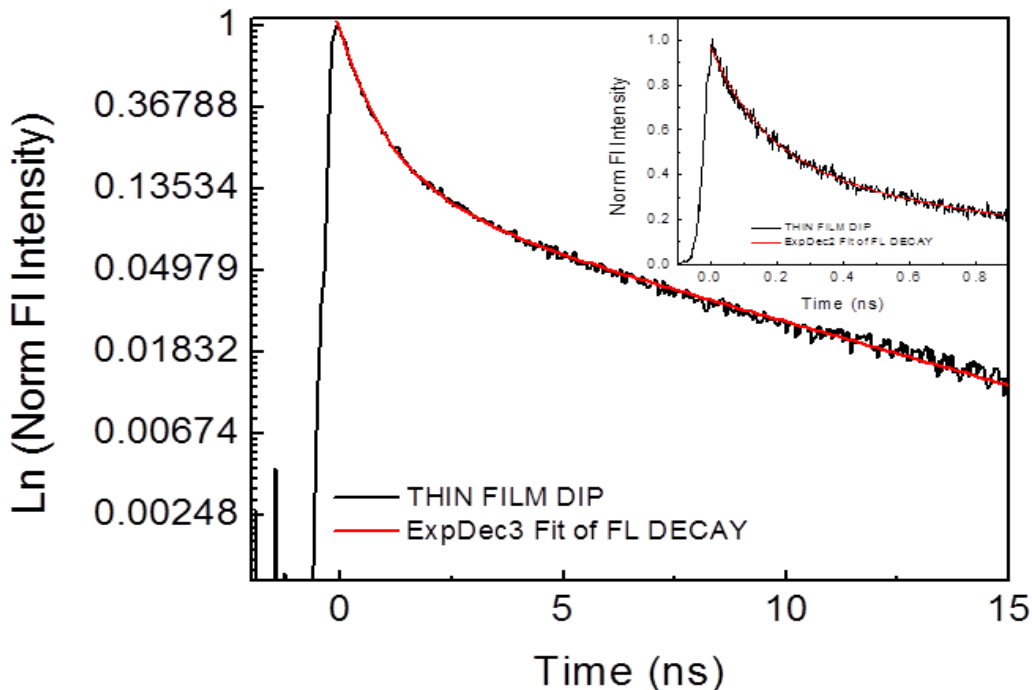

Figure 4.6 Normalized fluorescence decay of 100 nm thick DIP thin film over 15 ns on a natural log scale. Inset plot shows 80% intensity loss within the first nanosecond of fluorescence decay.

overall profile of the decay curve in Figure 4.6 is reminiscent of the behavior of solid tetracene, where SF leads to a prompt fluorescence decay followed by a much longer-lived delayed fluorescence.[8] Given the similarity of their crystal packing, it was suspected that SF might play some role in the singlet relaxation in **DIP**. But when the PL decay of **DIP** was analyzed in detail, clear differences emerge between the behavior of the two crystals. First, the slow component in tetracene is true delayed fluorescence, where the later time spectrum is identical to that of the prompt fluorescence. This is not the case for **DIP**, where the PL evolves to be dominated by a low energy peak, as shown in Figure 4.7. In tetracene, the delayed fluorescence arises from a dark triplet population that is interconverting with the bright singlets. The role of the triplet makes the fluorescence decay susceptible to the influence of a magnetic field.[24-25] It was found that application of magnetic fields up to 7000 Gauss had no observable effect on the **DIP** fluorescence decay. Finally, a strong intensity dependence of the long-lived component of the decay was not observed, which would have been expected if it really results from a bimolecular recombination of triplet excitons. The decay of the delayed fluorescence in tetracene, on the other hand, does show a pronounced intensity dependence.[26-27] SF in **DIP** would be significantly more uphill energetically than that in tetracene, since $2E(T_1)-E(S_1)=2050$ cm^{-1} for the molecule in solution.[13] It may be that the energy barrier is sufficient to prevent SF in **DIP**, although the spectral lineshapes (and thus the electronic

structure of the singlet excitons) also appear to be quite different from those observed in crystalline tetracene.
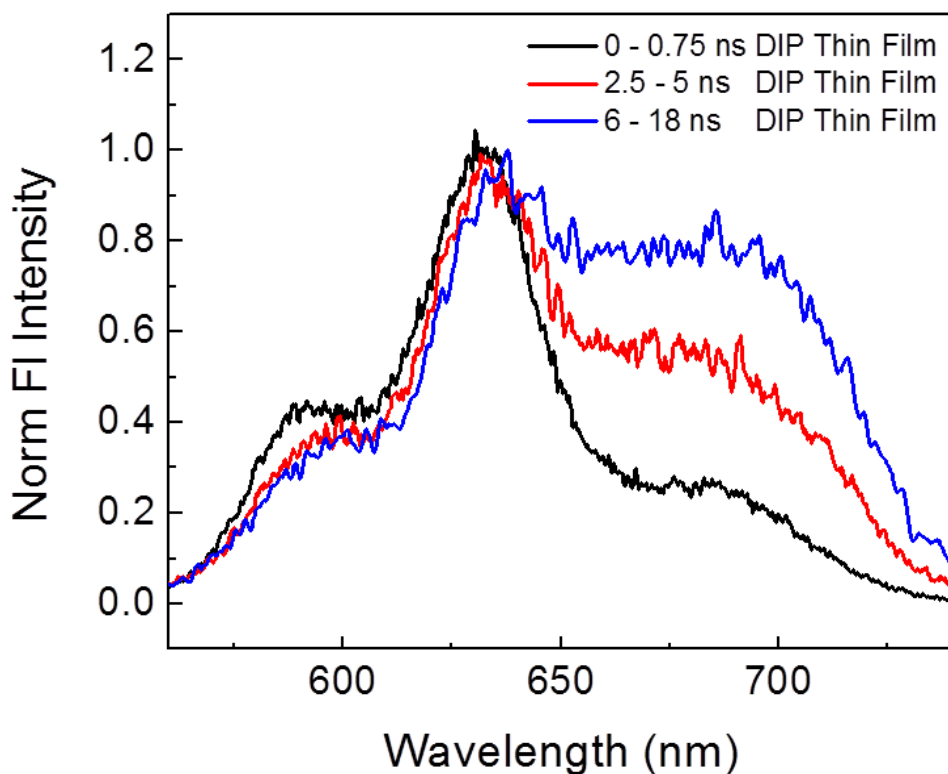
Figure 4.7 Normalized fluorescence spectra of DIP thin film integrated from 0 – 0.75 ns (black line), 2.5 – 5 ns (red line), and 6 – 18 ns (blue line) showing a red shift at later times.

Since triplet formation and delayed fluorescence can be ruled out, the long-lived PL must originate from other singlet species. The broad peak at 690 nm that is prominent at later times in Figure 4.7 strongly suggests that the bulk of the long-lived states are excimers. The herringbone packing in a pristine DIP crystal would seem to preclude excimer formation, but structural defects can give rise to cofacial molecular arrangements that enable excimer formation, as

observed in other herringbone crystals like anthracene.[3,28-29] The lack of a pronounced rise time for the 690 nm feature suggests that the excimer emission arises from defect sites within the films that are directly excited by the laser.

4.5. Thin Film Femtosecond Transient Absorption

In order to probe the ultimate fate of the **DIP** excited state population, femtosecond TA experiments were needed. These experiments again suffered from low signal levels. **DIP** tends to crystallize with its long axis close to perpendicular to the growth substrate.[30] Since its transition dipole moment is parallel to its long molecular axis, it cannot couple well to the incoming light field whose polarization is perpendicular to the surface normal. Nevertheless, TA signals were obtained at relatively high pump pulse fluences. At these fluences, clear evidence for exciton-exciton annihilation on the picosecond timescale can be seen. Figure 4.8 shows the normalized decays of the **DIP** TA induced absorption signal, integrated over the range 650-750 nm. The initial decay become much more rapid as the excitation density is increased from 10^{18} cm^{-3} to 10^{19} cm^{-3}. By using a simple model for the exciton–exciton annihilation,[27,31] an expression can be derived for the decay of the singlet population, $n_S(t)$:

$$\frac{\partial n_S}{\partial t} = -k_S n_S - k_{ee} n_S^2 \qquad (1)$$

$$n_S(t) = \left[-\frac{k_{ee}}{k_S} + \left(\frac{1}{n_S(0)} + \frac{k_{ee}}{k_S} \right) e^{k_S t} \right] \qquad (2)$$

Where k_S is the intrinsic singlet decay rate and k_{ee} is the exciton-exciton annihilation rate. If $1/k_S$ is fixed to be 170 ps, the value obtained from the early

time PL decay, the curves in Figure 4.8 can be fit with k_{ee} = 2x10^{-9} cm^3/s. This value of k_{ee} is almost a factor of 5 smaller than that obtained for crystalline tetracene and β-perylene using a similar analysis.[27,32] The small value of k_{ee} was surprising in light of the large exciton diffusion lengths reported for **DIP**, since k_{ee} should be directly proportional to the exciton diffusion constant.[33] However, in tetracene the singlet exciton is J-type[34-36], while in **DIP** it appears to be H-type. It is possible that the reduced oscillator strength of the H-type exciton either reduces its energy transfer rate or its radius of interaction. If this is the case, **DIP** would provide a good example of how exciton-exciton annihilation can be affected by the exciton's electronic structure.
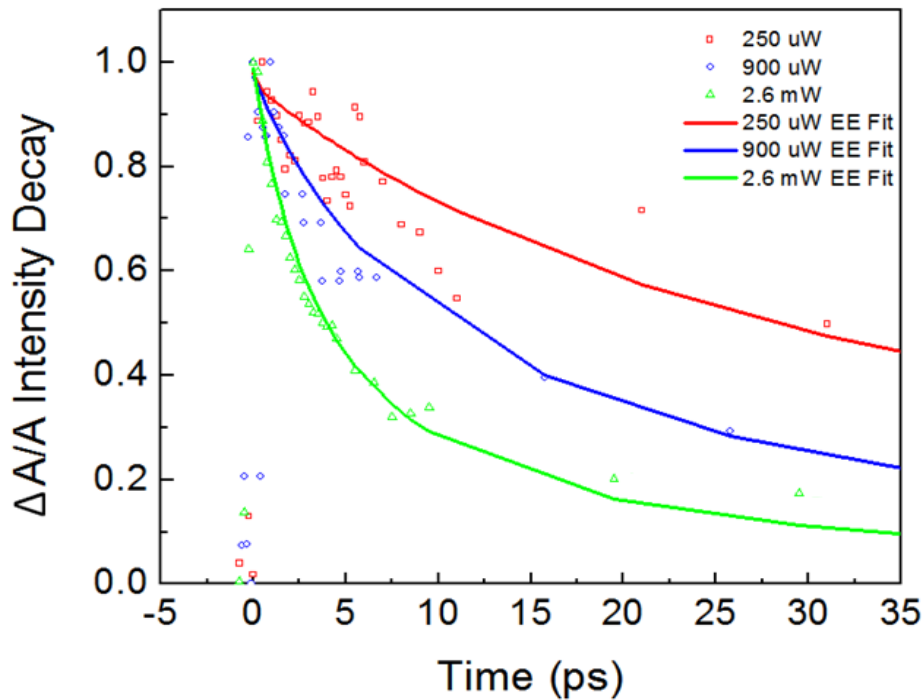
Figure 4.8 Early time transient absorption signal decays of DIP thin film integrated from 650 – 750 nm measured at three different powers at the sample: 250 uW (red open squares), 900 uW (blue open circles), and 2.6 mW (green open triangles). Overlayed in corresponding colors are exciton-exciton annihilation fits with kee = 2x10-9 cm3/s (see Equation 2).

Once singlet exciton-exciton annihilation is taken into account, the subsequent evolution of the TA data is straightforward to analyze. The data at all wavelengths can be fit using a single exponential decay with a time constant τ_S = 170 ps and a constant offset. The necessity of the offset can be seen from the spectral data shown in Figure 4.9. At a delay of 1 ps, the signal is dominated by a broad induced absorption overlaid with sharp features located at 550 nm, 520 nm and 480 nm, which is assigned to the S_0-S_1 bleach. The absorption decays with a time constant of τ_S = 170 ps, but at a delay of 1 ns, the remaining signal has both positive and negative features that remain constant. The negative peaks at 550 nm, 510 nm and 480 nm are close to the peaks in the steady-state absorption spectrum in Figure 4.2, but are slightly blue-shifted. Furthermore, there are positive peaks between the negative peaks, and the signal overall has a derivative appearance rather than a well-defined excited state absorption feature.

Figure 4.9 Transient absorption spectra of DIP thin film at 0 ps (black), 1 ps (red), and 1 ns (blue).

4.6. Nonradiative Heating Effects on Thin Film Absorption Spectrum

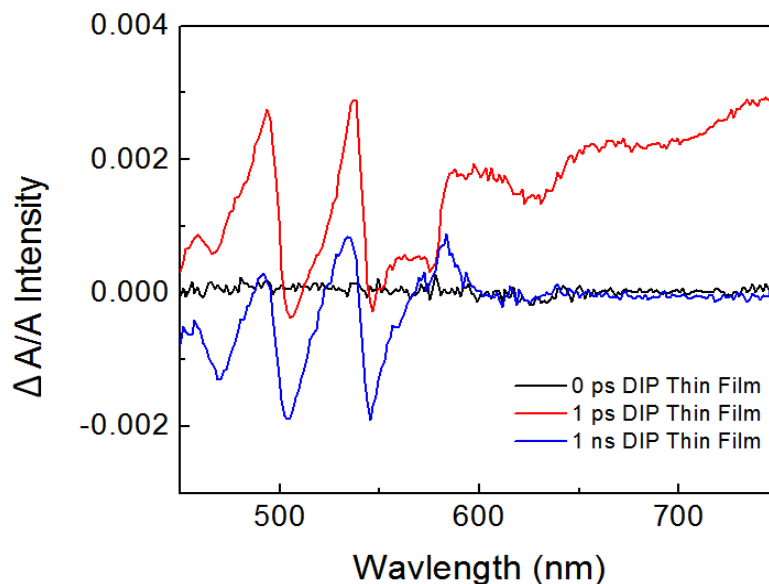There are two possible explanations to be considered for the behavior of the TA spectrum at long delays. The first possibility is that the overlap of the bleach and the TA spectrum of a long-lived excited state produced by relaxation of the singlet can be observed. In this case, the S_0-S_1 and the long-lived state absorption spectrum would have to overlap almost perfectly. The complete lack of absorption in the near infrared region would argue against these long-lived states being excimers or other types of charge-transfer states.[37] Since these time-resolved PL experiments also show no evidence for a large triplet population, the identity of this dark state is a bit of a mystery.

On the other hand, the 1 ns TA spectrum bears a strong resemblance to what has been seen in polycrystalline pentacene films after 400 nm excitation. This derivative-like bleach feature has been assigned this lineshape to a nonequilibrium heating effect rather than to overlapping bleach and excited state absorption features.[38-39] The basic idea is relatively simple. After the molecules relax nonradiatively, they deposit considerable energy into their environment and the local temperature can be much greater than the ambient temperature. The higher temperature typically leads to a blueshift of the S_0-S_1 absorption spectrum. The differential absorption signal measures the difference between a cold (pump pulse off) and hot (pump pulse on) ground state absorption, even in the absence of any excited state population. If it is assumed that the entire energy of a 400 nm photon is temporarily localized within a region of 10 molecules, and assuming

a heat capacity of 300 J/mol K[40], a local temperature rise on the order of 100-200 K can be estimated. The absorption spectrum of a **DIP** thin film at elevated temperatures was taken, with the results shown in Figure 4.10a. The difference can be taken of the appropriately scaled 450 K and 300 K absorption spectra and compare it to the 1 ns TA spectrum. The two spectra are overlaid in Figure 4.10b. The qualitative similarity of the two spectra suggests that a significant portion of the TA spectrum results from hot ground state. By the same token, if the difference of the TA signal and the bleach signal calculated from the 300 K absorption spectrum had been taken in order to obtain the induced absorption of the purported long-lived state, a spectrum very similar to the 450 K absorption would have been obtained, i.e. a shifted and broadened version of the 300 K absorption spectrum. This was in fact the first approach to analyzing the data, and it was the similarity of the S_0-S_1 spectrum and calculated excited state spectrum that motivated reanalyzing the TA data in terms of thermal effects. It should be emphasized that the estimate of a 150 K temperature jump is based on a qualitative comparison of the TA and absorption spectra and has considerable uncertainty. But this temperature rise is well within the range observed in other solid-state systems with chromophores that undergo rapid internal conversion.[41-42] The transformation of photon energy into heat is a highly localized and transient process, since over the course of a few ns the heat will diffuse into the bulk sample, leading to a much smaller overall temperature rise. Typically even large transient temperature jumps do not lead to permanent

sample damage.[43]   Furthermore, DIP thin films on gold have been found to be stable under sustained heating up to 150 °C[44], comparable to our estimated temperature jump. In our TA experiments, no permanent changes in the optical properties of the samples were observed. The main effect of the heating is to generate a transient hot ground state absorption that makes it difficult to extract quantitative information on residual long-lived excited states.
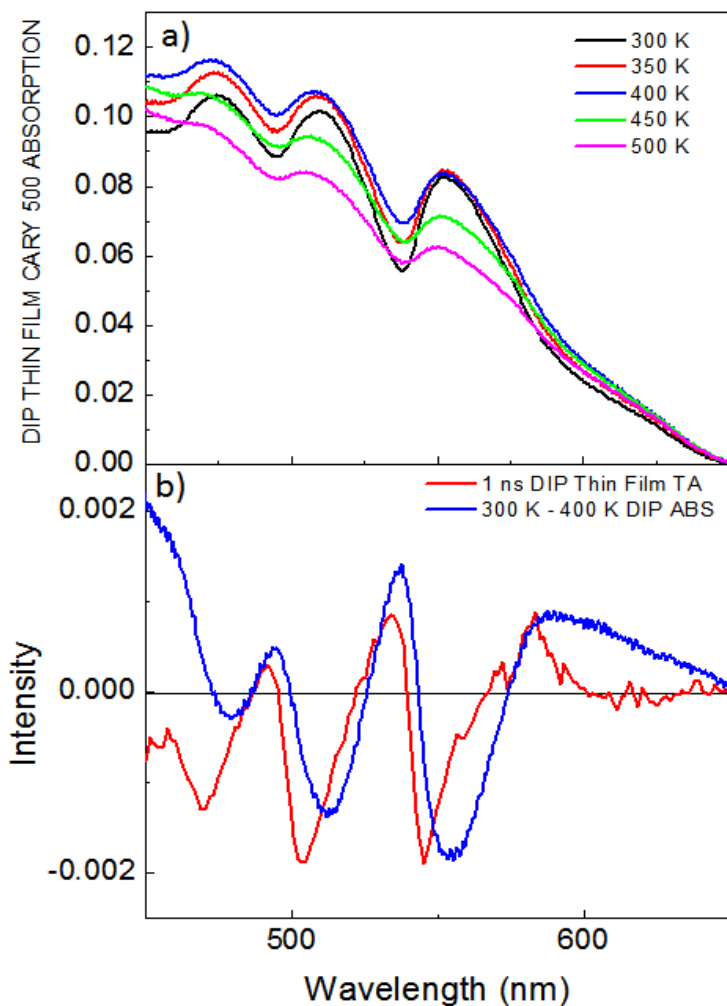

Figure 4.10 Absorption spectra of DIP thin film at temperatures ranging from 300 – 500 K (a, top). The difference spectrum between 400 K and 300 K absorption spectra overlaid with the 1 ns transient absorption spectrum of DIP thin film (b, bottom).

4.7. Comparison with Literature and Implications for Device Dynamics

These experimental results on solid **DIP** merit some discussion. First, the internal conversion process that returns the singlet excited state back to the ground state can be considered. If it is the same mechanism as for isolated **DIP** molecules in solution, then it must be accelerated by a factor of 5 in the solid film. But since molecular internal conversion is expected to be hindered in a constrained crystal environment, it is possible that this mechanism is no longer operative in the solid-state. Theoretical work by Settels et al. has identified an alternative mechanism in which dimer states have conical intersections that can provide fast pathways back to S_0.[45] They found that this mechanism was not effective in a pristine **DIP** crystal, but that it was very sensitive to intermolecular geometries and could become important at grain boundaries or defects. Rapid migration of the initially created excitons to such sites, followed by internal conversion, could provide a physical explanation for the observed internal conversion. No evidence could be found for a significant singlet relaxation channel leading to a different type of long-lived state, like a triplet or charge-separated state. The PL data clearly show that there is a population of long-lived states that can survive for 10 ns or longer. But it is likely that these long-lived emissive species represent only a small fraction of the total excitations. If all the emitting species have similar radiative rates, making the amplitudes of the different exponential decays proportional to their associated populations, then they comprise 10% or less of the total excitations.

Rapid internal conversion would suggest that singlet excitons do not have the opportunity to diffuse over long distances before they relax back to the ground state. If this is the case, however, it is hard to understand the large (10-100 nm) exciton diffusion lengths reported for **DIP**.[46-48] It is possible that the long-lived species observed in the PL data may be responsible for photocurrent generation in organic photovoltaic devices. However, recent studies of **DIP**-C_{60} bilayer organic photovoltaics suggested that that photoexcitation of the electron acceptor C_{60}, plays an important role in generating photocurrent in these devices.[49-50] This is consistent with this work's spectroscopic results showing that most photoexcited **DIP** molecules relax back to the ground state within a few hundred picoseconds. Photoexcited C_{60} molecules, on the other hand, can undergo rapid intersystem crossing to form long-lived triplet excitons that can diffuse over 30 nm.[51-52] **DIP** may be most useful as a charge transporting medium and perhaps also as a way to induce order in neighboring thin films composed of other molecules, rather than as a source of ionizable mobile excitons.

4.8 Conclusion

The photophysical dynamics of the organic semiconductor molecule **DIP** in both dilute solution and in solid films have been studied. By itself, **DIP** in its excited singlet state undergoes a rapid (0.89 ns) internal conversion back to its ground state. In solid form, multiple excited state species are formed with lifetimes ranging from 170 ps to 6.5 ns. TA experiments indicate that the majority

of the excited state population undergoes internal conversion to form a hot ground state, leaving a minority of lower energy, longer–lived states. These results imply that despite its herringbone packing motif and high degree of crystalline order, **DIP** is not an ideal material to generate excitons in OPV devices. It is possible that chemical substitution could improve its excited state lifetime while retaining its stability and crystalline order.

REFERENCES

1. Tucker, S. A.; Bates, H. C.; Amszi, V. L.; Acree, W. E.; Lee, H.; Raddo, P. D.; Harvey, R. G.; Fetzer, J. C.; Dyker, G., Spectroscopic properties of polycyclic aromatic compounds. Part II. Fluorescence emission and quenching behavior of select acenaphthylene derivatives in organic nonelectrolyte solvents. *Anal. Chim. Acta* **1993,** *278*, 269-274.

2. Dunsbach, R.; Schmidt, R., Photophysical properties of some polycyclic conjugated hydrocarbons containing five-membered rings. *J. Photochem. Photobiol. A* **1994,** *83*, 7-13.

3. Ahn, T. S.; Muller, A. M.; Al-Kaysi, R. O.; Spano, F. C.; Norton, J. E.; Beljonne, D.; Bredas, J. L.; Bardeen, C. J., Experimental and theoretical study of temperature dependent exciton delocalization and relaxation in anthracene thin films. *J. Chem. Phys.* **2008,** *128*, 054505/1-054505/11.

4. Katoh, R.; Suzuki, K.; Furube, A.; Kotani, M.; Tokumaru, K., Fluorescence quantum yield of aromatic hydrocarbon crystals. *J. Phys. Chem. C* **2009,** *113*, 2961-2965.

5. Albrecht, W. G.; Coufal, H.; Haberkorn, R.; Michel-Beyerle, M. E., Excitation spectra of exciton fission in organic crystals. *Phys. Stat. Sol. B* **1978,** *89*, 261-265.

6. Eaton, S. W.; Shoer, L. E.; Karlen, S. D.; Dyar, S. M.; Margulies, E. A.; Veldkamp, B. S.; Ramanan, C.; Hartzler, D. A.; Savikhin, S.; Marks, T. J.; Wasielewski, M. R., Singlet exciton fission in polycrystalline thin films of a slip-stacked perylenediimide. *J. Am. Chem. Soc.* **2013,** *135*, 14701-14712.

7. Swenberg, C. E.; Stacy, W. T., Bimolecular radiationless transitions in crystalline tetracene. *Chem. Phys. Lett.* **1968,** *2*, 327-328.

8. Burdett, J. J.; Bardeen, C. J., The dynamics of singlet fission in crystalline tetracene and covalent analogs. *Acc. Chem. Res.* **2013,** *46*, 1312-1320.

9. Jundt, C.; Klein, G.; Sipp, B.; Moigne, J. L.; Joucla, M.; Villaeys, A. A., Exciton dynamics in pentacene thin films studied by pump-probe spectroscopy. *Chem. Phys. Lett.* **1995,** *241*, 84-88.

10. Rao, A.; Wilson, M. W. B.; Hodgkiss, J. M.; Albert-Seifried, S.; Bassler, H.; Friend, R. H., Exciton fission and charge generation via triplet excitons in pentacene/C60 bilayers. *J. Am. Chem. Soc.* **2010,** *132*, 12698-12703.

11. Wilson, M. W. B.; Rao, A.; Clark, J.; Kumar, R. S. S.; Brida, D.; Cerullo, G.; Friend, R. H., Ultrafast dynamics of exciton fission in polycrystalline pentacene. *J. Am. Chem. Soc.* **2011,** *133*, 11830-11833.

12. Nichols, V. M.; Rodriguez, M. T.; Piland, G. B.; Tham, F.; Nesterov, V. N.; Youngblood, W. J.; Bardeen, C. J., Assessing the potential of peropyrene as a singlet fission material: photophysical properties in solution and in the solid state. *J. Phys. Chem. C* **2013,** *117*, 16802-16810.

13. Schael, F.; Lohmannsroben, H.-G., Photophysical properties of the non-alternant polycyclic aromatic hydrocarbons periflanthene and 1,16-benzoperiflanthene in solution *J. Photochem. Photobiol. A* **1992,** *69*, 27-32.

14. Kohler, B. E.; Spiglanin, T. A., Structure and dynamics of excited singlet states of isolated diphenylhexatriene. *J. Chem. Phys.* **1984,** *80*, 5465-5471.

15. Jailaubekov, A. E.; Vengris, M.; Song, S.-H.; Kusumoto, T.; Hashimoto, H.; Larsen, D. S., Deconstructing the excited-state dynamics of β-carotene in solution. *J. Phys. Chem. A* **2011,** *115*, 3905-3916.

16. Zhang, D.; Horneber, A.; Mihaljevic, J.; Heinemeyer, U.; Braun, K.; Schreiber, F.; Scholz, R.; Meixner, A. J., Plasmon resonance modulated photoluminescence and Raman spectroscopy of diindenoperylene organic semiconductor thin film. *J. Lumin.* **2011,** *131*, 502-505.

17. Heinemeyer, U.; Scholz, R.; Gisslen, L.; Alonso, M. I.; Osso, J. O.; Garriga, M.; Hinderhofer, A.; Kytka, M.; Kowarik, S.; Gerlach, A.; Schreiber, F., Exciton-phonon coupling in diindenoperyelen thin films. *Phys. Rev. B* **2008,** *78*, 085210-1/085210-10.

18. Meinardi, F.; Cerminara, M.; Sassella, A.; Borghesi, A.; Spearman, P.; Bongiovanni, G.; Mura, A.; Tubino, R., Intrinsic exciton luminescence in odd and even numbered oligothiophenes. *Phys. Rev. Lett.* **2002,** *89*, 157403-1/157403/4.

19. Spano, F. C., Excitons in conjugated oligomer aggregates, films and crystals. *Ann. Rev. Phys. Chem.* **2006,** *57*, 217-243.

20. Spano, F. C., The spectral signatures of Frenkel polarons in H- and J-aggregates. *Acc. Chem. Res.* **2010,** *43*, 429-439.

21. Heilig, M.; Domhan, M.; Port, H., Optical properties and morphology of thin diindenoperylene films. *J. Lumin.* **2004,** *110*, 290-295.

22. Pope, M.; Swenberg, C. E., *Electronic processes in organic crystals and polymers*. Oxford University Press: New York, 1999.

23. Smith, M. B.; Michl, J., Singlet fission. *Chem. Rev.* **2010,** *110*, 6891-6936.

24. Geacintov, N.; Pope, M.; Vogel, F., Effect of magnetic field on the fluorescence of tetracene crystals: exciton fission. *Phys. Rev. Lett.* **1969,** *22*, 593-596.

25. Burdett, J. J.; Piland, G. B.; Bardeen, C. J., Magnetic field effects and the role of spin states in singlet fission. *Chem. Phys. Lett.* **2013,** *585,* 1-10.

26. Burdett, J. J.; Muller, A. M.; Gosztola, D.; Bardeen, C. J., Excited state dynamics in solid and monomeric tetracene: the roles of superradiance and exciton fission. *J. Chem. Phys.* **2010,** *133*, 144506/1-144506/12.

27. Burdett, J. J.; Gosztola, D.; Bardeen, C. J., The dependence of singlet exciton relaxation on excitation density and temperature in polycrystalline tetracene thin films: Kinetic evidence for a dark intermediate state and implications for singlet fission. *J. Chem. Phys.* **2011,** *135*, 214508/1-214508/10.

28. Fielding, P. E.; Jarnagin, R. C., "Excimer" and "Defect" Structure for Anthracene and Some Derivatives in Crystals, Thin Films, and Other Rigid Matrices. *J. Chem. Phys.* **1967,** *47*, 247-252.

29. Horiguchi, R.; Iwasaki, N.; Maruyama, Y., Time-Resolved and Temperature-Dependent Fluorescence Spectra of Anthracene and Pyrene in Crystalline and Liquid States. *J. Phys. Chem.* **1987,** *91*, 5135-5139.

30. Huang, Y. L.; Chen, W.; Huang, H.; Qi, D. C.; Chen, S.; Gao, Y. Y.; Pflaum, J.; Wee, A. T. S., Ultrathin films of diindenoperylene on graphite and SiO_2. *J. Phys. Chem. C* **2009,** *113*, 9251-9255.

31. Campillo, A. J.; Hyer, R. C.; Shapiro, S. L.; Swenberg, C. E., Exciton interactions in crystalline tetracene studied by single picosecond pulse excitation. *Chem. Phys. Lett.* **1977,** *48*, 495-500.

32. Yago, T.; Tamaki, Y.; Furube, A.; Katoh, R., Self-trapping limited exciton diffusion in a monomeric perylene crystal as revealed by femtosecond laser absorption microscopy. *Phys. Chem. Chem. Phys.* **2008,** *10*, 4435-4441.

33. Greene, B. I.; Millard, R. R., Singlet-exciton fusion in molecular solids: a direct subpicosecond determination of the time-dependent annihilation rates. *Phys. Rev. Lett.* **1985,** *55*, 1331-1334.

34. Lim, S. H.; Bjorklund, T. G.; Spano, F. C.; Bardeen, C. J., Exciton delocalization and superradiance in tetracene thin films and nanoaggregates. *Phys. Rev. Lett.* **2004,** *92*, 107402/1-107402/4.

35. Voigt, M.; Langner, A.; Schouwink, P.; Lupton, J. M.; Mahrt, R. F.; Sokolowski, M., Picosecond time resolved photoluminescence spectroscopy of a tetracene film on highly oriented pyrolytic graphite: dynamical relaxation, trap emission, and superradiance. *J. Chem. Phys.* **2007,** *127*, 114705/1-114705/8.

36. Camposeo, A.; Polo, M.; Tavazzi, S.; Silvestri, L.; Spearman, P.; Cingolani, R.; Pisignano, D., Polarized superradiance from delocalized exciton transitions in tetracene single crystals. *Phys. Rev. B* **2010,** *81*, 033306/1-033306/4.

37. Katoh, R.; Katoh, E.; Nakashima, N.; Yuuki, M.; Kotani, M., Near-IR absorption spectrum of aromatic excimers. *J. Phys. Chem. A* **1997,** *101*, 7725-7728.

38. Albert-Seifried, S.; Friend, R. H., Measurement of thermal modulation of optical absorption in pump-probe spectroscopy of semiconducting polymers. *Appl. Phys. Lett.* **2011,** *98*, 223304-1/223304-3.

39. Rao, A.; Wilson, M. W. B.; Albert-Seifried, S.; Petro, R. D.; Friend, R. H., Photophysics of pentacene thin films: the role of exciton fission and heating effects. *Phys. Rev. B* **2011,** *84*, 195411-1/195411-8.

40. Fulem, M.; Lastovka, V.; Straka, M.; Ruzicka, K.; Shaw, J. M., Heat capacities of tetracene and pentacene. *J. Chem. Eng. Data* **2008,** *53*, 2175-2181.

41. Wen, X.; Tolbert, W. A.; Dlott, D. D., Ultrafast Temperature Jump in Polymers: Phonons and Vibrations Heat up at Different Rates. *J. Chem. Phys.* **1993,** *99*, 4140-4151.

42. Mohammed, O. F.; Samartzis, P. C.; Zewail, A. H., Heating and Cooling Dynamics of Carbon Nanotubes Observed by Temperature-Jump Spectroscopy and Electron Microscopy. *J. Am. Chem. Soc.* **2009,** *131*, 16010-16011.

43. Chen, S.; Lee, I.-Y. S.; Tolber, W. A.; Wen, X.; Dlott, D. D., Applications of Ultrafast Temperature Jump Spectroscopy to Condensed Phase Molecular Dynamics. *J. Phys. Chem.* **1992,** *96*, 7178-7186.

44. Durr, A. C.; Schreiber, F.; Kelsch, M.; Carstanjen, H. D.; Dosch, H., Morphology and Thermal stability of Metal Contacts on Crystalline Organic Thin Films. *Adv. Mater.* **2002,** *14*, 961-963.

45. Settels, V.; Schubert, A.; Tafipolski, M.; Liu, W.; Stehr, V.; Topczak, A. K.; Pflaum, J.; Deibel, C.; Fink, R. F.; Engel, V.; Engels, B., Identification of ultrafast relaxation processes as a major reason for inefficient exciton diffusion in perylene-based organic semiconductors. *J. Am. Chem. Soc.* **2014,** *136*, 9327-9337.

46. Kurrle, D.; Pflaum, J., Exciton diffusion length in the organic semiconductor diindenoperylene. *Appl. Phys. Lett.* **2008,** *92*, 133306-1/133306-3.

47. Rim, S.-B.; Peumans, P., The effects of optical interference on exciton diffusion length measurements using photocurrent spectroscopy. *J. Appl. Phys.* **2008,** *103*, 124515-1/124515-5.

48. Lunt, R. R.; Giebink, N. C.; Belak, A. A.; Benziger, J. B.; Forrest, S. R., Exciton diffusion lengths of organic semiconductor thin films measured by spectrally resolved photoluminescence quenching. *J. Appl. Phys.* **2009,** *105*, 053711-1/053711-7.

49. Steindamm, A.; Brendel, M.; Topczak, A. K.; Pflaum, J., Thickness dependent effects of an intermediate molecular blocking layer on the optoelectronic characteristics of organic bilayer photovoltaic cells. *Appl. Phys. Lett.* **2012,** *101*, 143302-1/143301-4.

50. Zhou, Y.; Taima, T.; Kuwabara, T.; Takahashi, K., Efficient small-molecule photovoltaic cells using a crystalline diindenoperylene film as a nanostructured template. *Adv. Mater.* **2013,** *25*, 6069-6075.

51. Peumans, P.; Yakimov, A.; Forrest, S. R., Small molecular weight organic thin-film photodetectors and solar cells. *J. Appl. Phys.* **2003,** *93*, 3693-3723.

52. Qin, D.; Gu, P.; Dhar, R. S.; Razavipour, S. G.; Ban, D., Measuring the exciton diffusion length of C60 in organic planar heterojunction solar cells. *Phys. Stat. Sol. A* **2011,** *208*, 1967-1971.

CHAPTER 5

Direct Detection of $S_0 - T_1$ Transition Using a Custom High Pressure Absorption Cell

5.1 Introduction

The stabilization of singlet energy levels that can be brought about in solid samples from crystallization prevented SF in the alpha polymorph of crystallized Peropyrene (**PP**) as discussed in Chapter 3. The singlet energy level is a very important piece of the singlet fission mechanism and the loss of energy can upset the requirement of $2E(T_1) \leq E(S_1)$ for a given molecule. Singlet energy level sensitivity with environmental factors can be explained by the large transition dipole moment between S_0 and S_1 state for a spin allowed transition (discussed in further detail on page 8, Chapter 1, of this work). By the same argument, the lack of transition dipole moment strength between the S_0 and T_1 state suggests that triplet states would be far less sensitive to the same environmental factors. In order to predict whether singlet fission is energetically possible, it is evident that knowing the extent to which both the singlet and triplet energies shift due to crystallization is necessary. As a first step to improving our knowledge in this area, solutions of molecules can are studied in this chapter. However, even the triplet energies of molecules in solution are not always straightforward to determine. Standard absorption experiments are not sufficient to determine a true triplet energy level because the $S_0 - T_1$ transition dipole moment is very small.

5.1.1 Triplet Energy Determination in the Literature

The triplet energy level of peropyrene was determined via triplet –triplet sensitization.[1] However, this method is approximate, gives the energy as a range and not a discrete number, and is indirect. Other more complicated experimental methods for determining triplet energy levels include photoacoustic calorimetry[2,3] and heavy atom effect absorption experiments[4-7]. A more direct, simple, and proven method of triplet energy determination is high pressure oxygen induced singlet-triplet absorption. Introduced in 1957 by Evans[8,9], this method increases the transition dipole moment of the $S_0 - T_1$ transition using high pressures of oxygen and manipulating Beer's Law:

$$A = \varepsilon BC \tag{5.1}$$

In which A is absorption, ε is the molar extinction factor, B is the cell pathlength and C is the concentration of a sample. An absorption cell with a pathlength greater than the standard 1 cm length increases the value of B and an overpressure of oxygen is used to increase the transition dipole moment of $S_0 - T_1$, which is related to ε. It was first thought that increased $S_0 - T_1$ transition was due to heavy atom effects from the oxygen, however the most recent argument attributes the enhanced absorption to interactions between the aromatic molecule's excited state and the charge transfer state of the aromatic molecule-oxygen complex formed.[10,11] In principle, the only difference between an ambient pressure absorption spectrum and a pressurized absorption spectrum would be the $S_0 - T_1$ absorption spectrum. This underlying spectrum could easily be

obtained by subtracting the ambient pressure spectrum from the pressurized spectrum.

5.2 High Pressure Cell

A custom absorption cell modeled after Evan's cell was designed in the Bardeen group and built by the UCR Machine Shop (see Figure 5.1 and 5.2). The overall pathlength of the cell was 10 cm and the windows installed at either end of the cell were 1" wide and 5/8" thick UV quartz. The cell fit into a Cary 500 absorption spectrometer and could be secured using 4 screws that fit through the base of the cell and into the Cary 500 housing (see Figure 5.3).
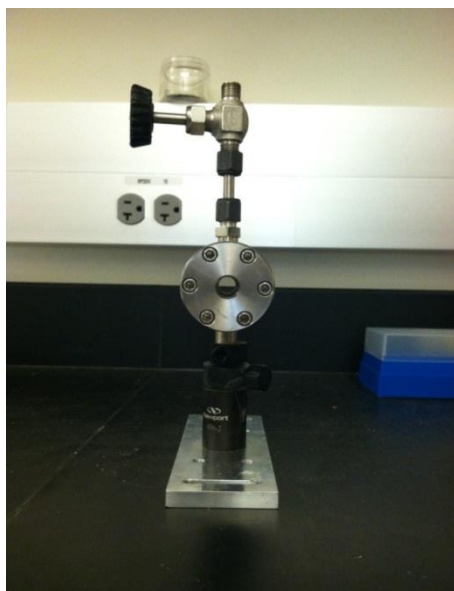

Figure 5.1 High pressure absorption cell with base, front view.

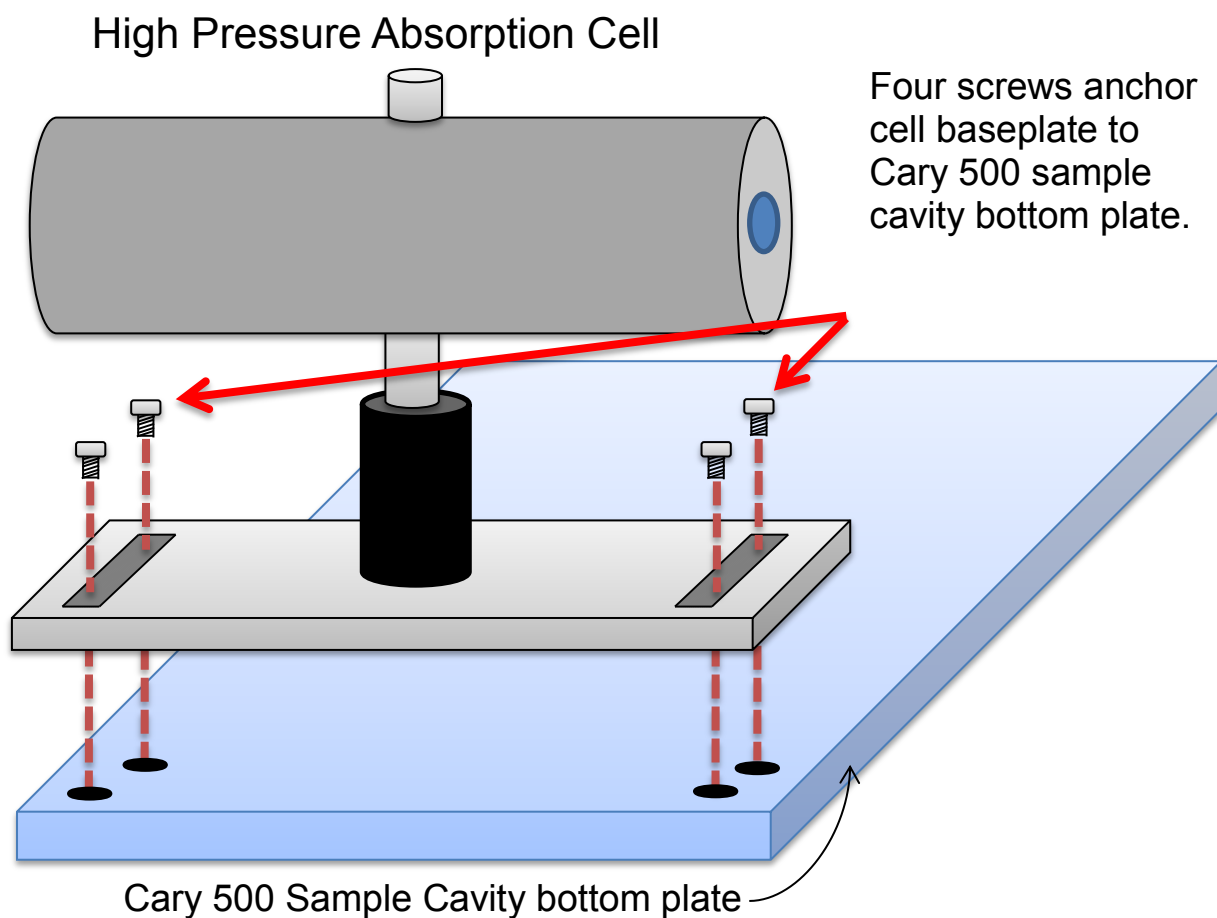**Figure 5.2** Side view of high pressure absorption cell with base in Cary 500 sample cavity.

High Pressure Absorption Cell

Four screws anchor cell baseplate to Cary 500 sample cavity bottom plate.

Cary 500 Sample Cavity bottom plate

Figure 5.3 Mounting diagram for high pressure cell in Cary 500 Spectrometer.

5.3 Anthracene Derivative Series

The first molecular series chosen to study and validate the experimental setup was anthracene derivatives. The $S_0 - T_1$ transition of 9-methylanthracene (**9MA**) and other derivatives has already been determined previously and was also used by Evans et al. in their high pressure cell. An attractive property of anthracene and its derivatives is high solubility, capable of creating concentrations of nearly 1 M in chloroform, giving an even higher absorption

value using Beers Law. Anthracene also has a high triplet energy level (14,500 cm^{-1}). However, the relaxed excited singlet state energy does not have sufficient energy to fission into two triplets and so singlet fission competes with excited singlet state relaxation. Singlet and triplet absorption can be used to study the effects of anthracene substitution on singlet and triplet energy levels. The goal would be the ability to fine tune both the singlet and triplet energy levels via substitution in order to increase the triplet quantum yield efficiency. Ideally, for anthracene, substitution would lead to the relaxed singlet energy shifting higher in energy while the triplet energy remains at 14,500 cm^{-1}. However, another approach would be to find substitutions that shift the singlet energy higher and shifts the triplet energy lower so that $E_{S1} > 2E_{T1}$.

Solutions used in experiments were always in chloroform at concentrations of at least 0.3 M. The concentration was limited by the solubility of each anthracene derivative. The cell was filled nearly to the top (see Figure 5.4) to allow as much surface area of the solution as possible to be exposed to the overpressure of oxygen. After filling the cell using a Pasteur pipet or a syringe, the cell was mounted into the Cary 500 for an ambient pressure scan that would be used at the reference spectrum. The cell was attached to an oxygen tank with a special oxygen regulator capable of regulating pressures up to 3,000 p.s.i. The oxygen was opened very slowly to ensure all possible leaks could be identified and plumbing tightened if necessary. Once the exposed cell pressure reached 2,000 p.s.i., 5 – 10 minutes were allowed to pass before closing the cell valve

first (see Figure 5.5) and then the tank valve. After both valves were closed, a pressure release valve was opened slowly and the cell was removed from the oxygen gas line. Once removed, the cell was shaken by hand gently for at least 15 minutes. After 15 minutes of gentle shaking, the cell was placed back into the Cary 500 and aligned straight in the cavity. The alignment method should be determined by the user and kept consistent. For example, in the data presented in this chapter, alignment was performed by placing a piece of very thick card stock flush against a lip on each side wall (see Figure 5.6) which left a gap less than 0.5 cm across between the absorption cell and the card edge. This provided a straight reference edge (the cardstock) against which the cell was aligned. In the future, the cell base could be built onto in order to provide some kind of mechanical alignment, for example, two vertical rods that could fix the cell position. After alignment a scan was taken from 1200 to 400 nm, scanning at a rate of 3.5 nm **PER** minute.
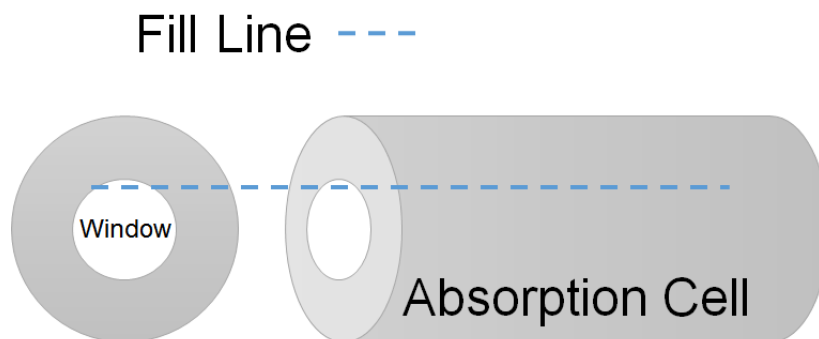

Figure 5.4. Illustration of absorption cell indicating maximum sample fill line. This fill line was used in order to maximize surface area in contact with oxygen in order to aid oxygen diffusion into the solution.
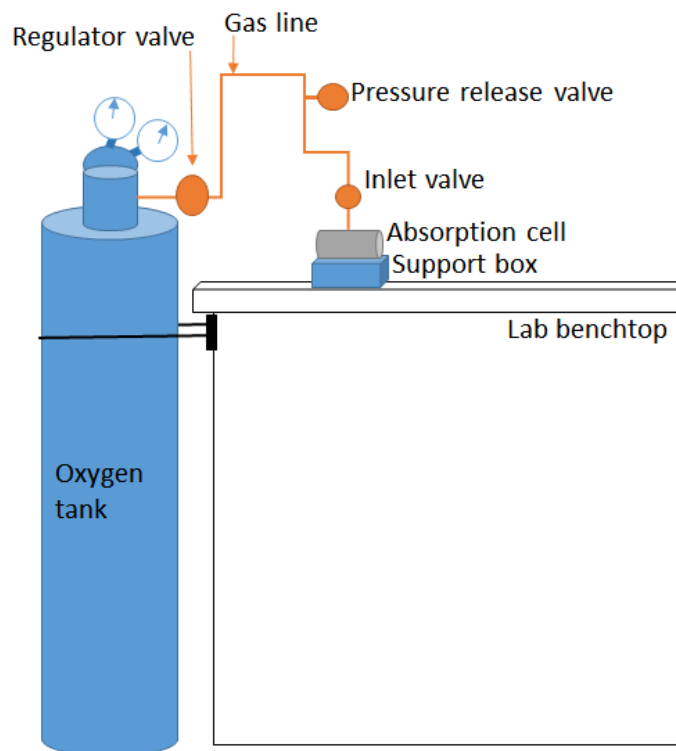
Figure 5.5 Illustration of cell pressurizing step experimental setup.
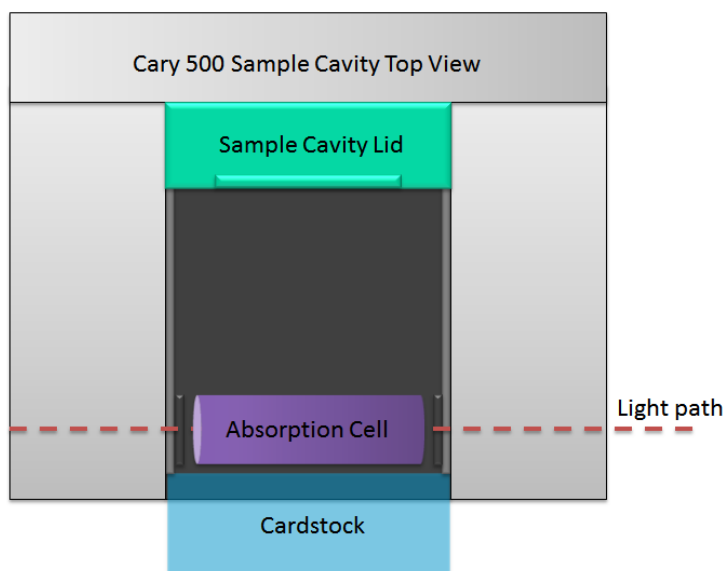

Figure 5.6 Top view of Cary 500 spectrometer with absorption cell mounted. Transparent blue rectangle represents position of a cut piece of cardstock used to create a visible straight reference edge as close to the absorption cell side as possible for alignment purposes.

5.3.1 Cell Characterization

The first set of scans taken were to characterize the cell's absorption in the Cary 500. This was done by taking an absorption spectra of the cell empty and without windows installed, empty with one window installed, empty with both windows installed, filled with chloroform blank solvent, and lastly with a solution of 9-methyl anthracene (**9MA)** in chloroform (see Figure 5.7). It can be seen that there is some inherent shape of the absorption spectrum without any solvent or sample in it, and that with 0, 1 or 2 windows installed, the spectrum remains very similar from 600 – 1200 nm. The addition of a blank solvent, chloroform, increases the absorption of wavelengths less than 300 as would be expected for an organic solvent and introduces peaks in the NIR that are probably chloroform overtones.[12] The addition of **9MA** saturates the absorption below 400 nm
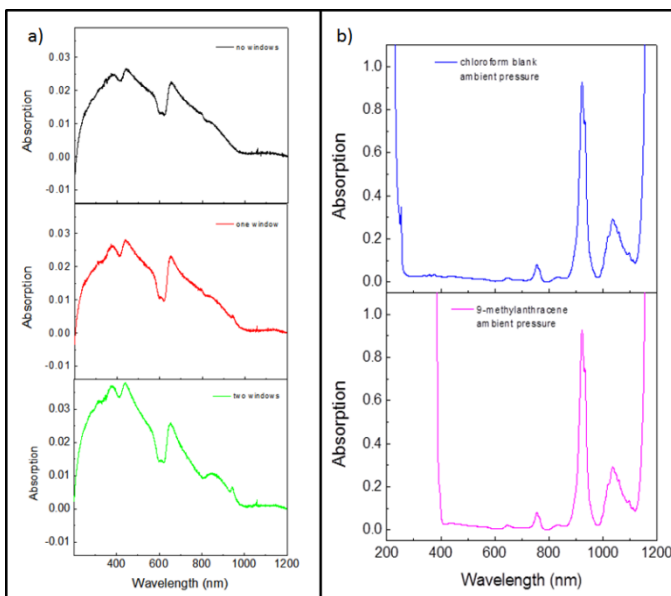

Figure 5.7 Panel a shows the **a**bsorption spectra of the high pressure cell in a Cary 500 without windows installed (black line), with one window installed (red line), and with two windows installed (bue line). Panel b shows the absorption spectra of pressurized chloroform blank (top, bue line) and pressurized 9MA n chloroform (bottom, pink line) in high pressure cell.

5.3.2 Triplet Absorption Spectra

In order to validate the high pressure absorption method, the triplet absorption spectrum of 9MA was extracted first and checked against Evan's data. Evans verified their triplet absorption peaks by comparing the lowest energy peak with the highest energy peak of **9MA's** phosphorescent spectrum. They validated their method through excellent agreement between the two.[9] Figure 5.8 below shows the 9MA triplet absorption spectrum obtained from the high pressure absorption cell introduced in this chapter overlaid with the values from Evan's research.
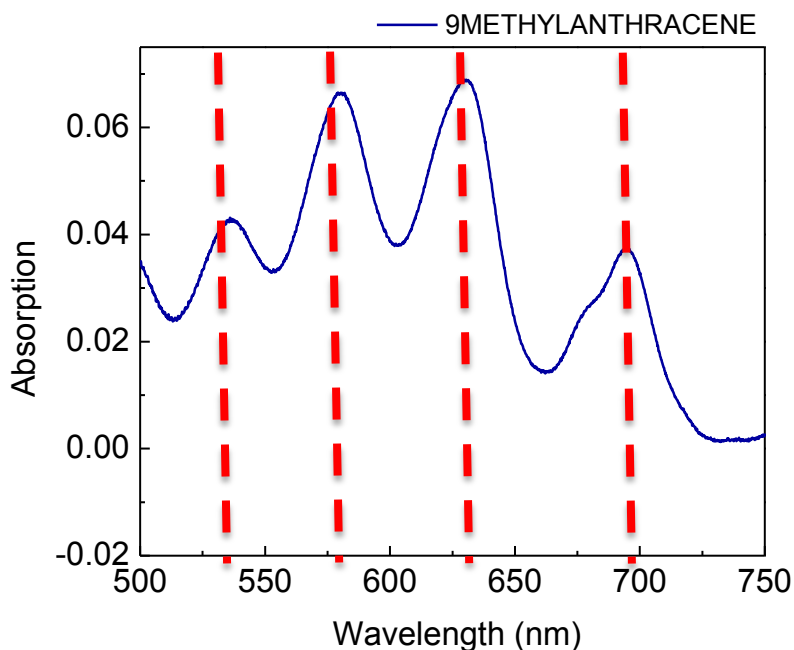

Figure 5.8 Extracted triplet absorption spectrum of 9MA (blue solid line) overlaid with Evan's triplet absorption peak values (dashed red lines).

Five different anthracene derivatives were measured using the high pressure cell and, partially because the literature values were known, extracting triplet spectra was relatively straightforward. Figure 5.9 shows the extracted triplet spectra whose values between 550 and 700 nm match those from the Evans paper.[9]
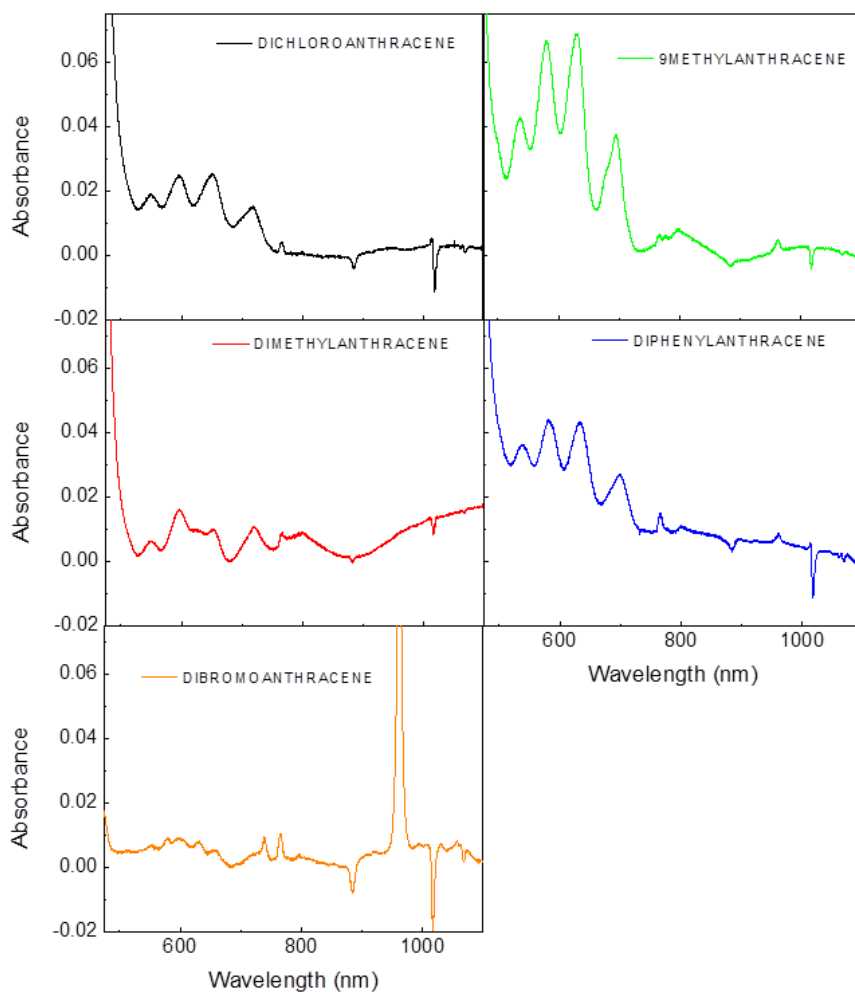

Figure 5.9 Extracted triplet absorption spectra of 9,10-dichloroanthracene (black), 9,10-dimethylanthhracene (red), 9-methylanthracene (green), diphenylanthracene (blue), and 9,10-dibromoanthracene (orange). Spectra obtained by subtracting ambient pressure absorption spectrum from pressurized absorption spectrum.

5.4 Current Issues

Even though the cell itself and solvent produces lineshapes and peaks in the absorption spectra, it was thought that all of this could be treated as background. The hope was initially that a simple subtraction of the ambient pressure spectrum from the pressurized spectrum would yield the triplet absorption spectrum. However, it turns out that in addition to solvent peaks, there is also oxygen induced effects such as baseline shifting that are introduced (see Figure 5.10). At 400 nm and 800 nm the spectrometer switching light sources which causes a discontinuity in the absorption spectrum at each. Additionally, while the UV/VIS region is relatively stable, the NIR baseline absorption currently has reproducibility issues which results in a rolling of the baseline upon ambient spectrum subtraction. All of these are issues that need to be addressed before a routine subtraction method can be used regardless of solvent or sample.

Solubility is also a problem with this experiment. Not all organic compounds can make solutions with concentrations close to 1 M. The absorption of the highest extracted peak in the 9MA scan is about 0.07. Using Beer's Law (Equation 5.1), 10 cm for the pathlength, and 0.7 M for the concentration, a molar absorptivity of 0.01 can be extracted for the $S_0 - T_1$ transition. Using this molar absorptivity value, in order to achieve a triplet absorption peak of at least 0.02 (in order to be distinguishable from experimental artifact peaks in the NIR region), a lower limit of 0.3 M concentration can be established. The sensitivity of the experimental setup needs to be increased if solutions with lower concentrations

have to be used. One possible method of addressing this would be to increase the sensitivity of each scan although that means longer scan times. It is also possible that a sensitive enough data workup procedure could extract very weak triplet absorption peaks. A third option would be to dissolve more oxygen into the solution, possibly with higher pressures or more efficient shaking methods.
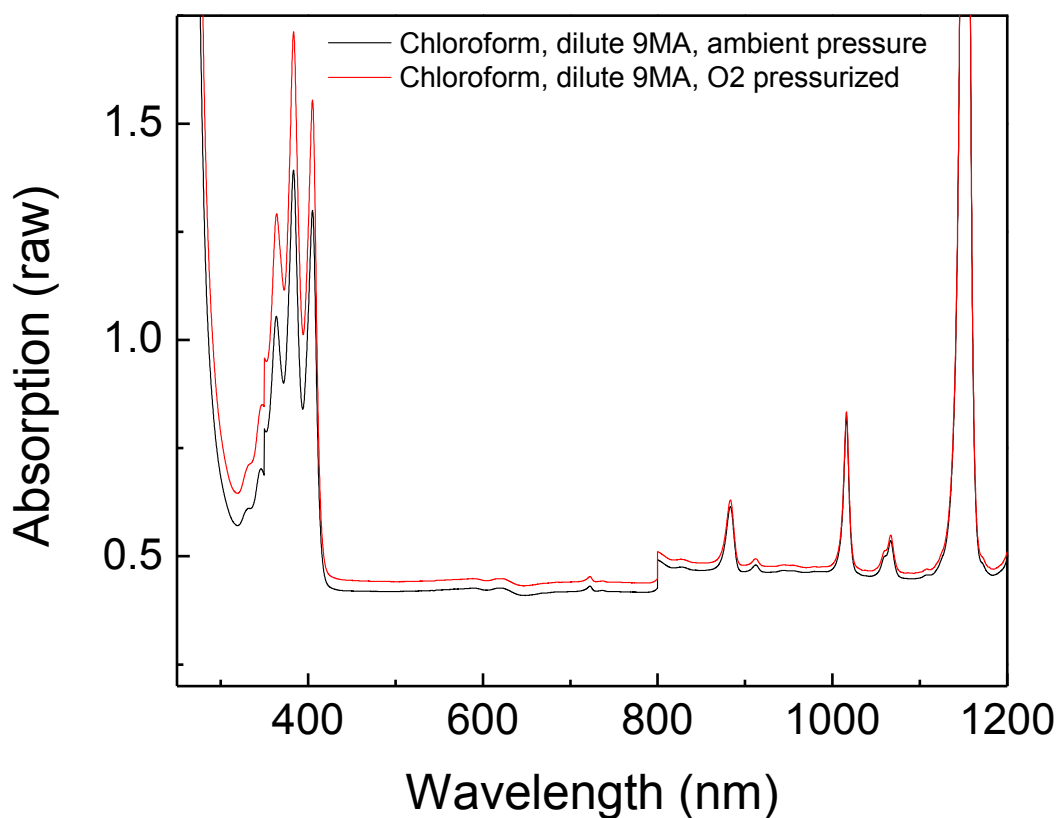

Figure 5.10 Overlay of raw absorption spectra of chloform with very dilute 9MA at ambient pressure and pressurized with oxygen.

5.5 Conclusion and Future Work

In conclusion, a high pressure triplet absorption cell was designed, built, and used to successfully extract S_0-T_1 absorption spectra for a set of anthracene derivatives. Future work to improve the method includes more experiments to optimize the shaking method and time. One possibility for improving the shaking method could be utilizing sonication. Additional experiments to optimize the instrument sensitivity would also greatly improve data analysis. After addressing these issues and also those with general data work-up and sample solubility, this experiment would be able to quickly and directly measure the triplet energy levels of organic compounds. This would be particularly helpful with screening molecules for use as singlet fission materials as it would give a directly measured triplet energy levels that could be compared with directly measured singlet energy levels. This experimental setup could also validate theoretical models designed to determine triplet energies as it gives a direct and discrete triplet energy measurement. Lastly, easy and quick direct measurement of triplet energy levels could also be useful for experiments in which the triplet energy is important for other reasons, such as UV filters which could be tested for their ability to sensitize singlet oxygen.

References

1. Wenzel, U.; Lohmannsroben, H. G., Photophysical and Fluorescence Quenching Properties of Peropyrene in Solution. *J. Photochem. Photobio. A* **1996,** *96*, 13-18.

2. Goodman, J.; Lavilla, J., The Energetics and Kinetics of Relaxed Alkene Triplet States as Determined by Pulsed Time-Resolved Photoacoustic Calorimetry. *Chem. Phys. Lett.* **1987**, *141*, 149-153.

3. Caldwell, R.; Misawa, H.; Peters, K.; Goodman, J., Use of Pulsed Time-ResolvedPhotoacoustic Calorimetry to Determine the Strain Energy of trans-1-Phenylcyclohexene and the Energy of the Relaxed 1-Phenylcylohexene Triplet. *J. Am. Chem. Soc.* **1986,** *108*, 6803-6805.

4. McClure, D. Triplet-Singlet Transitions in Organic Molecules. Lifetime Measurements of the Triplet State. *J. Chem. Phys,* **1949,** *17,* 905 – 910.

5. Weissman, S.; Yuester, P. Effects of Perturbations on Phosphorescence: Luminescence of Metal Organic Complexes. *J. Chem. Phys.* **1949**, *17*, 1182-1188.

6. Hans,P.; Blake, N.; McClure, D. Singlet-Triplet Absorption Bands in Some Halogen Substituted Aromatic Compounds. *J. Chem. Phys,* **1954,** *22,* 255-258

7. Kasha, M. Collisional Perturbation of Spin-Orbital Coupling and the Mechanism of Fluorescence Quenching. A Visual Demonstration of the Perturbation. *J. Chem. Phys.* **1952**, *20*, 71-74.

8. Evans, D. Magnetic Perturbation of the Lowest Triplet States of Aromatic Molecules by Dissolved Oxygen. *Nature,* **1956,** *178,* 534-535.

9. Evans, D. Perturbation of Singlet–Triplet Transitions of Aromatic Molecules by oxygen under pressure. *J. Chem. Soc.,* **1957,** 1351-1357.

10. Mulliken, R.; Tsubomura, H. Molecular Complexes and their Spectra. XII. Ultraviolet Absorption Spectra Caused by the Interaction of Oxygen with Organic Molecules. *J. Am. Soc.* **1960,** *82,* 5966-5974.

11. Hoijtink, G. Influence of Paramagnetic Molecules on Singlet-Triplet Transitions. *Mol. Phys.* **1960,** *3,* 67-70.

12. Futami, Y.; Ozaki, Y.; Hamada, Y.; Wojcik, M.; Ozaki, Y., Solvent Dependence of Absorption Intensities and Wavenumbers of the Fundamental and First Overtone of NH Stretching Vibration of Pyrrole Studied by Near-Infrared/Infrared Spectroscopy and DFT Calculations. *J. Phys. Chem. A.,* **2011,** *115,* 1194-1198.

CHAPTER 6

Conclusion

6.1 Summary and Conclusions

Singlet fission (SF) was introduced and its history covered briefly in the Introduction of this work. Current molecules that exhibit SF were also covered, bringing into light the need for new molecules with desirable properties that would optimize their use in photovoltaic (PV) cells: (1) a higher triplet energy to facilitate more efficient energy transfer to inorganic semiconductors, (2) a triplet yield near 200% (or 100% SF efficiency), and (3) a greater photostability for daily sun exposure. It was established that while the acene family has produced many SF molecules, the rylene family warrants investigation for future SF candidate molecules. For example, perylene (**PER**) is one conjugated aromatic hydrocarbon member of the rylene family that undergoes SF with low SF efficiency but is a very photostable molecule. In Chapter 3, Peropyrene (**PP**) was introduced as a derivative molecule of **PER** whose energetics and expected rylene family photostability retention single it out as an ideal candidate for SF. After characterizing the monomer in multiple solutions and discovering a dark state near the bright emissive state which perturbs the bright state, solid-state studies done on the **α-PP** crystal polymorph (see figure 6.1 for comparison of **α-PP** and an edge-to-face herringbone packing motif illustration) proved disappointing in that the **PP** crystals did not exhibit SF. It was concluded that the

lack of SF was due to the lowered energy of the **α-PP** excited state, probably due to overlapping π orbitals creating an excimer state. It was also hypothesized that this lowered excited singlet state would probably not exist in an edge-to-face herringbone packing structure, similar to that of tetracene. An edge-to-face herringbone packing motif would eliminate excessive π orbital overlap and prevent an excimer state from forming. **PP** highlighted the importance of knowing
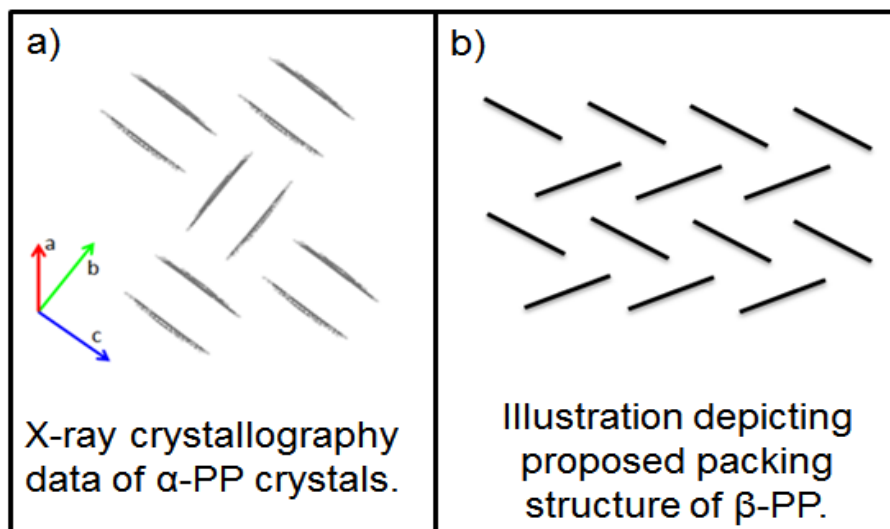

Figure 6.1 X-ray crystallography data of α-peropyrene polymorph showing pairwise herringbone packing structure (a). Panel (b) shows an illustration of the proposed crystal packing structure of β-peropyrene with edge-to-face herringbbone packing motif.

and choosing, if the option is available to, the crystal packing structure of a molecule and its impact on the ability of the molecule to undergo SF. The seemingly exaggerated dependence of **PP**'s fluorescence lifetime on solvent (nearly a factor of 2 difference between cyclohexane and acetonitrile) also shed light on state mixing. Using two photon absorption to access dark states (of different symmetry than the ground state), a second state was found close in

energy to the excited singlet state. Using perturbation theory, it was concluded that the mixing of this bright and dark state was creating a new state from which the fluorescence was actually emitting and was also responsible for the drastic differences of the apparent fluorescence lifetime in different solvents.

In Chapter 4, Diindenoperylene (**DIP**) was introduced as a second rylene family member SF candidate due to its herringbone packing motif, high crystallinity, and high triplet energy, 10,300 cm^{-1}, despite an "uphill" SF energetic scheme, $2E(T^1) - E(S_1) = -2,400$ cm^{-1}. After confirming a rapid (0.88 ns) internal conversion back to the ground state in the monomer form, solid state studies did not show any signs of SF. In fact, about 80% of the excited singlet state underwent internal conversion within the first 200 ps and the remaining singlet state population populated multiple long lived (up to 6.5 ns) lower energy states. Based on these findings, it was concluded that DIP not only does not exhibit SF but also would not be useful as a source of mobile excitons, for example in a photovoltaic device. However, **DIP** is already used in PV devices (see Chapter 4 for discussion) because of its high order of crystallinity, which is capable of inducing crystallinity in neighboring molecules.

Peropyrene is an example of how the crystal packing structure of a material can affect its ability to function as a singlet fission material. Additionally, DIP, although it had a desirable crystal packing structure illustrated how energetics also affect a materials singlet fission ability. When considering the energetic requirement for singlet fission, the triplet energy is just as important as

the singlet energy. Singlet energies can be easily determined using absorption and fluorescence experiments, however the triplet energy is be more difficult to elucidate due to the fact that the S_0-T_1 transition is spin forbidden. Clearly, a method that can directly detect the triplet energy of a molecule would be very useful and even necessary when screening molecules for singlet fission. In order to address this need, a high pressure absorption cell was built on site at UCR by the campus machine shop, and is introduced in Chapter 5. The cell, engineered to withstand up to 3,000 p.s.i. of O_2 gas, was pressurized up to 2,000 p.s.i. and fully dismantled and rebuilt for every single sample to be tested. The robust design proved capable of withstanding the constant handling and high pressures. One note of caution, the only part that has failed to date is the glass window which can and will crack if the cell is pressurized without properly tightening down the end screws or if the screws are overly tightened. It was concluded that through the use of chloroform as the solvent, concentrations above 0.3 M, and 2,000 p.s.i. of oxygen, the S_0-T_1 absorption transition dipole moment was increased up to an extinction coefficient value of 0.01 and the absorption of ground state molecules directly to the lowest energy triplet state could be observed. Furthermore, the actual triplet absorption spectrum was able to be extracted with excellent agreement with values previously reported in the literature (see Chapter 5 for more discussion). However, the experiment is not without its own problems as the introduction of oxygen and pressure seems to cause data workup problems. Upon pressurization of the sample in the cell, the

ambient pressure background spectrum shifts and new peaks are introduced, possibly due to overtones from the chloroform solvent. Also, the absorption spectra have low reproducibility and stability at longer wavelengths (800 – 1200 nm). A third problem is the change of lamp source used by the spectrometer which causes discontinuity in the absorption spectrum.

6.2 Future Work

In order to achieve the goal of increased PV cell efficiency by utilizing SF the next step would be integration of an optimal SF material into PV cells. The vast majority of currently produced solar cells are silicon based, and technology advances have dramatically decreased the cost and increased the efficiency of large scale production. Rather than increasing the efficiency of a solely organic PV, the most efficient and practical route forward that would realize the use of SF to increase the overall efficiency of PV cells would be interfacing a SF material with silicon, an inorganic bandgap material.

While **α-PP** and **DIP** are two rylenes that did not prove to be capable of serving as singlet fission materials, the rylene family itself still remains one of the most promising sources of SF materials. Recent work by Wasielewski has shown perylenediimides and *tert*-butyl-substituted terrylenes to be very capable singlet fission materials, with a 200% triplet yield in the terrylenes[1-2]. For use in PV cells however, *tert*-butyl-substituted terrylene's triplet energy of 9,000 cm^{-1} would limit the cell's bandgap materials and even disqualify the use of silicon since its bandgap is higher in energy than terrylene's triplet. On the other hand, with its

117

high energy triplet (11,000 cm^{-1}), **PP** has great potential if another crystal polymorph, proposed in this work as the **β-PP** polymorph exists. This would be analogous to **PER**, which exhibits both α- and β- crystal packing motifs. As previously stated, the **β-PP** polymorph with its edge-to-face herringbone packing motif could avoid excessive π orbital overlap between neighboring molecules, potentially preventing an excimer state from forming and retaining a high singlet energy level suitable for SF. Another possible avenue of continued **PP** research would be looking into the effects of substitution on singlet and triplet energy levels and on crystal packing structure. **PP** is still the closest rylene family member molecule to being a photostable, highly efficient SF molecule with a high triplet energy level. Future experiments for **DIP** already include work being done on utilizing **DIP** to dilute pentacene (**PEN**) molecules in crystalline thin films. **DIP** is suited for this because it has the exact same crystal packing structure as **PEN** and is similar in size to **PEN**. Again, substitution could prove to be a successful means of manipulating **DIP**'s energetics into being suitable for SF, especially if substitution can occur without interrupting the highly crystalline nature of the molecule.

In fact, the triplet absorption cell introduced and discussed in Chapter 5 could prove to be a useful tool for substitution studies, as it can be used to directly determine the triplet energy quickly, which would prove powerful when surveying many molecules at a time. The next step with the high pressure absorption cell is to determine an efficient and standardized data work-up

method. Assuming a future molecule's solubility does not allow for concentrations of 0.3M+, the induced triplet absorption transitions would be very small and possibly not visible by eye during data collection. In addition, if testing a molecule that has no previous triplet studies, there would not be a range that the data workup could focus on. A robust and tested data work-up method would need to address baseline changes upon pressurization, introduction of oxygen, and at discontinuous points where the lamp source changes in the instrument (e.g. 400 nm and 800 nm) across the entire tested wavelength range. Potential applications for this cell include any soluble molecule whose triplet energy is of interest. Exact $S_0 - T_1$ transition energy levels of future SF candidate molecules and substituted molecules, such as **PP** or anthracene derivatives would certainly be useful information when conducting survey or substitution effect studies. Additionally, the triplet energy of UV filter molecules that are currently used in sunscreens, such as avobenzone or octocrylene[3] are also of great interest and could be determined using the high pressure absorption cell.

REFERENCES

1. Eaton, S.W.; Miller, S.A.; Margulies, E.A.; Shoer, L.E.; Schaller, R.D.; Wasielewski, M.R., Singlet exciton Fission in Thin Films of tert-Butyl-Substituted Terrylenes. *J. Phys. Chem. A.,* **2015**, *119*, 4151-4161.

2. Eaton, S.W.; Wasielewski, M.R.; et al., Singlet Exciton Fission in Polycrystalline Thin Films of a Slip-Staked Perylenediimide., *J. Am. Chem. Soc.*, **2013**, *135*, 14701-14712.

3. Hanson, K.M.; Gratton, E.; Bardeen, C.J., Sunscreen Enhancement of UV-Induced Reactive Oxygen Species In The Skin. *Free Radical Biology & Medicine,* **2006,** *41,* 1205-1212